Chitosan Nanoparticles for Mucosal Vaccination – Understanding the Particle Formation Process and Formulation for Nasal Application

Dissertation zur Erlangung des Doktorgrades
der Mathematisch-Naturwissenschaftlichen Fakultät
der Christian-Albrechts-Universität zu Kiel

vorgelegt von
Judith Maria Heidland

Kiel 2018

Erste Gutachterin	Prof. Dr. Regina Scherließ
Zweite Gutachterin	Prof. Dr. Susanne Sebens
Tag der mündlichen Prüfung	16. Juli 2018
Zum Druck genehmigt	17. Juli 2018

gez. Prof. Dr. Frank Kempken, Dekan

Conference contributions

Oral presentations

- J. Heidland, R. Scherließ, Nano-in-microparticles for dry powder vaccination via the respiratory tract, CRS German Chapter Annual Meeting, March 2017

- J. Heidland, O. Helm, M. Lettau, E. Winter, S. Sebens, R. Scherließ, Nano-in-microparticles for Dry Powder Vaccination – Nasal Application and Uptake in Immune Competent Cells, Respiratory Drug Delivery, Tucson, Arizona, United States, April 2018, *Posters on the Podium Short Talk*

Poster presentations

- J. Heidland, R. Scherließ, NiM powders for nasal vaccination – insights into particle forming process, 10th World Meeting on Pharmaceutics, Biopharmaceutics and Technology, Glasgow, United Kingdom, April 2016

- J. Heidland, R. Scherließ, Nano-in-microparticle powders for mucosal vaccination – understanding the particle forming process, Drug Delivery to the Lungs 27, Edinburgh, United Kingdom, December 2016

- J. Heidland, R. Scherließ, Nano-in-microparticles for dry powder vaccination – possible for nasal application?, Drug Delivery to the Lungs 2017, Edinburgh, United Kingdom, December 2017, *Best academic poster award*

- J. Heidland, R. Scherließ, Aerodynamic characterisation of a nano-in-microparticulate formulation for dry powder vaccination, 11th World Meeting on Pharmaceutics, Biopharmaceutics and Technology, Granada, Spain, March 2018

- J. Heidland, O. Helm, M. Lettau, E. Winter, S. Sebens, R. Scherließ, Nano-in-microparticles for Dry Powder Vaccination – Nasal Application and Uptake in Immune Competent Cells, Respiratory Drug Delivery, Tucson, Arizona, United States, April 2018

After climbing a great hill,
one only finds that there are many more hills to climb.

Nelson Mandela

Table of contents

1 Introduction and Objectives

1.1 Introduction

In 1980 the World Health Organisation (WHO) declared smallpox eradicated due to an effective, internationally coordinated mass vaccination campaign. In another success story, polio was defeated in all but some remaining geographical pockets and infectious diseases such as diphtheria or tetanus are not life-threatening anymore [1]. Vaccination in general can be regarded as one of the most cost-effective health-care interventions; diseases such as cancer, HIV and tuberculosis for which preventive or therapeutic vaccines are not available (yet) however lack such effective therapy [2]. The public's overall positive perception of vaccination took a hit when in 1998 *The Lancet* published a paper linking the measles-mumps-rubella vaccine with autism even though the paper was later withdrawn because it was found to be erroneous and misleading [3].

Furthermore, it is very difficult to develop vaccines for pathogens with a high antigenic drift because their surface antigens change [4] and in case of the influenza virus this even leads to the need for a new vaccine every year because the surface antigens are used as antigens in the vaccine. In some years, e.g. the winter 2017/18, this vaccine does not match the actually circulating influenza isolates [5,6] and thus, the public's vaccination willingness is yet lower. It can therefore be inferred that there is a need for the development of novel and broader effective vaccines conferring protection even against fast shifting antigens, which are simultaneously safe to use.

Today, vaccines are mostly formulated as solutions or suspensions for injection. The antigen usually consists of live attenuated pathogens, whole inactivated organisms or inactivated bacterial toxins. Especially the attenuated pathogens are considered highly immunogenic while being minimally virulent. However, with those pathogens there is still a risk of regaining virulence [7]. Consequently, those vaccines carry the risk of severe adverse effects and even the break-out of the disease the vaccine was supposed to prevent. Having made this experience, safety is ranked very important in vaccine development nowadays and accordingly newly developed vaccines will probably not

contain live attenuated pathogens [4]. Inactivated organisms are safer but also less immunogenic in comparison to live attenuated pathogens. The lack in immunogenicity will be even more pronounced if only subunits instead of the whole organism are used as antigen. These could be a toxin or a capsular polysaccharide from encapsulated bacteria [4]. To overcome this lack in immunogenicity, adjuvants that enhance, modulate and/or prolong the resulting immune response are used [8]. Adjuvants furthermore allow the reduction of antigen load and antigen doses while stabilising the vaccine formulation during storage [9]. For this purpose, nowadays mostly alum is used but the implementation of new adjuvants, especially if utilising other routes of administration than injection, is sought after. Nanoparticles (NPs), for example, have been identified as potential antigen carriers that simultaneously exhibit adjuvant properties [10]. Other potential new adjuvants include chitosan, emulsions or pattern recognition ligands [11–13].

Alternative routes of administration (other than injection) are considered because the parenteral route is generally not known to induce a strong mucosal but merely systemic immunity. Mucosal immunisation with a particulate antigen which can be processed locally has been shown to induce both mucosal and systemic immunity [14], rendering it a favourable route of vaccine administration. This does not come as a surprise, since most pathogens enter the body via a mucosa. Nasal administration, being one opportunity for mucosal administration, bears the advantage of being independent of sterile equipment for administration and the nasal tissue is easily accessible as well as highly vascularised [15]. Challenges associated with this route of administration include achieving a sufficient dwell time of the formulation on the mucosa (to ensure uptake into and activation of antigen presenting cells, APCs) due to mucociliary clearance and the complex geometry of the nose with a narrow entrance and further narrow passages [16].

1.2 Objectives

The aim of this work is to investigate NPs as potential antigen carriers for vaccine formulations. Chitosan will be used as particle forming polymer because it is widely discussed in literature as excipient in vaccines due to its adjuvant potential [10,17–19]. The understanding of the particle formation process between chitosan and a counterion by ionic gelation and influencing factors on that process as well as the optimisation of the loading of a model antigen in the NPs will be part of this work.

To make the NPs applicable they will be incorporated into a microparticle matrix (Nano-in-Microparticle, NiM), which is suitable for nasal administration, as schematically shown in Figure 1-1.

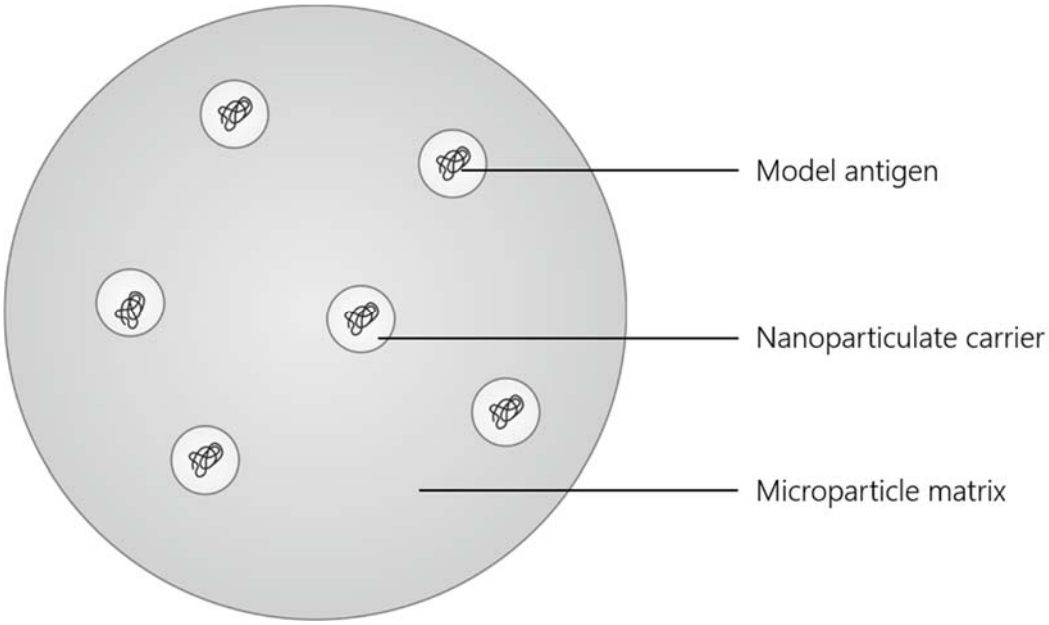

Figure 1-1. Scheme of the proposed NiM formulation.

The developed formulation will be investigated regarding its aerodynamic behaviour in terms of dispersibility from nasal powder device, nasal deposition and fine particle fraction (FPF). Upon deposition the microparticle matrix should dissolve and release the NPs. The *in vitro* uptake of those redispersed NPs into human dendritic cells (DCs) will be assessed to gain a first idea of the particles' potential for vaccine delivery.

2 Theoretical Background

2.1 Anatomy and Physiology of the Nose

The nasal cavity has gained more and more interest in the academic community and in the pharmaceutical industry by offering a potential as an administration route not only for local but also for systemic drug delivery [20–22]. It is of particular interest for nose-to-brain delivery (bypassing the blood-brain barrier) of substances such as fentanyl [23]. Due to the presence of many immune competent cells in the nasal tissue, it is furthermore a particularly interesting administration site for vaccines [15,24].

2.1.1 Anatomy of the Nose

The nose can be divided into the outer and the inner nose. The latter is separated into two (usually dissimilar) halves by the nasal septum (*septum nasi*). Each half can be subdivided into the nasal vestibule (*vestibulum nasi*) and the nasal cavity (*cavum nasi*). At the transition between the nasal vestibule and cavity the nasal valve (*limen nasi*) is located, an important structure as it usually exhibits the narrowest diameter in the inner nose and thus has considerable impact on respiration and particle deposition. The air is accelerated here before slowing down and being swirled in the anterior nasal cavity which exhibits broader structures [25]. Each nasal cavity is confined dorsally by the posterior nasal aperture (*choana*) and both halves are merged in the nasopharynx [26]. Each nasal cavity has a volume of approximately 7.5 mL in an adult [21]. A schematic image of the nose, depicting details in the nasal cavity is shown in Figure 2-1.

Each lateral nasal wall holds three bony turbinates (*conchae nasales*) which are covered by mucous membranes. They increase the specific surface area of the nasal cavity to approximately 130 cm^2 for both nasal cavities (150 cm^2 total surface area of the nose) in adults [27]. The turbinates simultaneously structure the nasal cavity in three passages (*meatus nasi*): the inferior nasal passage between the nasal floor and the inferior turbinate, the middle nasal passage between the inferior and the middle turbinate and the upper passage between the middle and superior turbinate. Above the latter the

olfactory region is located. Furthermore, the lateral walls of the nasal cavity are connected to the nasal sinuses (*sinus paranasales*) via narrow openings [26].

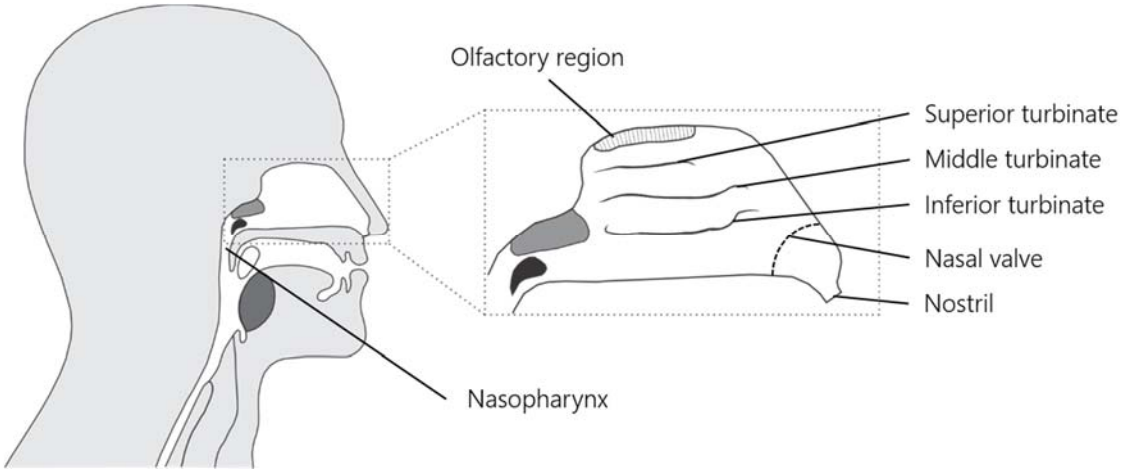

Figure 2-1. Sagittal section of the upper airways with details of the nasal cavity, adapted from [28]. Details on depicted tonsils are explained in section 2.2.1.1.

The inner nose is covered by either respiratory or olfactory mucous membranes [25]. The olfactory mucosa can be found in the olfactory region and is characterised by the presence of Bowman's glands. Enzymes secreted by those glands serve olfaction.

The other parts of the nose, including the nasal turbinates and sinuses, are covered by the respiratory mucosa which is highly vascularised [29]. It consists of a multi-layered ciliated epithelium and comprises mucous glands [30]. The epithelium is covered by secretions which form a double layer, as depicted in Figure 2-2.

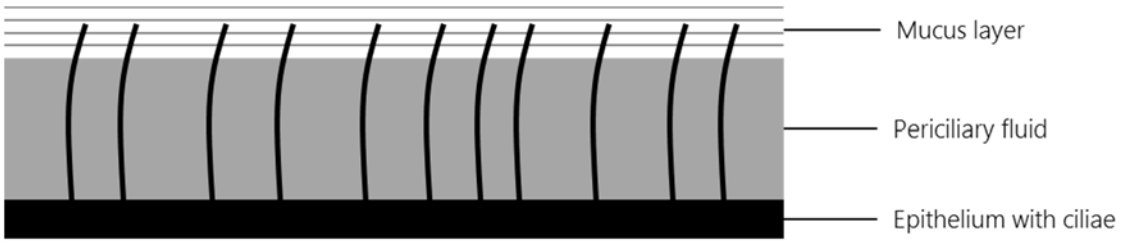

Figure 2-2. Secretions covering the nasal epithelium which can be divided in the periciliary fluid (7 - 10 µm) and the mucus layer (0.5 - 2 µm), adapted from [31].

The periciliary fluid, which is depicted in grey in the illustration, is of low viscosity while the mucus layer above exhibits a higher viscosity and non-Newtonian viscoelastic properties. It consists of 95 % water, 2 - 3 % glycoproteins, 1 % other proteins, 1 % salts and < 1 % lipids and is replaced approximately every 15 min [31]. Being a glycoprotein,

mucin is the principal polymeric component in the mucus and its quaternary structure is responsible for its gel-forming properties. It has a polyanionic character at neutral pH because of many sulphate and sialic residues [32]. The mucus and entrapped particles are moved to the nasopharynx due to ciliary action at a rate of (usually) 4 - 6 mm min^{-1}. There can be variation due to diseases and in between individuals [21,31].

In contrast to the posterior parts of the nasal cavity, the anterior parts (including the front surfaces of the turbinates) are coated with non-ciliated epithelium. Thus, removal from those regions is slower [21].

2.1.2 Physiology of the Nose

The nose is the preferred airway for respiration during sleep, rest and mild exercise. Nasal breathing is even obligatory in neonates [25,33]. Moreover, filtration and conditioning of the air as well as olfaction are functions of the nose [31]. The smell perception takes place in the olfactory region located in the superior part of the nasal cavity [26]. The inhaled air mostly flows through the middle nasal passage, exhaled air through the inferior nasal passage as well [30]. While the air is inhaled, it gets warmed (to 31 - 34 °C) and humidified by evaporation of nasal fluids. Furthermore, the air is cleared from airborne contaminants (or drug particles and droplets) which are entrapped in the nasal hairs and the mucus. The particle filtration efficiency from the air is dependent on the size and foremost due to inertial impaction. Particles above 10 µm are to be expected to deposit in the nose [21].

2.2 Vaccination

The observation that one person usually does not suffer from the same disease more than once has already been made in ancient times. It led to the practice of inoculation of healthy persons with small amounts of infectious material obtained from persons infected with smallpox, with the aim of achieving immunity while lowering risks associated with the naturally occurring disease (mortality of 20 - 30 %) [34,35]. In China

this practise was already documented a thousand years before Edward Jenner started with the modern vaccination. In 1796, rather than inoculating with infectious material obtained from patients who were suffering from smallpox, he used material obtained from cowpox. He did this because he observed an immunity of milkmaids against smallpox after having suffered from cowpox, a harmless infection for humans. Hence, inoculation with cowpox led to a comparable immunity against smallpox while minimising risk of adverse effects [34]. Due to this tremendous success the word "vaccination" was derived from the latin word *vacca* for cow.

In the late 19th century Paul Koch identified microorganisms as a cause of infectious diseases and Louis Pasteur developed the first attenuation method for pathogens [34]. Those pathogens were less infectious while maintaining their immunogenic properties leading to the development of vaccines against rabies and cholera [36]. In the following, killed pathogens were utilised for vaccines as antigens. In the 1920s even antigens only containing inactivated toxins, so called toxoids, from diphtheria and tetanus were adopted [34,37]. While decreasing the risk of severe adverse effects more and more by using smaller parts of the pathogen, the immunogenicity is lowered as well. Hence, adjuvants (derived from the latin word *adjuvare* for helping) were used with the aim to enhance and prolong the immune response [34]. More information on this topic will be provided in chapter 2.3.1.

In vaccination adverse effects are an important topic because they are only sparsely tolerated. This is because vaccines are given to healthy persons in contrast to other medication, which is given to sick persons. Those patients bear greater adverse effects because the disease they suffer from is (usually) worse. A distinction can be drawn between adverse effects related to the vaccine, those associated with the vaccination procedure and those arising simultaneously with the vaccination by chance [38]. At present, most vaccines are administered intramuscularly. Hence, adverse effects are likely to occur due to the injection procedure (e.g. accidental needle sticks, use of contaminated needles) [7]. Figure 2-3 shows the potential impact of adverse events on the success of a vaccination campaign.

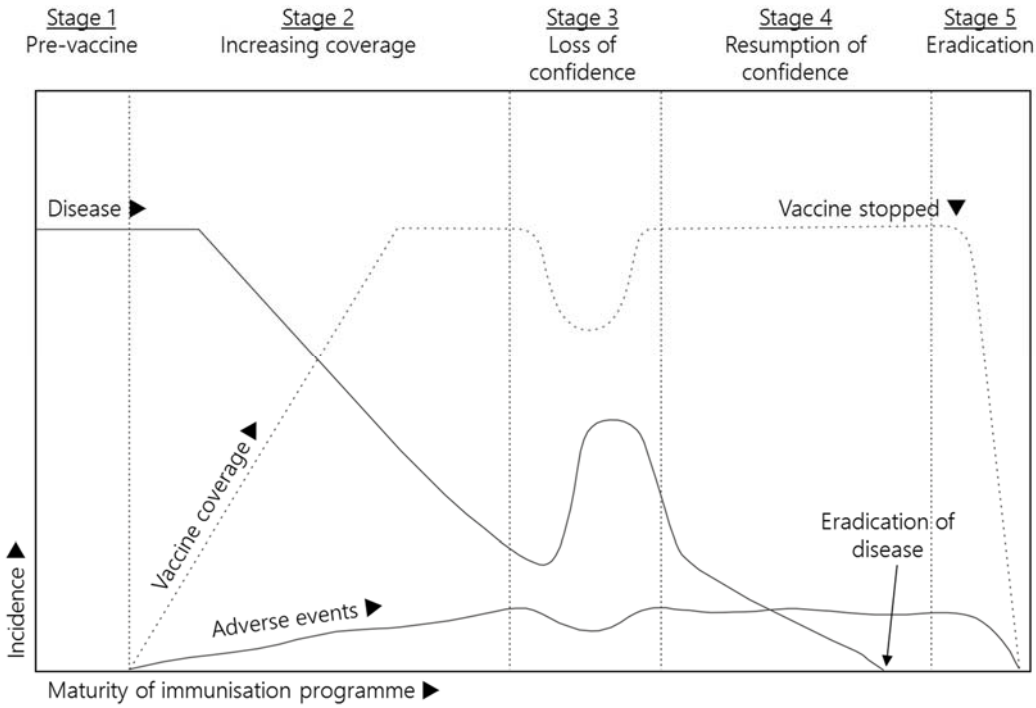

Figure 2-3. Potential stages in the evaluation of an immunisation programme linking the disease's incidence, vaccine coverage and adverse events, adapted from [39].

In stage 1 (before a vaccine is available), the disease incidence is high. When the vaccine becomes available, the vaccine coverage increases and simultaneously the disease incidence decreases. With rising vaccine doses applied, the number of adverse events (vaccine-related, vaccination process-related and coincidental) increases (stage 2). After a while the threats of the disease become less visible due to low incidence, on the other hand the adverse events come to the fore resulting in loss of public confidence in the vaccine. Therefore, vaccine coverage falls again (stage 3) which concurrently raises the probability of new outbreaks of the disease. Triggered by such an outbreak, the trust in the vaccine increases again, vaccine coverage increases (stage 4) and eventually the disease is eradicated. It is only at this time that the vaccine application can be stopped (stage 5) [39]. This figure stresses not only the need for public awareness campaigns about the threats of infectious diseases but also shows the need for new vaccines and/or other administration routes, which are associated with less adverse events because the success of an immunisation programme relies on it. Nasal vaccines (formulated as liquid or dry powder) are not administered invasively and hence might be a promising alternative to the nowadays commonly used parenteral vaccines

because they bear not such a high risk of vaccination-related adverse events, as accidental needle sticks [28].

2.2.1 Immunological Principles

The immune system can be divided into the innate and the adaptive immune system. Both systems are necessary to effectively defeat pathogens. While the innate immune system is activated within hours, the adaptive one takes days when it has not encountered the pathogen before. Once it has, it is the most effective part of the immune system [40]. Both systems consist of cellular and humoral (soluble) components [1]. Granulocytes, natural killer cells, macrophages and DCs are cells, which belong to the innate immune system. The latter two cell types are APCs that are able to activate T- and B-lymphocytes, which represent the cellular components of the adaptive immune system. For this reason, macrophages and, in particular, DCs form an important link between the innate and the adaptive immune system. The humoral components are the complement system and soluble antibodies (immunoglobulins, Ig) for the innate and the adaptive immune system, respectively. The complement system, consisting of many plasma proteins, provides the fastest response to a pathogen (within hours). It eventually results in the lysis of the pathogen [40]. Alternatively, the pathogen can be phagocytosed and eliminated by the cellular components of the innate immune system. Those cells recognise the pathogens due to so called pathogen-associated molecular patterns which are present on many pathogens but not on body's own cells [1]. The APCs not only eliminate the antigen, but furthermore present it via major histocompatibility complex I (MHC-I) or MHC-II to T- and B-lymphocytes which is key to activate the adaptive immune system [40]. Whether an antigen is presented via MHC-I or MHC-II is dependent on its type. An endogenous antigen (e.g. virus in an infected cell) is degraded by the proteasome complex and presented via MHCI-I to $CD8^+$ cytotoxic T-cells [41]. By contrast, antigens, which are phagocytosed, are degraded by a pH decrease and cytotoxic molecules and presented via MHC-II for recognition by cluster of differentiation 4^+ ($CD4^+$) T-cells. This stimulates the CD4+ T-cells to mature into

helper T-cells (T_H) type 1 or 2. Those can be differentiated based on the secreted cytokines [1]. While T_H1 cells favour the development of a cellular immune response, T_H2 cells favour the development of a humoral immune response by activation of B-cells that develop into plasma cells releasing the humoral component of the adaptive immune system – antibodies. Depending on the activating cytokine, different isotypes of antibodies can be produced [1,42]. Those usually lead to the lysis of the infected cells. At the end of an infection, another type of T-cells (regulatory T-cells) supresses further T-cell responses.

Both, T- and B-lymphocytes form memory cells, which can intervene much faster upon re-infection than it was possible during the primary infection. A balanced immune response (cellular and humoral) after vaccination is considered optimal nowadays [42].

2.2.1.1 Nose-Associated Lymphoid Tissue

While injected antigens evoke systemic immune responses, antigens which are administered at a mucosa also evoke a local immune response via the mucosal immune system. This is part of the adaptive immune system and belongs to the secondary lymphoid organs [40]. The nose-associated lymphoid tissue (NALT) is the site of the mucosal immune system in the upper airways and located in the human pharynx, as shown in Figure 2-4.

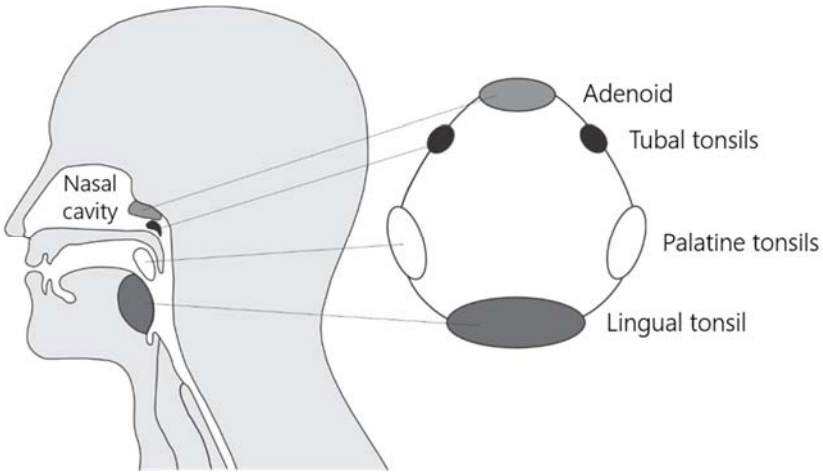

Figure 2-4. Pharyngeal lymphoid tissue of Waldeyer's ring, taken from [43].

It was first described in 1984 by Waldeyer and named after him. The NALT consists of the adenoid (or nasopharyngeal tonsil), the paired tubal and paired palatine tonsils and

the lingual tonsil [43]. In children the NALT is potentially distributed throughout the nasal cavity, increasing the chance of a contact between the antigen and the lymphoid tissue and therefore improving the potential immune response in children after administration of an intranasal vaccine [28,31].

The NALT comprises all immunocompetent cells that are necessary to induce an immune response: DCs, macrophages, T- and B-lymphocytes and microfold cells (M-cells) [44]. The M-cells are specialised epithelial cells which can take up particles up to a size of 10 µm [45] and deliver them by transcellular vesicular transport to underlying immune cells that can process them [24]. M-cells and DCs are however not only present in the confined structure of the NALT but are distributed throughout the respiratory mucosa [10,46]. Pathogens or particles that are deposited in the nasal cavity can either be taken up by cells in the respiratory mucosa after overcoming the mucus layer or in the adenoid where they are transported to by mucociliary clearance [10,15]. Different mechanisms for particle uptake are displayed in Figure 2-5.

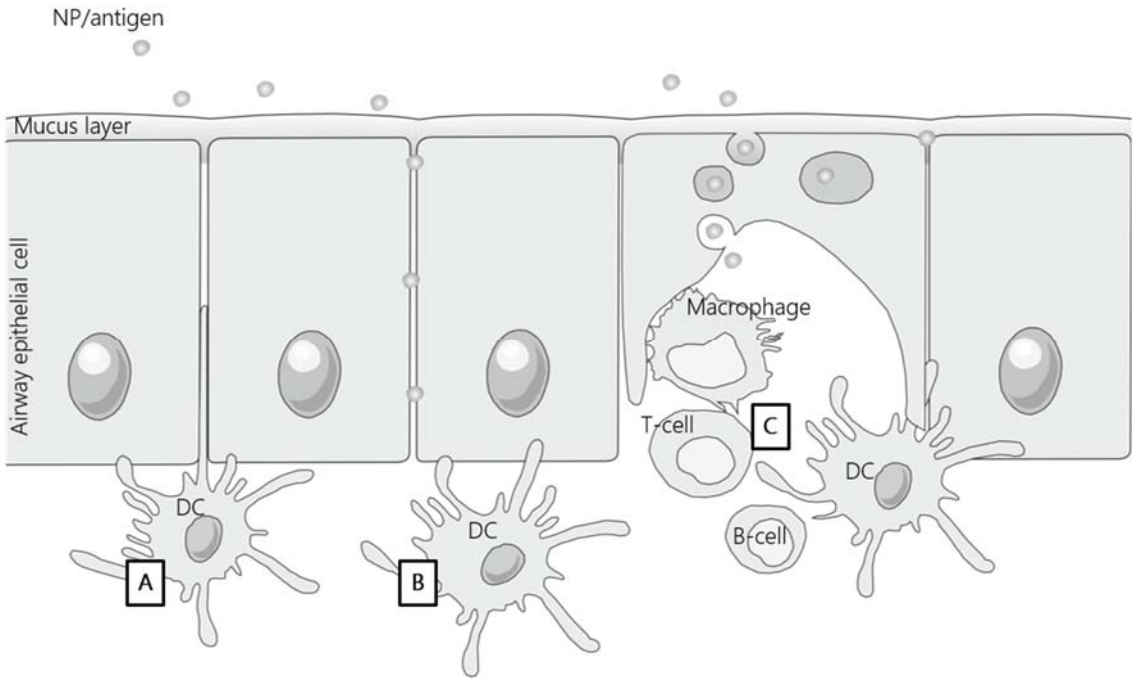

Figure 2-5. Routes of mucosal immune induction in nasal and airways epithelia by antigen loaded NPs, taken from [10].

NPs can be taken up directly by DCs via transepithelial dendrites (A). Alternatively, NPs can passively permeate through epithelial junctions and then be taken up by underlying DCs (B). Another option is the transcellular transport through M-cells and delivery to immune cells that are present in the underlying pocket (C). Other possibilities include uptake of the NP via endocytosis in an epithelial cell, which can trigger the immune response by the release of cytokines, or presentation via MHC-I to T-lymphocytes.

Particles with sizes ranging from a few hundred nanometres up to a few micrometres can be taken up by DCs [47]. Hamdy et al. described NPs as preferred over microparticles if targeting DCs because smaller particles are rather taken up by DCs while macrophages ingest larger particles [48]. Different preferred NP sizes are described in the literature, e.g. 20 - 80 nm [10] or 250 - 400 nm [49], depending on parameters such as the flexibility of the NP. Concluding from the abovementioned literature sources, this project aimed for particle sizes below 500 nm to enable preferred uptake into DCs.

Activated DCs either stimulate a local immune response by presenting the antigen to neighbouring lymphocytes or migrate to lymph nodes (in the nose preferably to the posterior cervical lymph nodes) to stimulate an additional immune response. Depending on the lymph node in which the further processing takes place, different types of antibodies are produced by plasma cells. While the posterior cervical lymph nodes induce so called homing of immunocompetent cells and thus a local immune response (plasma cells release IgA) as well, the processing in the superior cervical lymph nodes and the spleen rather leads to a systemic immune response (plasma cells release IgG and IgM) [50]. Homing is the migration of lymphocytes back to their original tissues. Due to homing receptors, which bind tissue-specific chemokines, cytokines or adhesion molecules, lymphocytes find their original mucosa. Moreover, homing is directed by chemotaxis controlling the lymphocyte migration [40,51].

In addition, plasma cells releasing IgA can appear not only at the mucosal site of primary infection or immunisation, but also at distant mucosal sites. This feature is referred to as the “common mucosal immune system” [15,52]. The extent to which IgA is

expressed at those distant mucosal sites by plasma cells is dependent on the route of primary infection, e.g. infection or immunisation via the nose not only stimulates an immune response in the respiratory tract but also results in a strong genital-vaginal mucosal immune response [51]. Secretory IgA (sIgA) antibodies are usually found in a dimeric or multimeric form in mucosal secretions and are relatively resistant to enzymatic degradation. Those antibodies play a leading role in the neutralisation of pathogens prior to infection directly in the mucosa [24].

2.2.2 Immunisation Strategies

Usually an immunisation is a preventive action, which can be divided into the active and the passive immunisation. Another field is the therapeutic immunisation.

In case of an active immunisation a vaccine is administered to an antigen naïve individual. This induces an immune response building up over 10 - 14 days which leads to the development of memory T- and B-lymphocytes [34]. Usually this immunisation is repeated within a short period of time (two to four weeks) to boost the affinity of the secreted antibodies. This achieved immunity can last life-long [1,53]. Passive immunisation on the other hand does not provide a long-lasting but immediate immunity. It is performed in emergencies by administrating antibodies after an infection that one is not immune to, e.g. tetanus or snake venom [40]. In contrast, therapeutic vaccines are developed as future cures to pre-existing conditions such as cancer, chronic infections (HIV, hepatitis, tuberculosis) or Alzheimer's disease, just to name a few [54–57].

2.2.3 Routes of Administration

Vaccines can be delivered to humans via different administration routes. Nowadays, the most typically used is the intramuscular (or subcutaneous) injection [7]. This route however bears some disadvantages and thus other administration routes have been under research. Needle-free routes are the cutaneous and the mucosal immunisation,

i.e. nasal, oral, pulmonary or ocular immunisation [7]. Slütter et al. listed advantages and disadvantages of different administration routes as shown in Table 2-1 [58].

Table 2-1. Advantages and disadvantages of different vaccine administration routes, taken from [58].

Immunisation route	*Advantages*	*Disadvantages*
Parenteral	• Powerful systemic immune response • Accurate dosing	• Invasive • Limited mucosal immune response
Nasal	• Non-invasive • Mucosal and systemic immune response • Easily accessible • Little degradation (compared to oral)	• Mucociliary clearance • Inefficient uptake of soluble antigens
Oral	• Non-invasive • Mucosal and systemic immune response • Large surface area	• Vaccine digestion in stomach and gut • Inefficient uptake of soluble antigens • Mucosal tolerance
Pulmonary	• Non-invasive • Mucosal and systemic immune response • Little degradation (compared to oral)	• Delivery of antigen highly variable between persons • Clearance from lungs
Dermal	• Non or minimally invasive • Large, easily accessible application area • High density of immune cells in skin • Mucosal immune response possible	• May require (minimally) invasive technology • Less established technology

In addition to Table 2-1 it might be said that after parenteral vaccination no mucosal immunity instead of a limited one is to be expected because the antigen will most likely not be processed locally. The same is true if a soluble antigen is used in nasal vaccination. The problem with the soluble antigen will probably not be the uptake but rather the local processing, which is key in inducing a mucosal immune response.

Most pathogens enter the body via a mucosa, consequently this route is very promising for vaccination [28,59]. Especially the nasal vaccination has been of great interest because the nose is not only easily accessible but also highly vascularised and furthermore comprises the immune competent NALT. Moreover, immune responses can be induced at distant mucosal sites, as mentioned before in chapter 2.2.1.1. Another advantage is the potential of self-administration, enabling the easy immunisation of large population groups [60]. Mucosal vaccination is nonetheless very challenging as illustrated by the low number of registered mucosal vaccines. Most of them are for oral use (i.e. cholera, polio, rotavirus) and only Fluenz® (marketed as FluMist™ in the United States, USA, and in Canada), a vaccine against influenza, for nasal use. In this product, a live attenuated virus is used as antigen [61].

The challenges, mentioned in Table 2-1, have yet to be overcome. The requirements for the formulation are thus increased compared to injected vaccines. More light will be shed on this topic in the following chapter 2.3.

2.3 Vaccine Formulations

Registered vaccines can be divided into three categories as described earlier. Vaccines contain live attenuated pathogens, killed pathogens or subunits (toxoids or surface proteins). The immunogenicity is highest for the live attenuated pathogens, decreased in killed pathogens and even lower for subunit antigens. Hence, the need for adjuvants to enhance the immune reaction is greatest in subunit vaccines [62]. With decreasing immunogenicity, the safety of a vaccine increases. A live attenuated pathogen as antigen bears the highest risk of adverse effects because the pathogen might become virulent again and even evoke the disease it was supposed to protect against [4].

In addition to the antigen, vaccine formulations usually include stabilisers (to stabilise the antigen), inactivation substances (e.g. formalin to transform toxins to toxoids), residues from the manufacturing process (e.g. cellular components of hen's eggs, antibiotics), preservatives (to prevent a contamination of the vaccine) and adjuvants

(enhancement of the immune reaction) [63]. The latter will be further discussed in the following chapter 2.3.1 because they are particularly important in subunit vaccines that are administered intranasally.

2.3.1 Adjuvants

The use of adjuvants has a long history. Aluminium hydroxide and phosphate, commonly referred to as alum, have been used for almost 90 years to enhance the immune response to a vaccine [64]. Alum is the most widely used and most frequently studied adjuvant. Its effect probably relies on a depot effect (slow release of the adsorbed antigen). Moreover, Alum leads *in vivo* to the secretion of high levels of antigen-specific antibodies, hence to a preferential humoral immune response. If a cellular immune response however is needed (e.g. intracellular pathogen), alum will not be suitable [64,65].

A mere 20 years ago another adjuvant, MF59 (microfluidised emulsion 59), was first used in an influenza vaccine (Fluad®, Novartis, Switzerland) [64,66] even though the use of emulsions as adjuvant has been studied since 1930 (Freund's Complete Adjuvant). MF59 is an oil-in-water emulsion that mostly consists of squalene and is stabilised by polysorbate 80 and sorbitane trioleate 85 [64]. Many other adjuvants are discussed in the literature not only regarding their immune enhancing capacity but also its pathway, which might direct the immune response towards a humoral and/or a cellular mediated one [67]. Different postulated mechanisms include depot formation, recruitment of immune cells, activation of the inflammasome, enhancement of antigen presentation by MHC molecules or immunomodulation [9].

Moreover, it must be differentiated between adjuvants being effective after parenteral injection and those after mucosal administration. Newsted et al. state that in 2015 none of the licensed adjuvants revealed a strong enhancement of the immune response after mucosal administration [68]. They furthermore report that mucosal adjuvants can be

separated into two groups: immunostimulators and vehicle delivery systems. Examples for those two groups are given in Table 2-2.

Table 2-2. Types of mucosal adjuvants, taken from [68].

Immunostimulatory adjuvants	*Vehicle delivery systems (Nanoparticles)*
• *Escerichia coli* heat labile enterotoxin	• Virus-like particles
• Cholera toxin	• Liposomes
• Pattern recognition ligands	• Nanogels/-emulsions
• Cytokines	
• Mast cell activators	

While immunostimulators directly activate innate immunity, delivery systems protect antigens from the environment and target M-cells [68]. Some adjuvants exhibit immunostimulatory properties and are delivery system at the same time, such as chitosan and its derivatives. Chitosan is not only a potent immunostimulant but also a relatively safe penetration enhancer by translocation of tight junctions between cells [69,70] making it a very promising adjuvant.

2.3.2 Special Requirements for a Nasal Nanovaccine

A nasal nanovaccine must deposit safely in the nose and be taken up into immune competent cells to induce an immune response. Excipients prolonging the dwell time on the nasal mucosa, easing the uptake and enhancing the immune response would thus be favourable [58]. The nanoparticles must be formulated in a way that ensures their deposition in the nose. This could either be done by the formulation as a liquid producing large enough droplets or as a dry powder in a suitable size range of above 10 µm (confer chapter 2.1.2). The use of a dry powder instead of a liquid as nasal vaccine alleviates storage and distribution requirements. Potentially not even refrigeration is necessary making a dry powder a favourable formulation, e.g. for mass vaccination campaigns in developing countries [31].

2.4 Nanoparticles

NPs were chosen as antigen carrier in this project. Therefore, this section gives a short overview of this topic.

The field of pharmaceutical nanoscience, which has grown considerably over the last 40 years, consists of many technologies, e.g. liposomes, nano-emulsions, polymeric NPs, carbon nanotubes or drug nanocrystals. Those are used for different applications in the field of cancer therapy, gene therapeutics, tissue engineering or vaccination [71]. Many applications exist for nanoscience, so many definitions exist for the definition of nano-objects. The FDA published a "guidance for industry" in 2014 that defines nano-objects as materials in the nanoscale range (with at least one dimension in the size range of approximately 1 nm to 100 nm) or materials/end products outside the nanoscale range up to 1 000 nm, provided they can exhibit different chemical or physical properties, or biological effects compared to larger-scale counterparts [72].

Polymeric NPs are usually produced by bottom-up techniques (in contrast to top-down techniques, e.g. milling). Bottom-up techniques start with atoms or molecules, which are built up to form NPs by, e.g. solvent evaporation or ionic gelation. The last technique is limited to charged polymers that react with a contrarily charged molecule resulting in precipitation. Depending on the chosen experimental setup, they can be in the nano-range.

3 Materials and Methods

3.1 Materials

3.1.1 Chitosan

In this project, chitosan was used as particle forming polymer. It is derived from chitin, a natural polysaccharide which is produced in a variety of living organisms such as funghi, crab and shrimp. Chitosan is obtained via partial deacetylation under strong alkaline conditions. The substance is a random copolymer of β-1,4-N-acetyl-D-glucosamine and β-1,4-D-glucosamine [73], as shown in Figure 3-1. Chitosan is characterised by its degree of deacetylation (DDA) giving the ratio between the acetylated and the deacetylated glucosamine units.

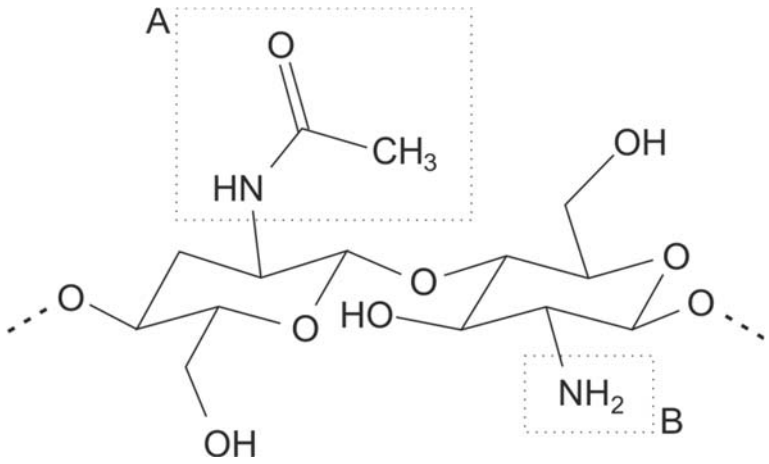

Figure 3-1. Chemical structure of chitosan depicting acetylated (A) and deacetylated (B) glucosamine units.

In addition to the DDA, the molecular weight characterises a chitosan quality. In the used chitosan products, it is indirectly described by the viscosity of a 1 % solution in 1 % acetic acid (HAc) at 20 °C. Accordingly, the viscosity is used as marker for molecular weight within this project. If the molecular weight increases, viscosity increases as well. DDA and molecular weight are only given as average values but because of chitosan's natural origin a statistical distribution is underlying these characteristics.

Chitosan has raised quite some interest as excipient in medicinal products. It is soluble in acids because of its free amino groups, resulting in positive charges. This cationic character gives the opportunity to utilise it as excipient to promote mucoadhesive

properties by binding with negative sialic residues of the mucus (confer chapter 2.1.1), to control drug release by gel formation or to enhance permeation by transiently opening tight junctions [74–76]. Chitosan is biocompatible, biodegradable, non-toxic and non-immunogenic [75]. As mentioned earlier (chapter 2.3.1) chitosan exhibits adjuvant properties if used for mucosal vaccination. All these characteristics make chitosan a very promising particle forming polymer in the field of vaccination [19].

Table 3-1 summarises the properties of the chitosan qualities used, given as mean values (confer above). In general, qualities from Heppe Medical Chitosan (Germany) exhibit narrower distributions for molecular weight compared to other suppliers. For every experiment, the used quality is denoted.

Table 3-1. Details of chitosan qualities (all obtained from Heppe Medical Chitosan, Germany) as stated by the supplier. For the quality Chitoscience 90/10 three batches were used, indicated by a-c.

Chitosan quality	*DDA, %*	*Viscosity of 1 % solution in 1 % HAc at 20 °C, mPa s*
Chitoscience 70/20	71.5	23
Chitoscience 70/50	69.1	45
Chitoscience 75/10	75.7	11
Chitoscience 80/20	78.7	23
Chitoscience 80/50	79.8	37
Chitoscience 85/10	84.4	10
Chitoscience 90/10a	90.1	15
Chitoscience 90/10b	88.1	8
Chitoscience 90/10c	87.7	14
Chitoscience 90/20	90.2	18
Chitoscience 90/200	88.5	220
Chitoscience 90/50	90.2	49
Chitoscience 95/10	96.1	15
Chitoceuticals 95/20	96.4	23

3.1.2 Sodium Carboxymethylcellulose

As second particle forming polymer sodium carboxymethylcellulose (CMC), a low viscosity carboxymethylcellulose sodium salt (Sigma-Aldrich, USA) was used. It is a semisynthetic, linear polysaccharide, shown in Figure 3-2. Its average degree of

substitution is 0.65 - 0.90 according to the product's specification. CMC qualities with a degree of substitution above 0.45 are soluble in water. In contrast to chitosan, CMC is negatively charged if dissolved in aqueous media between pH 2 and 10 [77].

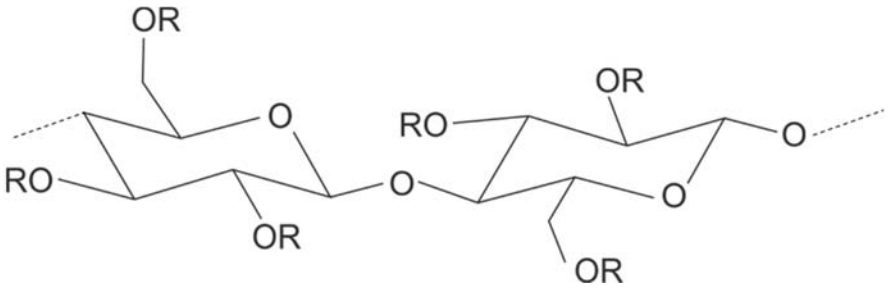

Figure 3-2. Chemical structure of CMC, R can be H or COONa.

In the pharmaceutical industry it is usually used as a thickening agent in gel formulations and oral suspensions, as a stabiliser for emulsions or as a binder for wet granulation [78]. In this project, given by its negative charge, it is used as a counterion for chitosan.

3.1.3 Sodium Deoxycholate

Sodium deoxycholate (DOC), obtained from Carl Roth, Germany, was used for some experiments as an alternative particle forming excipient, replacing CMC. With a molecular weight of 414.64 g mol^{-1}, it is a rather small molecule compared to the other particle forming excipients. The supplier states that solubility in water is 330 g L^{-1} at 15 °C. The chemical structure is depicted in Figure 3-3.

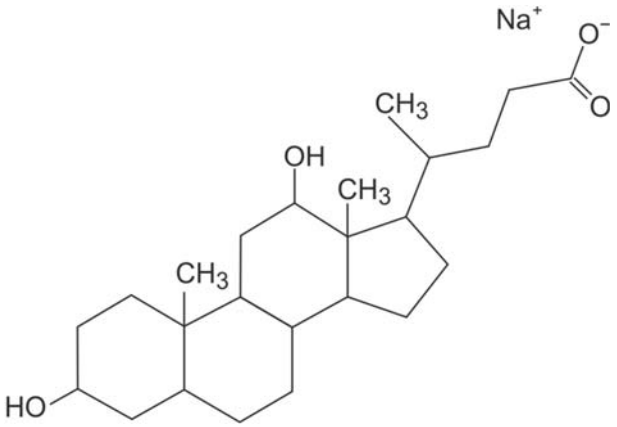

Figure 3-3. Chemical structure of DOC.

Naturally, this component can be found in the bile. It is the sodium salt of the secondary bile acid deoxycholic acid which is derived via dehydroxylation from primary bile acids by bacterial enzymes [26]. Salts from bile acids show permeation enhancing effects by temporary disruption of tight junctions. That is why they are among other things used as excipients in nasal drug delivery. Because of this permeation enhancing effect, which might facilitate particle uptake, it is of interest in the field of vaccination. Moreover, it increases the humoral immune response and it does not show toxic effects in concentrations of 0.5 - 1 % [79].

3.1.4 Ovalbumin

Ovalbumin (OVA) is the most abundant protein in egg white. It consists of 386 amino acids [80]. The glycoprotein's function has not yet been elucidated even though OVA was one of the first purified proteins [81]. During storage the native ovalbumin converts into a more stable form (S-Ovalbumin), showing an elevated degradation temperature of 86 °C compared to 78 °C for the native form. A lyophilised powder of > 98 % purity (Sigma-Aldrich, USA) with a molecular weight of 44.3 kDa and an isoelectric point (IEP) at pH 4.5 was used.

OVA is a well-established model protein for immunological studies in murine DCs [82,83]. The amino acids 257-264 (SIINFEKL) could be identified as the epitope inducing a cytotoxic T-cell response [84–86].

3.1.5 Mannitol

D-Mannitol (Figure 3-4) is a crystalline powder with a solubility of approximately 213 g L^{-1} at 20 °C, a melting point of 165 - 170 °C and a molecular weight of 182.18 g mol^{-1} [87]. Due to a very low glass transition temperature of -5 °C [88] mannitol is crystalline even after a fast drying process as spray drying. Being a non-reducing sugar alcohol makes it an attractive matrix material for microparticles. Reducing sugars in contrast could interact with free amino groups, which are present in every protein, in

a maillard reaction, potentially inactivating the protein. In the pharmaceutical industry, mannitol is used as an excipient in tablet or capsule formulations. Furthermore, it can be used as carrier in dry powder inhalation [88]. Bronchitol®, a product with mannitol as active pharmaceutical ingredient, has been on the market for the treatment of cystic fibrosis since 2012 [89]. In this work, Pearlitol® 300DC (Roquette, France) was used.

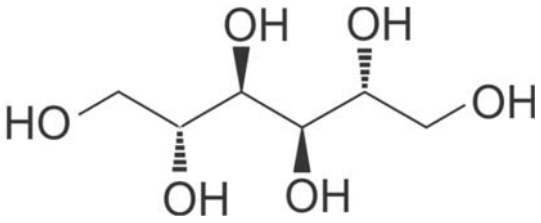

Figure 3-4. Chemical structure of D-Mannitol.

3.1.6 Fluorescein Isothiocyanate Isomer I

NPs were rendered visible for cell studies by the addition of fluorescein isothiocyanate isomer I (FITC) to chitosan. FITC, the derivative of fluorescein with an isothiocyanate group, is reactive towards amino groups which are present in many biomolecules [90]. It is a rather small molecule with a molecular weight of 389.4 g mol^{-1} [91], as shown in Figure 3-5. The used FITC had purity above 90 %, suitable for protein labelling (Sigma-Aldrich, USA).

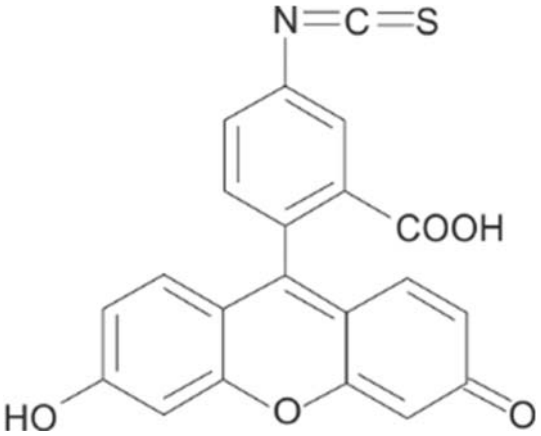

Figure 3-5. Chemical structure of FITC.

3.1.7 UDS Powder

The UDS powder (Aptar Pharma, France) was used for aerosolisation of the dry powder formulation. The UDS stands for unit dose system in this context. The UDS powder is a single dose and use device for nasal application. It is suitable for vaccination because such a formulation would only require a once at a time application. Figure 3-6 depicts the UDS powder with its inner construction.

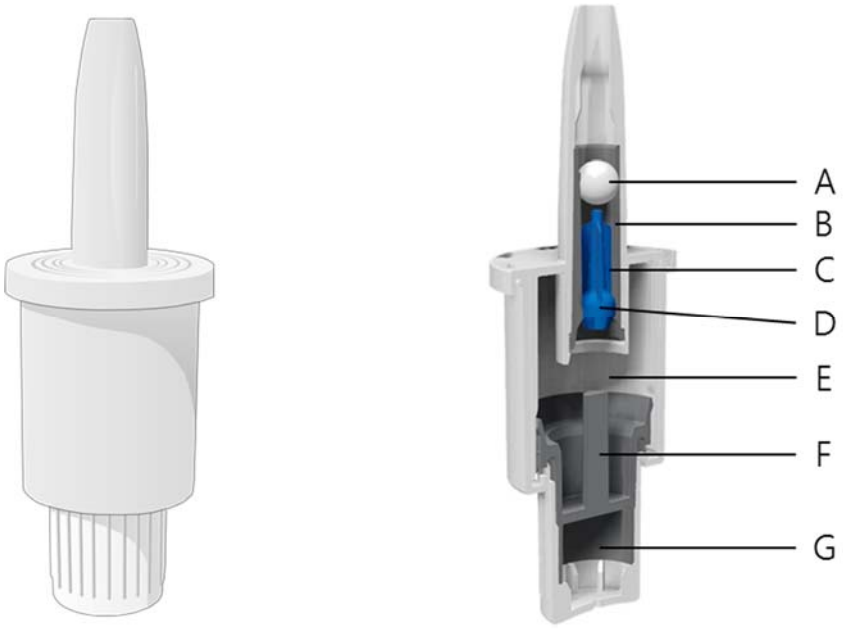

Figure 3-6. Image (left) and schematic figure of the UDS powder with inner construction (right), reprinted with permission from Aptar Pharma. Letters A to G indicate the functional components of the device.

Approximately 20 mg powder (C), exactly weighed, was filled manually into a cartridge (B) which is closed on one side with a plastic thorn (D) and on the other with a plastic ball (A). The cartridge was placed in the releasing tube prior to the final assembly using special assembly tools. The device was actuated by pressing the lower part (G) up. Doing so, the air (E) in the entire system was compressed, the bar (F) pushed up the thorn which then itself pushed up the ball. Consequently, the dose was released by expansion of the compressed air through the releasing tube.

3.2 Preparative Methods

3.2.1 Ionic Gelation

The particle formation method of NP consisting of chitosan and CMC was adapted from [92]. NPs were prepared by ionic gelation enabled by the contrarily charged particle forming polymers – chitosan positively and CMC or DOC negatively charged. The charges were obtained by dissolving the polymers in diluted HAc (chitosan) and in ultrapure water (CMC and DOC), respectively. They were left over night at room temperature to allow complete hydration. A standard concentration of 0.1 wt% for all polymers was used.

For experimental and cost-containment reasons, the batch size was typically set to 10 mL. The chitosan solution was filled into a small vessel and stirred by a magnetic stirrer (IKAMAG® RET, IKA®-Werke, Germany) at 700 rpm. The counterion solution (CMC or DOC) was added slowly by an automatic pipette (lowest dosing speed, Eppendorf Research® Pro, Eppendorf, Germany) to the chitosan solution. Directly after mixing the two solutions NPs formed resulting in a turbid suspension which was refrigerated for at least 30 min prior to further experiments.

If OVA was added as model antigen, the protein was dissolved in a concentration of 0.1 wt% in the chitosan solution shortly before NP production.

3.2.2 Processing of Nanoparticles

The particle formation by ionic gelation was not quantitative, meaning not all of the starting substances formed particles. Free chitosan, counterion (CMC or DOC) and (if added) OVA were present. If they were left in the solution, they would potentially affect the resulting NiM. Hence, prior to further processing, the nanosuspension was washed via centrifugation to eliminate any free components in the supernatant as follows:

Suspensions were separated by centrifugation according to size and density. The separation efficiency is influenced by the velocity and the radius of the centrifuge rotor.

Depending on the volume of the suspension that needs to be washed, different centrifugation schemes were utilised because the distance to the bottom of the tube (and thus the time for sedimentation) varied. All runs were performed at 15 °C because it was found that this reduced temperature helps to avoid that particles stick to each other and/or to the wall of the tube. Washing of 10 mL nanosuspension (in a 50 mL centrifuge tube) was done in one step for 60 min at 3 500 rcf. For a larger volume of 50 mL the suspension was filled in a 50 mL centrifuge tube (largest volume possible using the Eppendorf 5430R centrifuge, Eppendorf, Germany) and centrifuged in multiple steps (each 5, 10, 15, 30 or 60 min) at velocities of 1 878 - 7 197 rcf, as adapted from [92].

After each centrifugation step the supernatant was discarded into another centrifuge tube and centrifuged again. The centrifuge tube with the pellet was put on a shaker (Schüttelapparatur Typ B1, Edmund Bühler, Germany) to gently redisperse the NPs in the remaining drop of supernatant. At the end, all redispersed NP pellets were united and refilled to the desired volume with diluted HAc.

3.2.3 Fluorescence Labelling with Fluorescein Isothiocyanate Isomer I

The covalent binding of a fluorescent dye to chitosan has one benefit over an encapsulated fluorophore: The dye cannot be separated from the particle in cell experiments allowing reliable conclusions. The method to label chitosan with FITC was adapted from Colonna et al. [93]. After dissolving 100 mg chitosan in 10 mL 1 % HAc (giving a concentration of 10 mg mL^{-1}), 10 mL methanol was added to the mixture. Subsequently, 5 mL of a FITC (2 mg mL^{-1}) in methanol solution was added resulting in a ratio of chitosan to FITC of 10:1 and left to react for 3 h (constant stirring in the dark at room temperature). The binding takes places between the free amino groups of chitosan and the isothiocyanate groups of FITC, as shown in Figure 3-7.

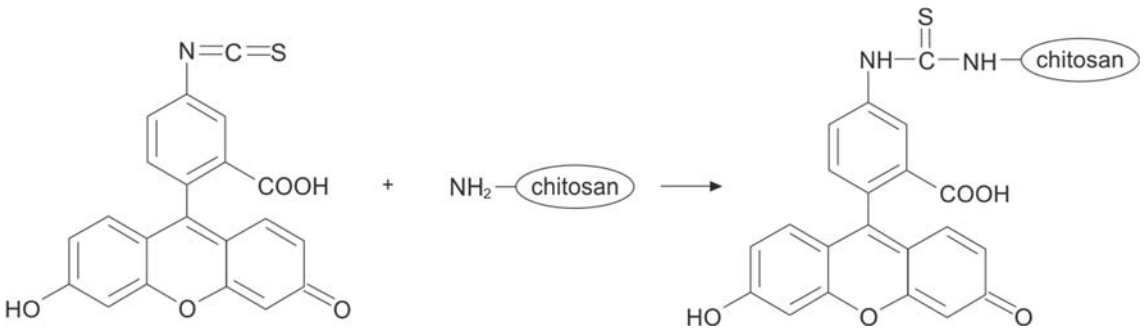

Figure 3-7. Reaction mechanism between FITC and chitosan.

After 3 h, the labelled polymer was precipitated with 1 M NaOH (above pH 10). The precipitated polymer was washed by centrifugation with methanol/water (75:25) to remove free FITC molecules. Centrifugation for 5 min at 7 197 rcf and 25 °C was repeated until no more colouring had been detected in the supernatant. The washed FITC-chitosan was dissolved in 1 % HAc and dialysed in the dark (room temperature) against water for 3 d to remove any remaining FITC. For this, a dialysis tube with a molecular weight cut off of 3.5 - 5 kDa (Spectra/Por® Float-A-Lyzer® G2, Spectrum, Netherlands) was used. Finally, to allow storage, the FITC-chitosan was freeze-dried (ALPHA 1-4 with LDC-1M, Martin Christ Gefriertrocknungsanlagen, Germany). When the FITC-chitosan was used for particle preparation, the initial weight was increased by 5 % to account for the added FITC.

3.2.4 Spray Drying

Microparticles were formed via spray drying. This technique is suitable, if large amounts of solvent must be dried. It is widely used in the food industry, for example to spray dry milk [94], as well as in the pharmaceutical industry, where microparticles are produced for numerous purposes. Spray dried powders are used in dry powder inhalation, as excipients in tablets or for transdermal dosage forms [94,95]. They usually consist of hollow spheres, however, depending on substance characteristics many different morphologies, e.g. indented particles, can prevail [95]. Spray drying is a very fast drying method. The fluid is atomised in small droplets which are mixed with a drying gas, usually air [96]. The smaller the droplets, the faster the drying because of increased

surface and increased vapour pressure due to a stronger curvature, leading to a lower boiling point allowing faster drying [94].

Figure 3-8 depicts the Mini Spray Dryer B-290 (Büchi Labortechnik, Switzerland) used in this study. The spray drying process can be separated into three process steps: (1) atomisation, (2) drying and (3) separation.

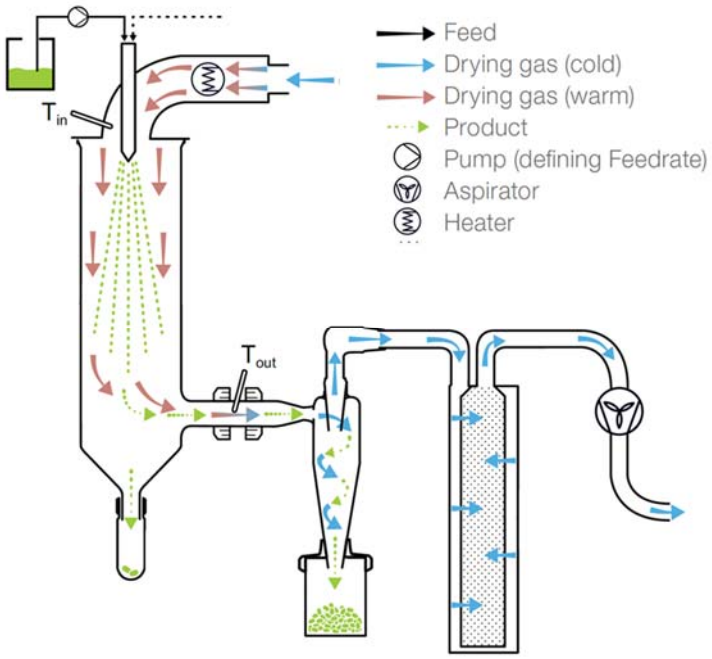

Figure 3-8. Schematic image of Mini Spray Dryer B-290 from Büchi Labortechnik, reprinted with permission from Büchi.

The Mini Spray dryer B-290 works with co-current flow: drying gas is led in feed direction. (1) The feed was atomised by either a two-fluid or an ultrasonic nozzle, shown in Figure 3-9.

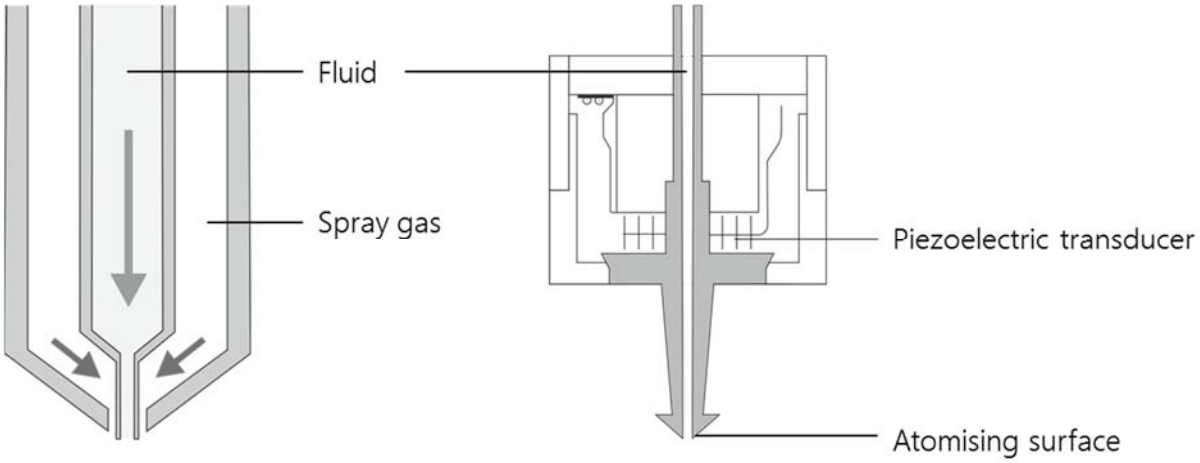

Figure 3-9. Schematic images of two-fluid (left) and ultrasonic nozzle (right) that were utilised in combination with the Mini Spray Dryer B-290

The two-fluid nozzle consists of two telescoped concentric pipes where the feed is delivered through the inner and the spray gas through the outer pipe. These two components collide outside the nozzle which reduces sticking tendencies. The droplet size is controlled by the diameter of the inner concentric pipe, by the feed rate and the spray gas flow and by characteristics of the liquid, such as viscosity and concentration. The ultrasonic nozzle generates droplets by high frequent vibration at the atomising surface [94,97]. Ceramic piezoelectric transducers convert high frequency (60 kHz) electrical energy from an external power generator into mechanical energy (vibration) at the atomising surface, breaking up the liquid feed into single droplets. The power output at the nozzle can be varied between 1 - 15 W to match the feed and the feed rate in particular. The mist is slower than that coming from a two-fluid nozzle. Droplet size generated by this nozzle is governed by the power on the atomising surface, the feed rate and by liquid characteristics. If water is dispersed, the mean volumetric diameter typically is 50 µm, the underlying distribution follows a logarithmic normal distribution [97].

(2) The second step is drying; this step is mostly dependent on the inlet temperature and the flow rate of the drying gas. This step takes less than a second. For that reason spray drying is a very mild drying technique as the product does not need to withstand high temperatures for a long time. The maximal temperature the product is exposed to in the co-current procedure is the outlet temperature measured at the transition

between drying chamber and cyclone. The product does not need to endure the inlet temperature because of the evaporation cold which shields it.

(3) The cyclone separates the dried powder particles from the air stream based on inertial forces. Particles that cannot be entrapped in the cyclone are separated from the airstream via a filter (those particles cannot be utilised; the filter only has the purpose of cleaning the air stream).

Only aqueous dispersions were spray dried in this work, hence the B-290 was operated in the open cycle mode (air was used for operation of the spray dryer, in the closed mode an inert gas would be used enabling spray drying of explosive liquids, e.g. ethanol). The standard spray drying parameters are summarised in Table 3-2.

Table 3-2. Standard spray drying parameters for two-fluid and ultrasonic nozzle.

Nozzle type	Two-fluid nozzle	Ultrasonic nozzle
Volume flow	35 m^3 h^{-1}	20 m^3 h^{-1}
Spray gas flow	473 L h^{-1}	Only needed for cooling of the nozzle
Inlet temperature	80 °C	110 °C
Outlet temperature	< 40 °C	< 40 °C
Feed rate	Adjusted to reach desired outlet temperature (10 - 15 %)	
Nozzle diameter	1.5 mm	-
Power output at nozzle	-	1 W

3.3 Design of Experiments

In order to maximise what can be learned from conducted experiments an experimental design was used. By varying several factors simultaneously, the number of required experiments for a given problem can be kept relatively small. The influencing factors can be identified by applying mathematical models. They can then be used to optimise or even to predict the results of future experiments.

In this thesis a central composite centre faced design was chosen to identify significant factors in spray drying utilising the ultrasonic nozzle. The design contained three factors at three levels including five centre points. The design of experiments (DoE) was generated using Modde Software (Version 10.1.1, Umetrics, Sweden) and resulted in 19

experiments. For model fitting only significant factors were considered while all others were excluded. This was performed individually for each response.

The model can be described by four factors, namely R2 (model fit), Q2 (estimation of future prediction precision), model validity (a test of diverse model problems) and reproducibility (variation between replicates) [98].

3.4 Analytical Methods

3.4.1 Determination of Molecular Weight

One of two main characteristics of chitosan's quality is its molecular weight. To gain more information about the molecular weight distribution size exclusion chromatography (SEC) experiments were performed.

3.4.1.1 Size Exclusion Chromatography

SEC is a liquid chromatographic separation method. In contrast to e.g. HPLC it does not separate substances according to their chemical reactivity but only by their molecular weight. Higher molecular weight substances are eluted earlier in comparison to those of lower molecular weight because they are less entrapped in the porous column material. Any interaction between the sample and the column material must be avoided if the aim is determining molecular weight or, more precisely, the hydrodynamic volume. The hydrodynamic volume can be derived from a calibration with linear polymer standards (e.g. pullulan) by means of the retention time. The hydrodynamic volume corresponds well with the molecular weight in case of a linear molecule. The estimated molecular weight of a branched polymer or one that interacts with the column material is likely to be underestimated when using this method (hydrodynamic volume smaller than molecular weight). The opposite case (hydrodynamic volume larger than molecular weight) might occur if a molecule generates a strong hydration shell resulting in a

shorter column retention time. If utilising a MALS detector the molar mass can be determined directly because the scattered light corresponds to the molecular weight.

Experiments were performed with a PL-GPC 50 Plus (Polymer Laboratories, USA). The system contains an integrated degasser and a differential refractive index detector (Polymer Laboratories, Varian Inc., USA). Additionally, a MALS detector (Mini DAWN Tristar, Wyatt) was utilised for the determination of molar mass, assuming a refractive index increment of 0.185 mL g^{-1} for chitosan (taken from [99]). For the separation by size, a PL aquagel OH Guard 8 µm precolumn followed by a PL aquagel OH 40 8 µm column and one PL aquagel OH 30 8 µm column (all Agilent Technologies, USA) in series were used. Samples (3 mg mL^{-1} dissolved in 1 % HAc) were eluted with a mixture of 0.25 M $NaNO_3$ und 0.01 M NaH_2PO_4 in water (pH 2.3) at a flow rate of 1.0 mg mL^{-1} and the column temperature was kept at 35 °C. Pullulan calibration was used to determine the hydrodynamic volume of the samples. Those values were compared to molecular weight obtained from MALS results.

3.4.2 Determination of Degree of Deacetylation

In addition to the molecular weight, the DDA is a crucial characteristic of chitosan. It was determined for selected chitosan qualities to gain a better understanding of the particle formation process.

3.4.2.1 ^{1}H-Nuclear Magnetic Resonance Spectroscopy

Nuclear Magnetic Resonance Spectroscopy (NMR) relies on the absorption of nuclear magnetic resonance in a high frequency range of 60 - 600 MHz enabling the determination of the chemical structure. The phenomenon can be observed for a few atoms, such as ^{1}H. ^{1}H nuclei can exhibit different spin conditions (+½, -½) corresponding to different energy levels. If an external magnetic field is applied the protons align and take spin conditions at different energy levels. By application of external energy (radio radiation), the nuclei on the lower energy level (number of nuclei

on this level slightly higher than nuclei on the higher energy level if no energy is applied) will absorb energy and will be lifted to the higher energy level. NMR detects this absorption and plots it against the magnetic field strength. Depending on the environment (solvent, nearby atoms) of a ^{1}H nucleus different signals (chemical shift) can be detected because the applied magnetic field is partially blocked. Those shifts are measured against a standard (usually deuterated sodium trimethylsilyl propionate, TSP) and are given in ppm [100]. All samples must be dissolved in deuterated solvents because protons present could lead to interferences.

^{1}H-NMR was utilised in this project to assess the DDA of chitosan. Experiments were performed by modifying the method of Lavertu et al. [101] to determine chitosan's DDA. Samples were dissolved in 2 % CD_3COOD (Carl Roth, Germany) to a concentration of 5 mg mL^{-1}. Measurements were performed with a BRUKER Avance III 300 MHz spectrometer (Bruker Corporation, USA) at 80 °C.

Chemical shifts of samples are related to the external standard TSP and given as ppm downfield from TSP. The DDA was determined using Equation (3-1), taken from [101].

$$DDA = \frac{H -_1 D}{H -_1 D + \frac{H - Ac}{3}} \times 100\ \% \qquad (3\text{-}1)$$

The variables used ($H\text{-}_1D$ and $H\text{-}Ac$ from the deacetylated and acetylated glucosamine units, respectively) are depicted in Figure 3-10.

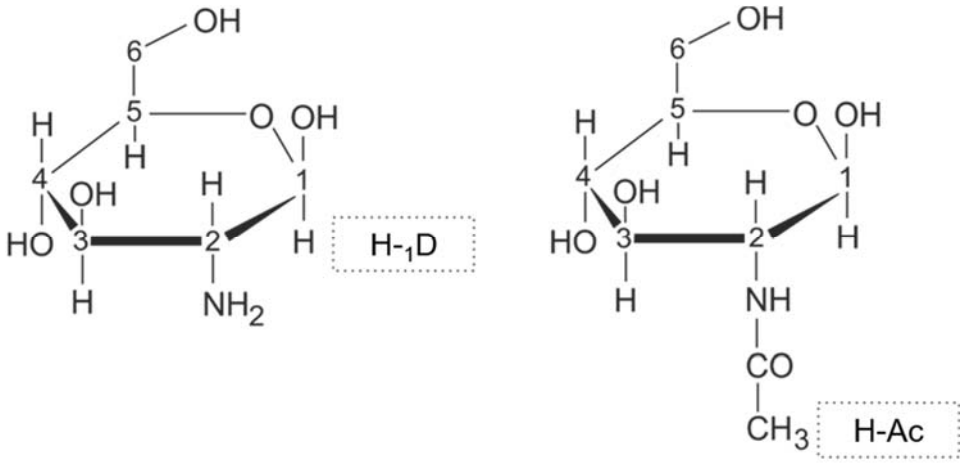

Figure 3-10. Positions of protons in chitosan monomers used for determination of DDA, adapted from [101].

3.4.3 Particle Size Determination

Particles cannot be described by only providing their diameter without specifying the method applied for determination. Most particle size measurement methods simplify particles to spheres while making different further assumptions (for example, about density). Hence, diameters measured are dependent on the technique and known input parameters. Particles can be equivalent to a sphere with the same weight, volume, length or aerodynamic behaviour.

Depending on particle size, different sizing techniques have been utilised for determination in this study. NPs were characterised by dynamic light scattering (DLS), giving an intensity-based particle diameter (z-average). Microparticles were measured with laser light diffraction resulting in a volume-based particle diameter.

3.4.3.1 Dynamic Light Scattering

Particles in the nanometre range usually do not undergo sedimentation but only Brownian motion. This random movement can be measured via dynamic light scattering, also known as photon correlation spectroscopy. Particles are illuminated with a laser and intensity fluctuations of the scattered light are subsequently measured [102]. The Stokes-Einstein-equation (Equation (3-2), taken from [103]) defines the relationship between Brownian motion and particle size. D_h stands for the hydrodynamic diameter, D_t for the translational diffusion coefficient, k_B for the Boltzmann's constant, T for temperature and η for dynamic viscosity, respectively.

$$D_h = \frac{k_B \times T}{3\pi \times \eta \times D_t} \qquad (3\text{-}2)$$

This formula implies that small particles or particles in an environment with low viscosity move faster than large particles or particles in an environment with high viscosity. Hence, the knowledge of a sample's viscosity at a given temperature is crucial for size determination. Particle size determined by DLS is usually given as z-average which is the normalised intensity weighted mean hydrodynamic size of measured particles. It is

derived from cumulants analysis of the measured correlation curve coming from a single particle size and a single exponential fit is applied to the autocorrelation function giving D_t. The deviation of the correlation function from this autocorrelation function is used for determination of the polydispersity index (PDI) [104]. It can vary between 0 and 1, 0 standing for a single particle size and 1 for widely distributed particle sizes. From the correlation function the intensity-based distribution can be calculated.

Viscosity and corresponding temperature were determined with the SV-10 Vibro-Viscometer (A&D Company, Japan) and the values utilised for subsequent DLS measurements. For those, the Zetasizer ZS Nano (Malvern Instruments, United Kingdom, UK) was used. Nanosuspensions were filled undiluted into disposable polystyrene cuvettes, placed in the Zetasizer and equilibrated for 2 min. The measurement consisted of three consecutive runs without a delay in between. Each run consisted of approximately 10 - 15 single measurements (exact number was determined automatically by the software). The laser emits light with a wavelength of 633 nm, the scattered light is detected at an angle of 173° (backscatter detection). This comprises advantages over a detection at 90°, for example, the option to measure higher concentration and the reduction of multiple light scattering (scattered light from one particle is subsequently scattered by another particle) [102]. Depending on the turbidity of the sample, the laser is more or less attenuated to avoid detector overload which is adapted by the Zetasizer automatically.

3.4.3.2 Laser Diffraction

Laser diffraction is a widely used technique as it allows evaluation of particle size in a very broad size range from 0.1 µm to several millimetres. The sample is exposed to laser light and based upon the angle and intensity of diffracted light the particle size (volume-based equivalent diameter) is determined based upon the Fraunhofer or the Mie theory. The Fraunhofer theory is especially advantageous because no additional optical parameters (e.g. refraction index) are needed for the analysis. The inflected light

is detected in an almost forward angle. Particle size is negatively correlated with diffraction angle [105]. Other phenomena such as absorption or reflection of light are not taken into account (in contrast to data evaluation according to the Mie theory).

For experiments within this work the laser diffraction sensor HELOS® (Sympatec, Germany) was used in combination with the Windox® 5 software (Sympatec, Germany) applying the Fraunhofer enhanced equation for data evaluation. Particles above 1 µm can be analysed using this equation. The helium neon laser emits light at a wavelength of 632 nm. Depending on the particle size different lenses, R2-R5, with measuring ranges from 0.25 - 87.5 µm to 0.5 - 875 µm, respectively, were used. Measurements were performed in triplicate. Two different dispersion modules were applied, the RODOS® dry dispersion module for size determination of powders and the SPRAYER® module (both Sympatec, Germany) for size determination of powders emitted from UDS powder device.

Using the RODOS® module the samples, which were fed manually, were dispersed via pressurised air. Particles below 10 µm were measured with a pressure of 3 bar while larger particles were measured with a dispersion pressure of 0.5 bar to prevent particle breakage while still ensuring efficient dispersion (determined experimentally). Measurements started at an optical concentration above 0.5 %.

To assess the dispersing power of the UDS powder, the SPRAYER® module was utilised. The actuation force was set to 60 N (automatic actuation), the distance to the measuring zone was set to 10 cm and a spray angle of 60° (mimicking the angle in which a nasal spray is usually applied *in vivo*) was used. Measurements started at an optical concentration above 0.5 % and particle size distributions were measured every 10 ms. For data extraction, a time point with steady optical concentration was chosen.

Cumulative frequency (Q3) and probability density function (q3*), representing the first derivative of the cumulative frequency, were plotted. Characteristic values of the particle size distribution x_{50}, x_{10} and x_{90}, corresponding to the median, the 10 % and the 90 % quantile were used for calculation of the span, Equation (3-3).

$$span = \frac{x_{90} - x_{10}}{x_{50}} \quad (3\text{-}3)$$

This value is especially useful for describing the distribution width when particle sizes are not normally distributed.

3.4.3.3 Scanning Electron Microscopy

Scanning electron microscopy (SEM) pictures were taken to visualise obtained microparticles and especially particle surface. In comparison to optical microscopy it allows a higher resolution suitable for particles in a low µm-range achieving magnifications up to 100 000-fold. A bundled electron beam is accelerated and directed onto the sample surface. Depending on the interactions between the sample and the electrons, different signals can be detected, including the emission of secondary electrons. Those can be received by a detector and used for the creation of an image after scanning a previously defined area of the sample surface [106].

Analysis of non-conductive samples, such as mannitol, often leads to build up of electrostatic charge. To be able to analyse those samples, their surface is covered with an electrically conductive layer. For this purpose the samples are fixed onto carbon stickers and sputtered with a Bal-Tec SCP 050 Sputter Coater (Leica Instruments, Germany) for 65 s to generate a thin gold layer on them. SEM pictures were taken with a Zeiss Ultra 55 Plus (Carl Zeiss, Germany) at a working voltage of 2 kV; signals were recorded from secondary electrons by an SE-2 detector.

3.4.4 Determination of Zeta Potential

The assessment of zeta potential (ZP) is especially important for samples that are solely stabilised by electrostatic charge (in comparison to sterically stabilised suspensions). By means of the ZP, the stability of such samples can be estimated. Suspensions with a ZP above +30 mV or below -30 mV are expected to be stable [107]. NPs produced in this

study were stabilised electrostatically. Hence, the ZP of the produced nanosuspensions and the redispersed NiM was evaluated.

As depicted in Figure 3-11 the ZP is the potential measured at the slipping plane. It must not be confused with the surface or the Stern potential, which is the potential at the margin of the first layer adhered to a particle. An electrical double layer exists around every particle [102].

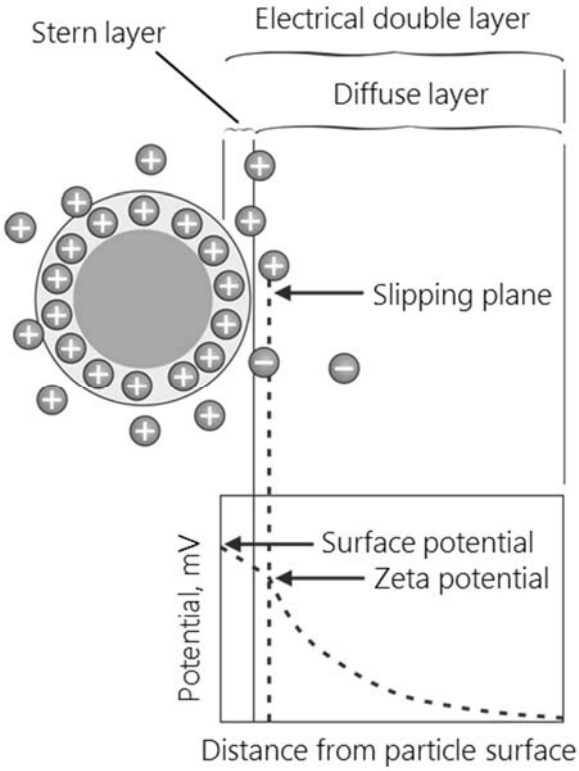

Figure 3-11. Distribution of potential around a charged particle, adapted from [102].

3.4.4.1 Laser Doppler Velocimetry

The ZP can be calculated from the electrophoretic mobility of a nanosuspension. It can be obtained by performing an electrophoresis experiment and determine the particles' velocity (proportional to measured fluctuation intensity of scattered light) by Laser Doppler Velocimetry. The ZP can be calculated from the electrophoretic mobility using the Henry equation (Equation (3-4), taken from [102]).

$$U_E = \frac{2\varepsilon \times \zeta \times f(ka)}{3\eta} \qquad (3\text{-}4)$$

ζ stands for the ZP, U_E represents the electrophoretic mobility, ε the dielectric constant and η the viscosity. For $f(ka)$, which denotes the Henry's function, two values are usually used as approximations: either 1.5 or 1.0. If measurement is performed in aqueous media with moderate electrolyte concentration $f(ka)$ is assumed to be 1.5, referred to as Smoluchowski approximation. The value of 1.0 is used for very small particles (below 200 nm) measured in a non-aqueous environment [102].

For the experiments performed within this work, the Zetasizer ZS Nano (Malvern Instruments, UK) in combination with folded capillary cells (Malvern Instruments, UK) was used. A potential is applied to the electrodes at both ends of the cell, thus charged particles move towards the electrode with opposite charge. Moving particles scatter light which is detected at an angle of 17° and combined with the reference beam. This fluctuating signal can be correlated to the speed of the particles [102]. ZP measurements were performed with a diluted nanosuspension in a ratio of nanosuspension to ultrapure water of 1:1 exhibiting conductivity below 1 mS cm^{-1}. Consequently, the viscosity of water has been used for the calculations, confer Equation (3-4). Measurements were started after an equilibration time of 60 s at a temperature of 25 °C. The measurement consisted of three runs without a delay in between; ten single measurements were performed in each run.

3.4.5 Characterisation of Interaction between Chitosan and CMC

Particle formation by ionic gelation is a spontaneous self-assembly of used substances. Hence, it is desirable to employ techniques that allow an understanding of particle formation and differences in particle formation depending on the excipients.

3.4.5.1 Isothermal Titration Calorimetry

Isothermal titration calorimetry (ITC) is a calorimetric technique that can be used to study interactions between molecules exploiting the fact that every reaction either

absorbs or releases energy. Traditionally, this technique is used to study interactions between a macromolecule (e.g. a protein) and a small ligand.

The experimental setup (Figure 3-12) consists of two cells (sample and reference) in an adiabatic jacket. Both cells are kept at exactly the same temperature. A syringe is inserted in the sample cell.

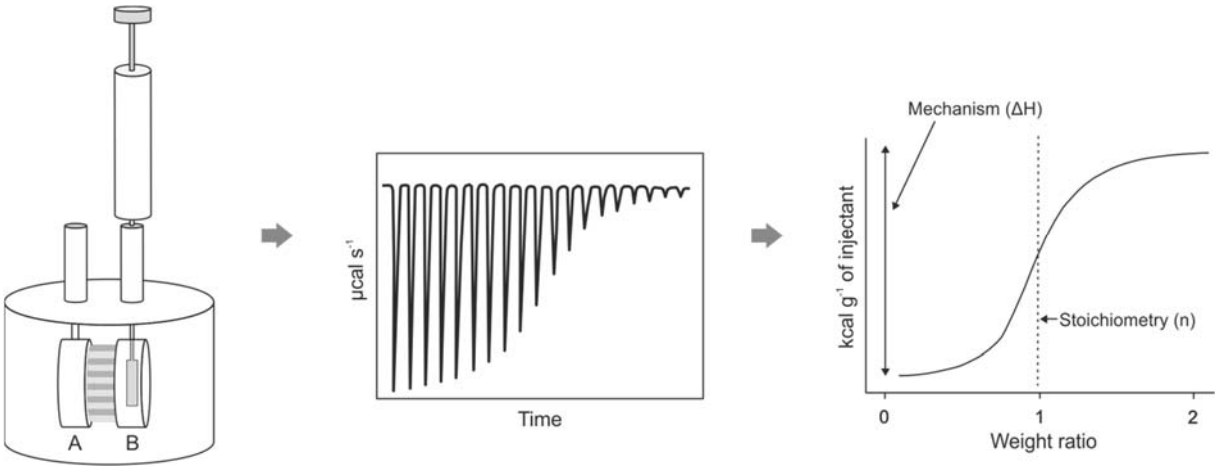

Figure 3-12. Images show the ITC experimental setup. The picture on the left shows the reference (A) and the sample cell with the syringe (B). The cells are placed in an adiabatic jacket allowing to work at isothermal conditions. Peltier elements between the cells measure heat differences after each titration step. The picture in the middle shows exemplary raw data for an exothermic reaction, each injection is represented by a peak. The picture on the right gives an exemplary result curve indicating the reaction's stoichiometry and enthalpy.

If a reaction takes place, the resulting energy change between the sample and the reference cell will be measured indirectly as the differential power applied to bring the two cells to the same temperature again [108]. Exothermic events thus result in negative and endothermic events in positive values for applied differential power. A great advantage of ITC is that it is a label-free technique so that the interactions can be studied between unmodified substances. Labelling of a substance might change its reactivity and hence the measured differential power.

Both, sample and reference cell, consist of an inert material, such as hastelloy or gold. If aqueous solvents are used, the reference cell is filled with ultrapure water. It is absolutely necessary to have the exact same solvent in sample cell and syringe to avoid large signals superposing the examined reaction by buffer mismatch. To ensure efficient

mixing, the syringe that serves simultaneously as stirrer is spirally formed. The concentration in the sample cell is usually lower than the concentration in the syringe because only low volumes are applied in each step. One titration step consists of approximately 1 - 25 µL [109], depending on the size of the sample cell. Generally, it can be said, the more titration steps have been performed, the weaker the reaction because more and more material already reacted. At some point the reaction is complete and instead of binding between the substances only dilution effects can be recognised. Data that can be gained from ITC experiments includes information about the interaction potential of two substances, the stoichiometry of a reaction and thermodynamic data as enthalpy and entropy which are decisive for a reaction to happen spontaneously. This is the case if the change in Gibb's energy G is negative. Equation (3-5) gives the influencing parameters on the Gibb's energy: The enthalpy H, the temperature T and the entropy S.

$$\Delta G = \Delta H - T \times \Delta S \qquad (3\text{-}5)$$

Two different ITC devices were utilised in this study, namely the MicroCal VP-ITC and the MicroCal PEAQ-ITC (both Malvern Instruments, UK). Both instruments have coin-shaped cells consisting of hastelloy. They can be operated at temperatures between 2 °C and 80 °C. Experiments were performed at 25 °C. The MicroCal VP-ITC has a cell volume of 1.4 mL and a syringe volume of 300 µL. A standard experiment consists of 35 injections with a spacing of 200 s. The injection volume was set to 8 µL (added over the course of 16 s), except for the first and the last injection with a volume of 1 µL. Those two data points are not included in the final evaluation. The first injection is used to prime the syringe for the first injection that is evaluated. Moreover, a stirring speed of 307 rpm has been used. Data evaluation was performed with the Origin Software (Malvern Instruments, UK). The MicroCal PEAQ-ITC has a cell volume of 200 µL and a syringe volume of 40 µL. A standard experiment here consists of 19 injections (spacing of 150 s) with an injection volume of 2 µL (added over the course of 4 s) each. A priming injection that is not included in final evaluation is done as well with a volume of 0.5 µL.

Stirring speed was set to 750 rpm. Data was evaluated with MicroCal PEAQ-ITC analysis software (Malvern Instruments, UK).

3.4.6 Determination of Protein Content

Proteins can be quantified by different techniques, such as fluorescent, spectroscopic or colorimetric methods. Fluorescent methods are based on self-fluorescence of amino acids, mostly of tryptophan which can be excited at 280 nm and subsequently emits light at 320 - 350 nm. Spectroscopic methods measure the tryptophan's absorption at 280 nm or the absorption of peptide bonds at 205 nm. While fluorescent and spectroscopic methods in general have the advantage of keeping the protein in its natural state, colorimetric methods allow a higher sensitivity as they are based on chemical reactions but concurrently are destructive. Nowadays, colorimetric methods are widely used [109]. Many different colorimetric assays can be applied; most of them can be obtained commercially. Usually they are either based on protein-dye binding or protein-copper chelation reactions. Depending on the sample and the accompanying substances (e.g. buffer salts), the best suited assay should be chosen [110]. In this study, the Pierce™ BCA Protein Assay Kit and the Micro BCA™ Protein Assay Kit (both Thermo Fisher Scientific, USA) with linear measuring ranges of 20 - 20 000 µg mL^{-1} and 0.5 - 20 µg mL^{-1}, respectively, were used. This assay is an example for protein-copper chelation reactions, as depicted in Figure 3-13. It was first developed by Smith et al. in 1985 [111]. Advantages of the bicinchoninic acid (BCA) assay include its linear response curve, an incubation time of 30 min (making time difference while pipetting samples into a 96 well micro test plate negligible compared to e.g. incubation of 5 min for a Bradford assay) and its compatibility with up to 5 % detergents [110].

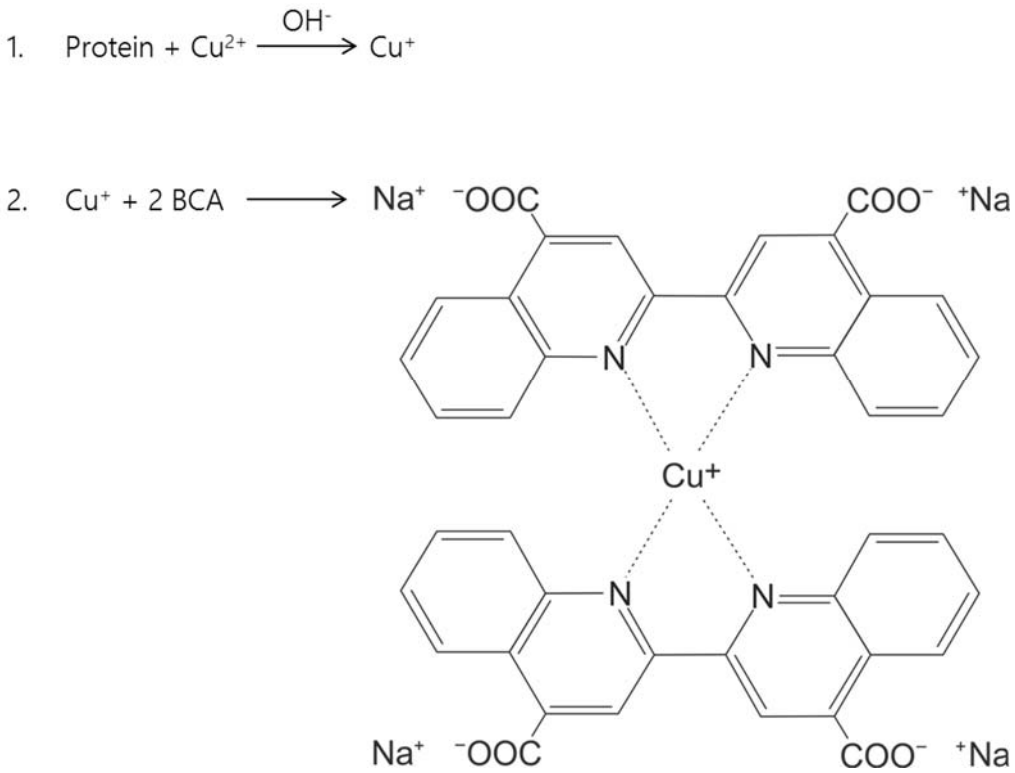

Figure 3-13. Reaction mechanism for the BCA assay in alkaline medium, adopted from [110].

This assay is a good choice for experiments in this study among the many available because it does not detect free amino groups but relies on the reducing capacity of a protein leading to a colour change from green to purple. An assay depending on free amino groups might give false positive results because chitosan exhibits free amino groups that could react in such an assay as well.

Determination of protein loading was performed indirectly by measuring the protein concentration in the supernatant after centrifugation of the NPs and precipitation of chitosan with NaOH. Subsequent dilution with 10x phosphate buffered saline (PBS) was intended to bring the samples' pH to 7.4. This way prepared samples were pipetted into 96 well micro test plate and freshly prepared BCA reaction mix was added. A 30 min incubation time at 37 °C was followed by a cool-down phase of another 30 min at room temperature. Afterwards the absorption values were measured with a plate reader (FLUOstar® Omega, BMG LABTECH, Germany) at a wavelength of 562 nm. Each measurement was executed in quadruplicate, results are given as mean.

The loading efficiency LE was calculated based on the non-encapsulated protein in the supernatant in comparison to the total amount of protein using Equation (3-6).

$$LE = 1 - \frac{non - encapsulated\ protein}{total\ protein} \times 100\ \% \qquad (3\text{-}6)$$

The loading capacity LC was calculated based on the non-encapsulated protein in the supernatant in comparison to the total amount of particle forming excipients using Equation (3-7).

$$LC = \frac{total\ protein - (non - encapsulated\ protein)}{total\ particle\ forming\ polymer} \times 100\ \% \qquad (3\text{-}7)$$

3.4.7 Determination of Hygroscopicity

Dynamic vapour sorption (DVS) was used to determine whether the developed NiM formulation was hygroscopic. It is a gravimetric technique, measuring the amount of solvent absorbed to and desorbed from the sample as a function of the relative vapour. Commonly, water vapour is used to adjust the relative humidity, but it is also possible to use organic solvents. DVS cannot only be used for investigation of hygroscopicity as done in this project but furthermore for, e.g. investigating polymorphism [112].

DVS measurements were performed using a DVS-Resolution (Surface Measurement Systems, UK) working at isothermal conditions (25 °C). To begin with, the sample (approximately 30 mg) was dried at a relative humidity of 0 %, and then the humidity was raised in 10 %-steps to 90 % and decreased again. The next humidity step was initiated if no significant change in mass (< 0.0005 % min^{-1}) was measured. This first cycle was followed by a second one to investigate whether irreversible events took place in the first cycle.

The hygroscopicity of the material was determined based on the weight increase of the powder at the end of the 80 % rH-step in the first cycle and classified according to the European Pharmacopoeia (Ph. Eur.).

3.4.8 Aerodynamic Characterisation

Assessing the *in vitro* aerodynamic performance of an inhalation formulation by performing an impaction analysis is a very common method. Such impaction analyses can be performed with the Next Generation Impactor (NGI, Copley Scientific, UK) which is described in the Ph. Eur. as apparatus E [113], depicted in Figure 3-14.

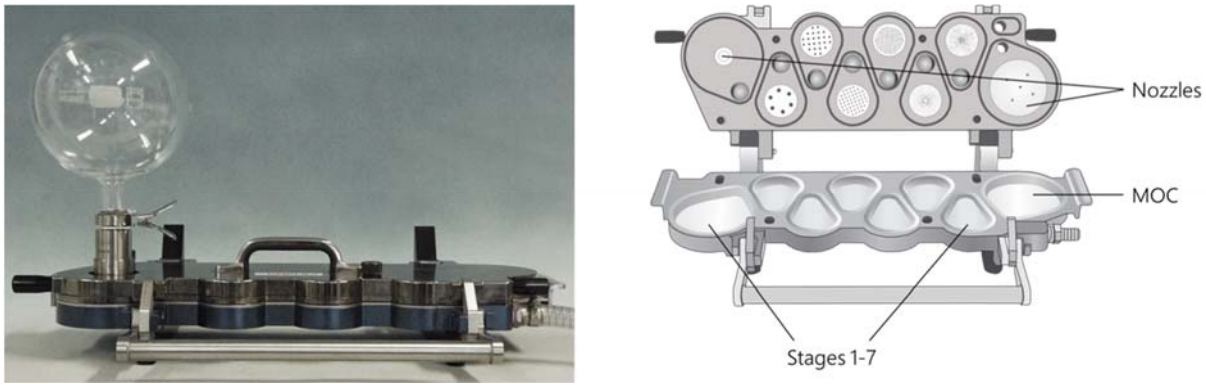

Figure 3-14. Image on the left shows the closed NGI connected to a 2 L nasal expansion chamber. On the right the scheme of the opened NGI with the seven stages and the MOC at the bottom and the respective nozzles in the lid can be seen.

The principle behind all impactors is the inertial deposition of the particles. The aerosolised formulation is sucked through the impactor or, more precisely, through a series of stages comprising nozzles with decreasing diameter. Depending on a particle's or droplet's characteristics it will deposit on a stage when it cannot follow the airstream anymore due to inertia. Any remaining particles will be deposited in the micro-orifice collector (MOC). Depending on the flow rate, the aerodynamic particle diameter cut offs can be calculated for each stage [114]. From those results the FPF, referring to the percentage of particles with an aerodynamic diameter below 5 µm, was calculated with the Copley Inhaler Testing Data Analysis Software (Copley Scientific, UK). The FPF is interesting if examining nasal products because when designing these, the aim is to obtain a predominantly nasal deposition and at the same time to keep the FPF as low as possible (due to regulatory requirements).

To assess nasal deposition, two different settings were chosen: the NGI in combination with the 2 L nasal expansion chamber (Figure 3-14, left) which is intended for nasal powders or a nasal cast (Figure 3-15), which is used without a connected NGI as well.

The nasal cast model (Boehringer Ingelheim, Germany) is based on a CT scan obtained from a male adult. It is divided into five segments: nostrils, nasal vestibule, lower turbinates, middle/upper turbinates and nasopharynx. Using the nasal cast, the regional deposition in the nose can be determined.

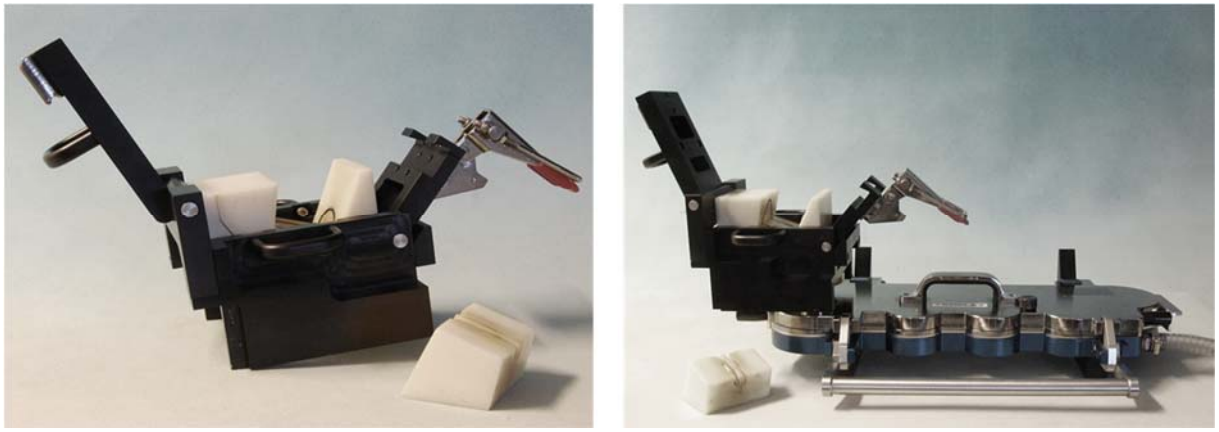

Figure 3-15. Images of opened nasal cast (left) depicting the modular setup of the nose model and nasal cast connected to the NGI (right).

All stages of the NGI and nasal expansion chamber or nasal cast were coated with a mixture of 1,2-propanediol (Sigma-Aldrich, USA) and 2-propanol (AppliChem, Germany) prior to measurement to avoid particle bouncing. For experiments with the nasal cast only, no air flow was applied. If the NGI was utilised (both in combination with nasal expansion chamber and nasal cast) it was operated at a flow rate of 15 L min^{-1}. This flow rate corresponds to the normal breathing rate of an adult. If the nasal cast was used two doses of NiM powder (40 mg) instead of one (20 mg) were applied by means of the UDS powder. After actuation(s) the flow was stopped and all components were separated and flushed with modified 10x PBS to obtain the samples. A D-mannitol assay (chapter 3.4.9) was used to quantify the obtained samples.

3.4.9 Quantification of Nano-in-Microparticles

NiM concentration in samples was quantified with a D-Mannitol Assay Kit (Abnova, Taiwan) as they mostly consist of mannitol. The assay is based upon the enzymatic reaction of mannitol dehydrogenase with D-mannitol converting it to D-fructose in the

presence of NAD being converted to NADH itself. NADH reduces a colourless molecule to a chromogen which can be detected at a wavelength of 450 nm [115].

Samples (dissolved in modified 10x PBS) were pipetted into a 96 well micro test plate. Calibration solutions were prepared with NiMs from the same batch as the samples. Both, samples and calibration solutions, were then mixed with assay buffer and the reaction mix prior to incubation for 20 min at 37 °C. Afterwards plates are left at room temperature for 30 min to allow cooling. Absorption at 450 nm was then measured with a plate reader (FLUOstar® Omega, BMG LABTECH, Germany).

3.4.10 Cell Culture

Experiments were performed at the Institute for Experimental Cancer Research at Kiel University and University Hospital of Schleswig-Holstein at Campus Kiel in Kiel, Germany.

Dendritic cells for *in vitro* uptake experiments were generated via elutriation from monocytes from healthy donors' blood monocytes following established protocols [116]. Written consent was obtained from all donors. After 5 d of differentiation culture, FITC-conjugated NiM powder was resuspended in a concentration of 2.1 mg mL^{-1} in culture medium and 100 µL of this suspension were added to the DCs (approximately 350 000 cells per mL per well). After 24 h of incubation, cells were washed with phosphate buffered saline, harvested with Accutase (Sigma-Aldrich, USA), washed again and then either analysed by flow cytometry (FACScalibur, BD, USA) or by image-cytometry (ImageStream®^{X} Mark II, Merck, Germany).

Collected flow cytometry data was analysed with WEASEL Flow Cytometry Software (Frank Battye, Australia). A first gating step was performed to identify living cells. This was done by plotting side- against forward-scattering (correspondent to granularity and size of the cells, respectively). The gate was set in a manner to exclude cell debris and particles not associated with cells. In a second step, the FITC+ cells, correspondent to

cells associated with NPs, were identified by plotting the FITC signal against the forward scatter and setting the gate by means of a negative control (cells without NP treatment).

By using image-cytometry an internalisation score (INS), the ratio of intra- to extracellular signal of interest (FITC-tagged NPs), could be determined. Following membrane counterstaining with anti CD11c-APC (BioLegend, USA) the NPs could be localised in- or outside the cell. A negative INS indicates extracellular localisation while a positive INS indicates intracellular localisation.

4 Results and Discussion

In the following chapter, the results obtained in this project are presented and discussed. First, the production and characterisation of NPs consisting of chitosan and two different counterions are described, followed by those particles' ability to be loaded with the model protein OVA. Then, the development and characterisation of a dosage form (dry powder) for those NPs are described. Towards the end, the results of first *in vitro* uptake experiments are provided.

4.1 Production and Characterisation of Nanoparticles Consisting of Chitosan and Carboxymethylcellulose

In this work the particle formation method for NP consisting of chitosan and sodium carboxymethylcellulose (CMC) as adapted from Diedrich [92] was further examined to gain a deeper understanding of the process. Schematically shown in Figure 4-1, it is based on the fact that the two polymers are contrarily charged and self-assemble as NPs upon mixing. The key part of it is a charge neutralisation of the free amino and carboxyl group. As each polymer (chitosan and CMC) has multiple free amino or carboxyl groups, respectively, this charge neutralisation takes place many times between two or more polymer strands resulting in a cross-linking of those.

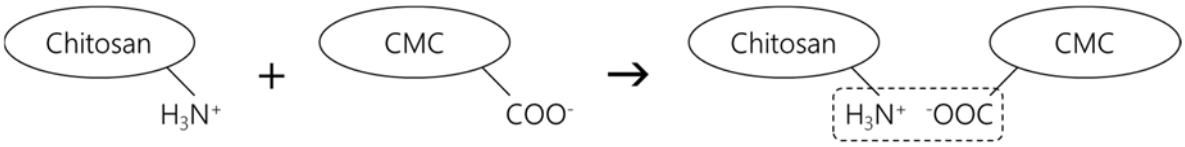

Figure 4-1. Scheme of the particle formation process between chitosan and CMC due to ionic binding between positively charged amino group and negatively charged carboxyl group.

In the following, influencing parameters on the process and their effects on the NPs have been investigated. NPs used as antigen carrier in mucosal vaccination should have a size suitable for preferential uptake in DC of at most 500 nm, as described in chapter 2.2.1.1.

Beneath the particle size, other parameters are crucial for the NPs, first of all particle stability. Moreover, the used chitosan quality, the mechanism of interaction, the addition sequence, the usage of stabilisers and the loading of a protein may have an impact on the resulting NPs and their size. Hence, those are discussed in the subsequent chapters as well.

4.1.1 Particle Stability

NPs with a ZP above +30 mV or below -30 mV are known to be stable in case that they are solely stabilised by charge and not (additionally) by steric configuration. To assess whether the stabilisation can be primarily ascribed to the electrostatic stabilisation, the ZP of obtained nanosuspensions was tested. If the nanosuspension agglomerated, when the ZP drops below +30 mV or rises above -30 mV, it can be used as stability indicator.

The measured ZP is highly dependent on the solvent used for the measurement. Hence, a dilution of the suspension might lead to a change of absolute value. On the other hand, dilution might also lead to less variance in data. Hence, in this project, an experiment to assess the effect of dilution on the absolute value and variance of ZP was performed utilising nanosuspensions that were diluted with water to different ratios. The results (Figure 4-2) indicated that a dilution of 1:2 with water should be preferred because, while resulting in almost the same absolute ZP value, the relative standard deviation (RSD) in between three performed runs was decreased substantially. This dilution has been used for all subsequently performed ZP measurements.

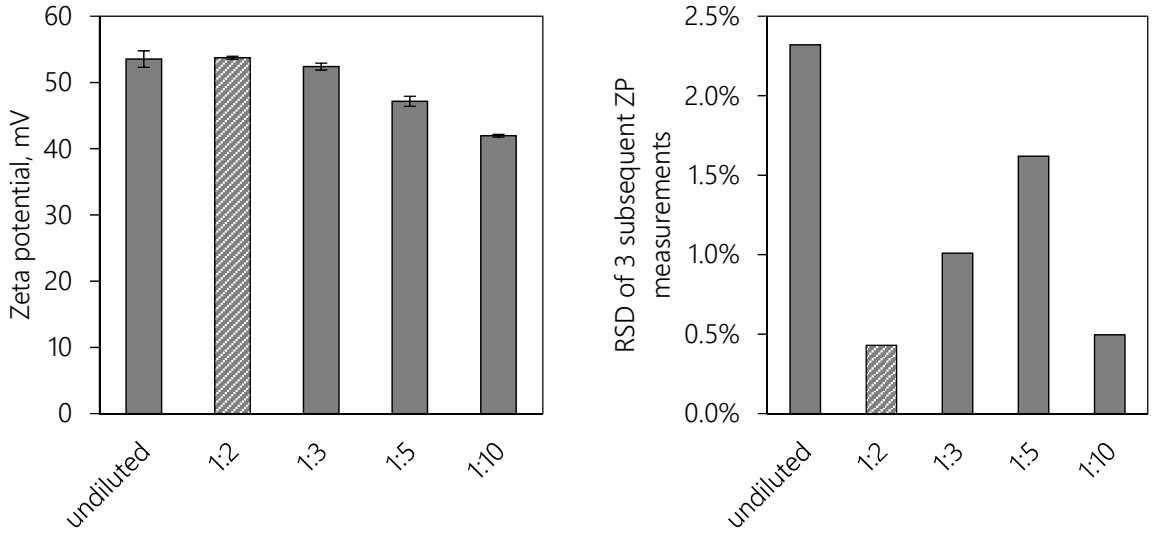

Figure 4-2. Diagram on the left shows the absolute ZP values for the different dilutions (numbers indicate the rate of dilution, n = 3, error bars = SD) while diagram on the right gives the RSD derived from the measurements.

To assess the likely stability of NPs, rising amounts (0.5 mL-steps) of a 0.1 wt% CMC solution were added to 5 mL of 0.1 wt% chitosan and the resulting ZP and size were determined for each nanosuspension. Results are depicted in Figure 4-3.

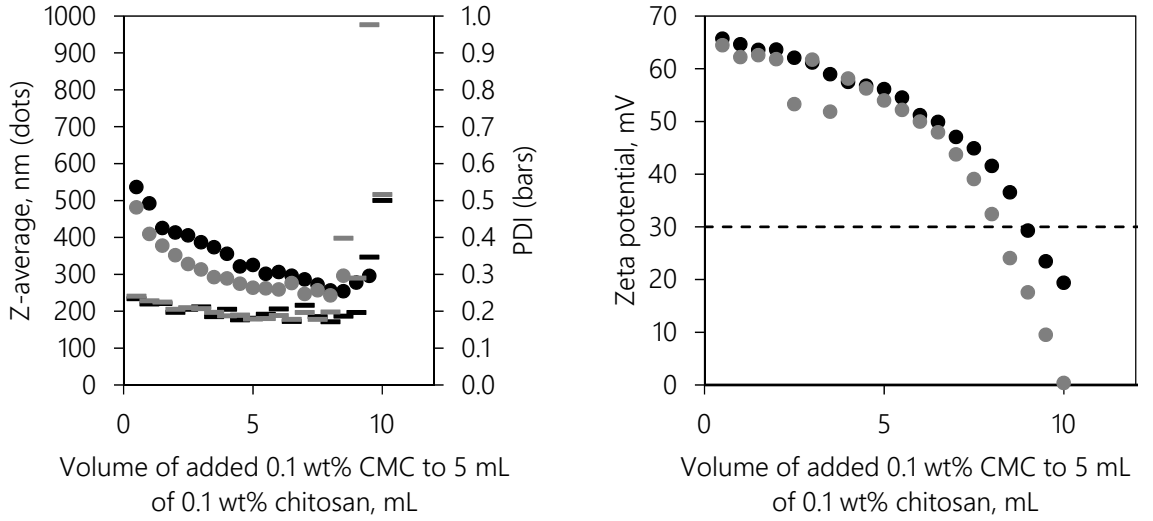

Figure 4-3. Particle size and PDI values (left) as well as corresponding ZP (right) are displayed for the experiment with chitosan 90/10c. Black circles (●) and bars (▪) correspond to the solvent 2 % HAc for chitosan, grey circles (●) and bars (▪) to 1 % HAc. The dotted line in the right diagram corresponds to aforementioned stability limit (above +30 mV) of electrostatically stabilised NPs (n = 1).

Results showed that the particle size decreased while adding more CMC and then increased drastically at some point (sizes exceeded 1 000 nm). The same was true for

the PDI values. The drastic increase in size and PDI could be observed in the reaction vessels as sedimenting agglomerates. Visual inspection moreover showed that the turbidity of the nanosuspension (confer chapter 4.1.5.3) increased with every titration step indicating more and more particle formation before sedimentation resulted in a clear supernatant. This sedimentation due to instability of the nanosuspension was at the same time as the drop of the corresponding ZP below +30 mV. Thus, it can be assumed that the NPs are foremost stabilised by charge.

An explanation for decreasing particle size when adding more CMC might be higher cross-linking between polymers that results in smaller, denser and/or more NPs. Furthermore, the influence of the acid strength becomes apparent in Figure 4-3. Particle size was slightly lower and the ZP dropped earlier below +30 mV if 1 % HAc was used. The resulting higher ZP values if the higher acid concentration of 2 % as opposed to 1 % was used were reasonable as more ions were present for electrostatic stabilisation.

In Figure 4-4 and Figure 4-5 it becomes apparent that the chitosan quality is decisive for NP formation as well. Figure 4-4 shows the resulting particle sizes and PDI values subject to the utilised chitosan quality.

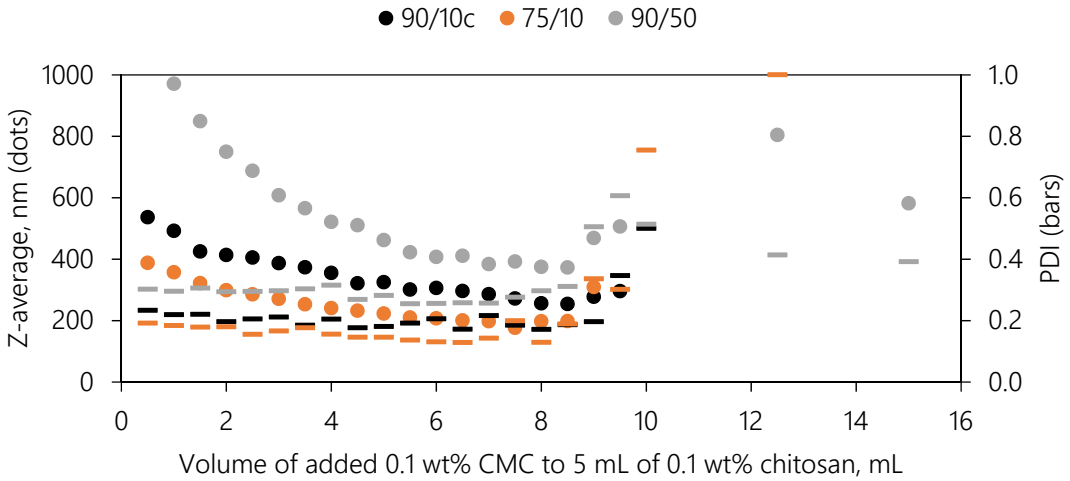

Figure 4-4. Particle sizes and PDI values for titration experiments with three different chitosan qualities (75/10, 90/10c, 90/50) (n = 1).

The particle size was positively correlated with the molecular weight of the chitosan, given here as viscosity. The different particle sizes of chitosan qualities 75/10 and 90/10c,

exhibiting the same nominal viscosity of 10 mPa s, can be explained by the varying actual viscosities reported in the certificates of analysis: 11 mPa s and 14 mPa s. This difference in viscosity accounted for the slightly different particle sizes of those two chitosan qualities (chitosan 90/10c resulting in larger particle sizes than chitosan 75/10). Chitosan 90/50 in contrast resulted in larger particles. The decrease in particle size with increasing CMC addition, however, was more pronounced. Details on the topic of particle size dependency on the chitosan quality can be found in chapter 4.1.4.

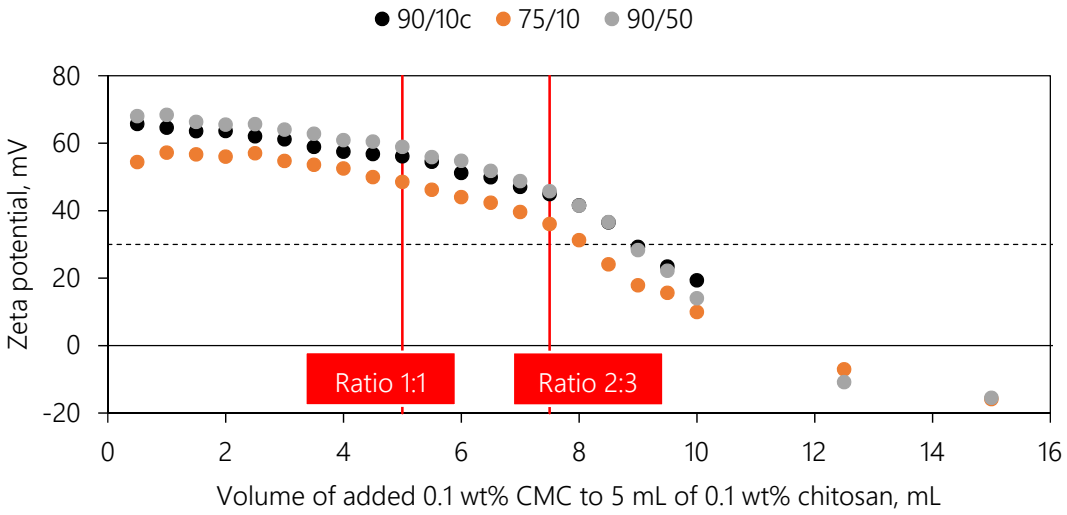

Figure 4-5. Corresponding ZP for titration experiments with three different chitosan qualities (75/10, 90/10c, 90/50). The dotted line in the right diagram corresponds to stability limit (above +30 mV) of electrostatically stabilised NPs. Red boxes indicate two stable ratios for NPs (n = 1).

The ZP results show another picture. There was no difference observable for those chitosan qualities exhibiting a similar degree of deacetylation (DDA, 90/10c and 90/50) while the chitosan with lower DDA (75/10) deviated in behaviour. This quality resulted in generally lower ZP. This led to unstable NPs at lower CMC concentrations compared to higher deacetylated qualities. The variation in size and ZP caused by the acid strength used for dissolution of chitosan prior to particle formation, which was shown for chitosan 90/10c (Figure 4-3), could be observed for the other qualities as well (data not shown). For further experiments two stable weight ratios of chitosan to CMC have been chosen: 1:1 and 2:3, as indicated in Figure 4-5. To summarise, it can be said that while

the molecular weight primarily influences the size of the particles, the DDA is crucial for particle stability.

4.1.2 Mechanism of Interaction Between Chitosan and Carboxymethylcellulose

ITC has been employed to gain a deeper understanding of the binding mechanism between chitosan and CMC during particle formation. This was done to determine whether differences observed in particle formation described in the previous chapter (4.1.1) as well as the impact on the size could be confirmed or even further confined. Compared to many other techniques, ITC holds the great advantage of working label-free. Thus, the actual particle formation process can be re-enacted and no labels alter the polymers resulting in a different particle formation. ITC works by injecting very small volumes (syringe) into a larger volume (cell). This is contrary to the standard experimental setup where two solutions in the same concentration were mixed in either equal volumes (ratio 1:1) or at least in similar dimensions (ratio 2:3). The concentrations of the excipients were adapted to fit the experimental setup of the ITC. The concentration of the polymer in the syringe (CMC) needed to be increased (0.9 wt% instead of 0.1 wt%) due to the small injected volume and to increase the concentration gradient even further the polymer in the cell (chitosan) was only dissolved to a concentration of 0.05 wt% instead of 0.1 wt%. Gradients of approximately 20 are recommended as starting conditions for ITC experiments and proved suitable for the following experiments. Those were performed with the three chitosan qualities previously discussed: 75/10, 90/10c and 90/50. Figure 4-6 delineates the resulting titration curves. Due to time constraints, the experiments could only be performed once.

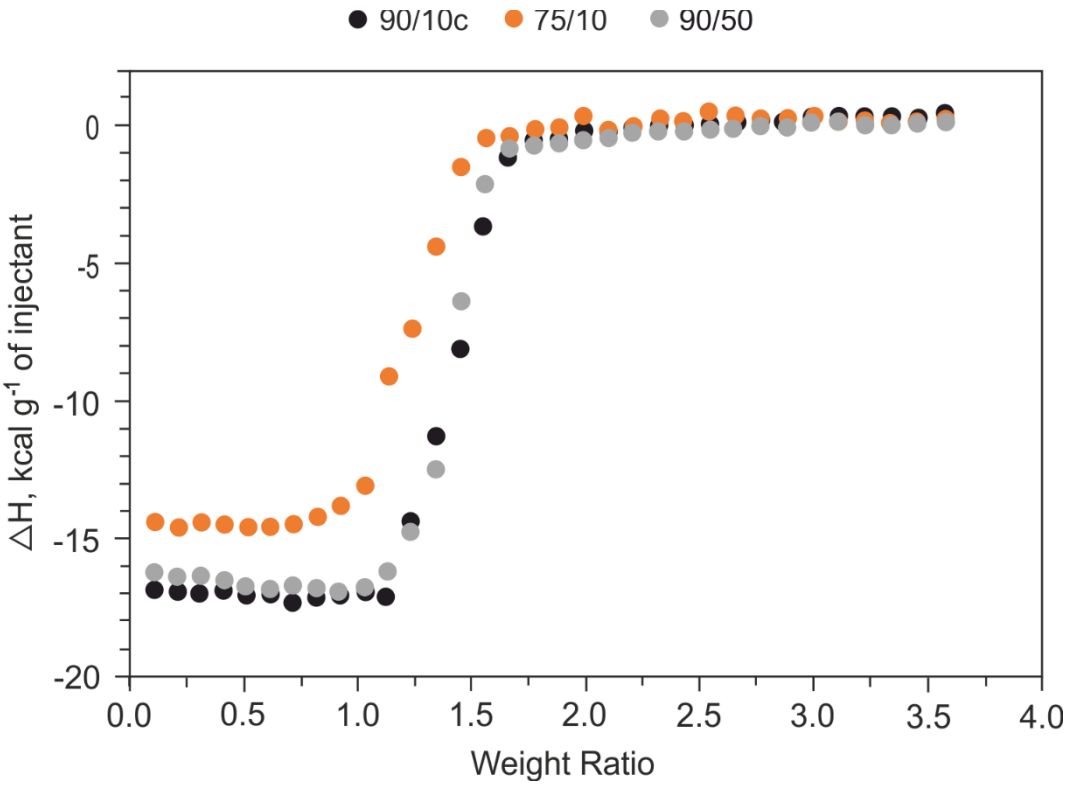

Figure 4-6. Binding curves for titration experiments with different chitosan qualities (cell) and CMC (syringe) as a function of the weight ratio between the two polymers (CMC to chitosan). The chitosan qualities showed differences in binding affinity varying the DDA and no difference varying molecular weight (n = 1).

Differences in particle forming process became obvious utilising ITC. Higher DDA led to a higher extent of chitosan reacting (curve is shifted to the right), probably leading to a higher particle yield (refer to chapter 4.1.5). Additionally, the particle formation mechanism changes, as indicated by the changed enthalpy. This was probably due to the changed amount of free amino groups available for reaction changing the cross-linking between the polymers. No influence of molecular weight on the particle forming process could be shown (curves for chitosan qualities with a DDA of 90 % look alike). By these trials the previous results (ZP values) from the particle preparation experiments could be confirmed. Higher DDA results in more (and intense) particle formation, even at small scale. No statement about expected size could be made based on the ITC experiments.

To gain further insights into the mechanisms that govern particle formation, the titration of CMC into chitosan 75/10 was repeated with the PEAQ-ITC. Here, the software not only calculated the binding curves but also created the so-called signature plot (Figure

4-7) which indicates whether a reaction is driven by change in enthalpy or by the product of entropy and temperature. While the value for the change in enthalpy can be taken directly from the experimental data, the Gibb's energy and entropy are calculated by the software. The course of a reaction is favoured if all values in the signature plot are negative [108].

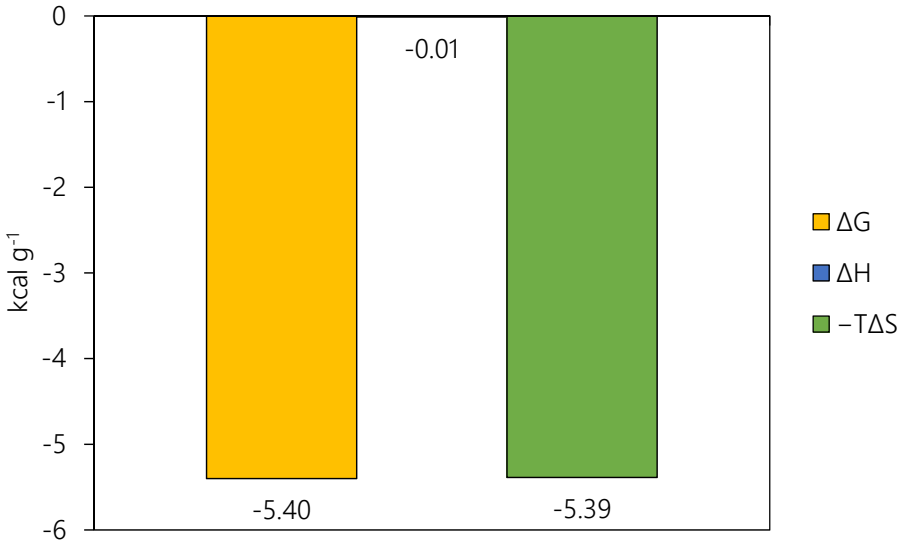

Figure 4-7. Signature plot from titration experiment with chitosan 75/10 and CMC indicating the Gibb's energy (ΔG), the enthalpy (ΔH) and the negative value of the product of temperature and entropy (-T ΔS).

The Gibb's energy is negative, thus a reaction takes place spontaneously. The binding between chitosan 75/10 and CMC is mainly driven by entropy, hence by hydrophobic interactions. Enthalpy (corresponding to hydrophilic binding) has a value of approximately zero, therefore it neither favours nor opposes the reaction [108]. This was not to be expected as the binding between chitosan and CMC is based on ionic gelation. Rather, it was expected to have a reaction dominated by hydrophilic interactions. The change in entropy might be related to the orientation change of polymers (coiled vs. straight) and hence different interaction with surrounding medium which result in large changes in entropy which are not dominated by hydrophobic interactions. Using this analysis tool of the PEAQ-ITC software allows interesting insights that would not have been obtainable by other techniques. However, for a deeper understanding of the thermodynamics further experiments (e.g. different chitosan qualities and temperatures) will be needed.

4.1.3 Addition Sequence

This subchapter examines to which extent the addition sequence (adding CMC to chitosan or vice versa) had an influence on the resulting NPs. That the addition sequence influences particle size has already been shown in a previous project [92].

The titration experiments performed within chapter 4.1.1 were repeated in an almost identical fashion, the only difference being that now chitosan was added to CMC. While the nanosuspensions obtained after adding CMC to chitosan showed an initial decrease in particle size as well as PDI and agglomeration if the corresponding ZP dropped below +30 mV (Figure 4-3), the nanosuspensions resulting from chitosan into CMC titration gave different results, shown in Figure 4-8.

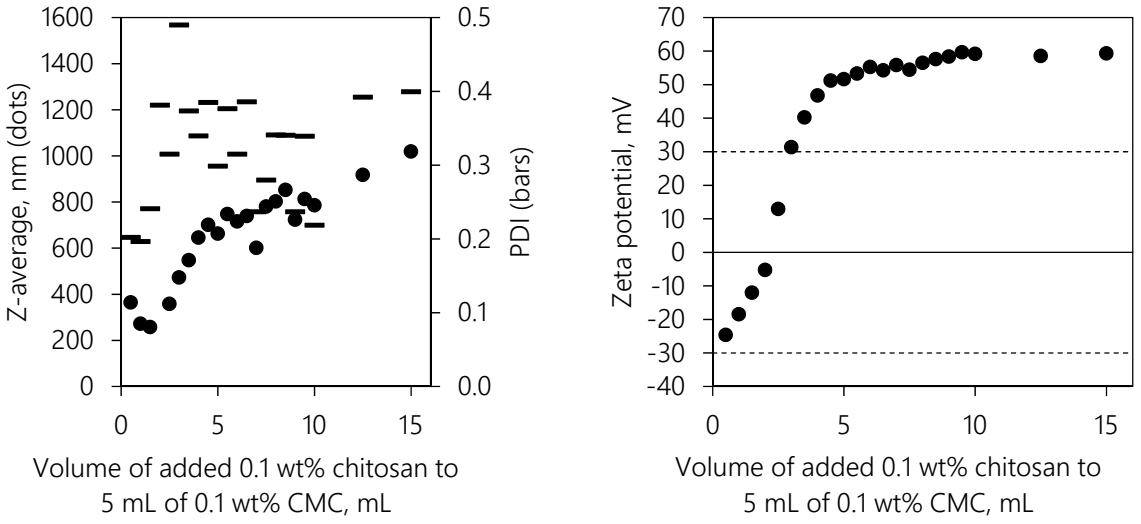

Figure 4-8. Particle size and PDI values (left) as well as corresponding ZP (right) are displayed for experiment with chitosan 90/10c. CMC was dissolved in water. The dotted lines in the right diagram correspond to stability limits (above +30 mV or below -30 mV) of electrostatically stabilised NPs (n = 1).

Negative ZP values were expected and measured for particles with only little addition of chitosan because the CMC dissolves as polyanion in water. However, the ZP was above -30 mV and rose continuously, indicating unstable NPs. All nanosuspensions that received up to 6.5 mL of chitosan formed agglomerates until the next day, even when the ZP indicated stable particles (above 3 mL addition of chitosan). This was probably due to the ZP change during particle formation resulting in unstable particles even though the final ZP indicates stable particles (above +30 mV). Measured sizes for NPs

were overall larger than in the reverse addition sequence (CMC into chitosan) and constantly increasing which was probably also a consequence of the ZP change from negative to positive. In contrast, if titrating CMC into chitosan the ZP was positive from the beginning and therefore led to overall more stable particles until ZP dropped below +30 mV.

To overcome this problem of changing ZP during particle formation, in another experiment it was tried to keep the ZP always below -30 mV. Here, the solvent for CMC was changed from water to PBS expecting particle stabilisation by keeping the ZP below -30 mV due to higher salt concentration and buffer capacity. Figure 4-9 depicts the respective results.

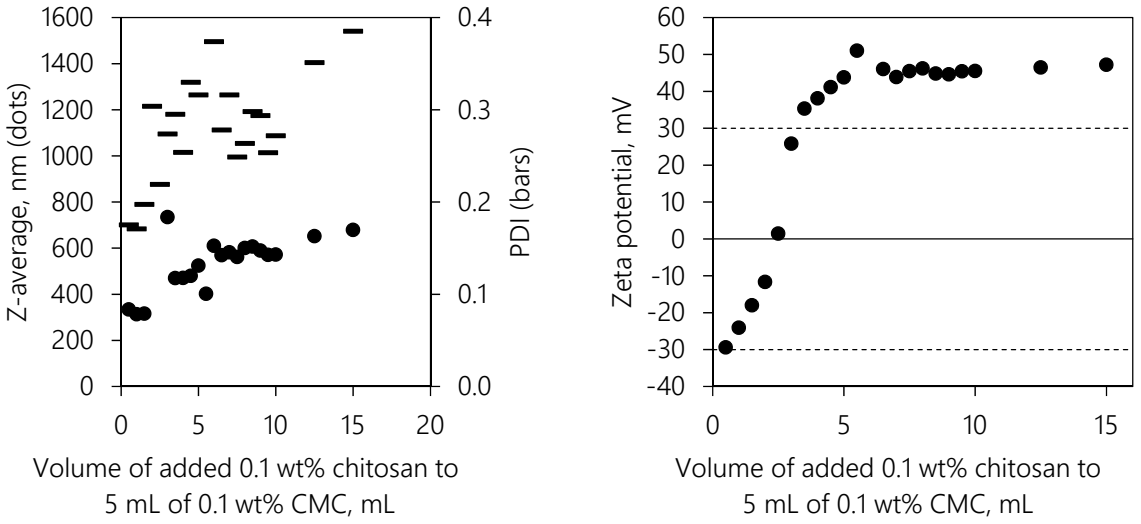

Figure 4-9. Particle size and PDI values (left) as well as corresponding ZP (right) are displayed for experiment with chitosan 90/10c. CMC was dissolved in PBS (n = 1).

The expected effect of lowering ZP by adding PBS did not materialise. Particles were overall a little more stable, showing agglomeration only for those samples with an addition of 2 - 3 mL chitosan solution. Particle sizes were a little lower if CMC was dissolved in PBS instead of water. This hints at a favourable effect of salt concentration on particle formation. Nonetheless, titrations of CMC into chitosan where CMC was dissolved in PBS were not performed within this project due to time constraints. Future projects should however keep this option in mind.

Altogether, from these experiments it can be summarised that the addition sequence influences the particle formation. If CMC was added to chitosan, resulting particles were smaller than if reversing this step. For comparison, the results for the previously selected stable ratios (1:1 and 2:3) are depicted in Table 4-1.

Table 4-1. Particle characteristics from titration experiments with chitosan 90/10c (dissolved in 2 % HAc) giving the values for ratios 1:1 and 2:3.

Ratio	*Addition sequence*	*Z-average, nm*	*PDI*	*ZP, mV*
1:1	CMC (water) added to chitosan	325.0	0.181	56.1
	Chitosan added to CMC (water)	662.7	0.298	51.6
	Chitosan added to CMC (PBS)	523.6	0.316	43.8
2:3	CMC (water) added to chitosan	271.6	0.185	44.9
	Chitosan added to CMC (water)	780.3	0.280	54.4
	Chitosan added to CMC (PBS)	561.6	0.249	45.5

The most likely explanation for this difference is the "passing" of the unstable ZP range (-30 mV to +30 mV) during particle formation introducing instability along the way. Other possible explanations include the differences in molecular weight of the participating polymers, charge density and/or orientation (linear vs. coiled polymer strands). The difference in molecular weight is unlikely because the particle formation process does not seem to be influenced by the varying molecular weight of the chitosan (further information on that topic can be found in chapter 4.1.2). The influence of the charge density cannot be distinguished because the exact charge density of the used CMC quality was not tested and the charge density of chitosan was varied. As also shown in chapter 4.1.2 the particle formation process generally is influenced by the charge density (hence, the DDA) resulting in lower enthalpy with lower DDA. Nevertheless the overall decreasing particle size if adding more CMC to chitosan is independent of the used chitosan quality. Therefore, this difference probably does not account for the differences occurring after changing the addition sequence. The influence of the orientation of the polymer cannot be assessed because no experiments were performed to determine it.

The results in this chapter showed that the addition of CMC to chitosan appears more suitable for formation of stable NPs in the desired size range. The lower particle sizes achieved by this addition sequence go along with smaller PDI values and thus, a narrower size distribution, which is also favourable. Following these results, adding CMC to chitosan was used in all successive experiments.

4.1.4 Particle Size

As the particle size is thought to be crucial for uptake in cells this chapter shows the influence of chitosan quality and chitosan to CMC ratio on the particle size. For this purpose, NPs were formed with numerous chitosan qualities in the selected stable ratios under standard experimental conditions. Particle sizes and respective PDI and ZP values obtained are shown in Table 4-2.

Adding CMC slowly (e.g. slow addition through a syringe or slow pouring from a beaker) was important for all nanosuspensions. If the CMC was added at once, particle size increased (data not shown). This increase with fast CMC addition was probably due to less time for NP formation.

Table 4-2. Particle size, PDI and ZP measured after particle formation with various chitosan qualities (n = 3, for clarity no standard deviation (SD) values were included). The chitosan qualities are ordered from top to bottom by rising viscosity.

Chitosan quality	*Ratio 1:1*			*Ratio 2:3*		
	Z-average, nm	*PDI*	*ZP, mV*	*Z-average, nm*	*PDI*	*ZP, mV*
90/10b	248.1	0.162	44.9	139.4	0.128	34.2
85/10	277.0	0.141	47.1	188.1	0.128	36.7
75/10	327.5	0.155	47.1	254.5	0.182	34.4
90/10c	351.9	0.191	51.9	252.8	0.186	41.7
90/10a	352.0	0.240	49.1	321.7	0.400	40.0
95/10	328.2	0.230	48.3	269.3	0.328	36.7
90/20	403.3	0.230	54.4	337.2	0.257	42.5
70/20	439.1	0.223	45.3	285.4	0.221	33.9
80/20	456.4	0.235	50.1	322.2	0.243	36.4
80/50	555.8	0.258	51.9	376.4	0.300	35.2
70/50	531.6	0.281	46.8	332.5	0.254	32.5
90/50	687.9	0.322	56.8	536.8	0.386	43.1
90/200	986.1	0.375	58.6	620.9	0.324	46.9

ZP values showed that all obtained nanosuspensions were stable. Generally, ZP was lower if more CMC was used in particle formation. The same tendency could be observed for size and PDI corresponding to the results from the first titration experiments (4.1.1). Size could be tuned by using different molecular weight chitosan (see Figure 4-10, chitosan qualities were ordered according to their molecular weight). The molecular weight (or as given for the chitosan qualities used: the viscosity) is positively correlated with particle size and PDI. To reach the targeted particle size of maximal 500 nm the viscosity should be kept below 50 mPa s (corresponding to an average molecular weight of approximately 150 kDa). The DDA on the other hand did not influence the particle size as much (see Figure 4-11, chitosan qualities were ordered by their DDA). Here, no trend with rising DDA could be observed. To summarise, with this production method for NPs only the molecular weight is decisive for particle size, while the DDA does not need to be considered.

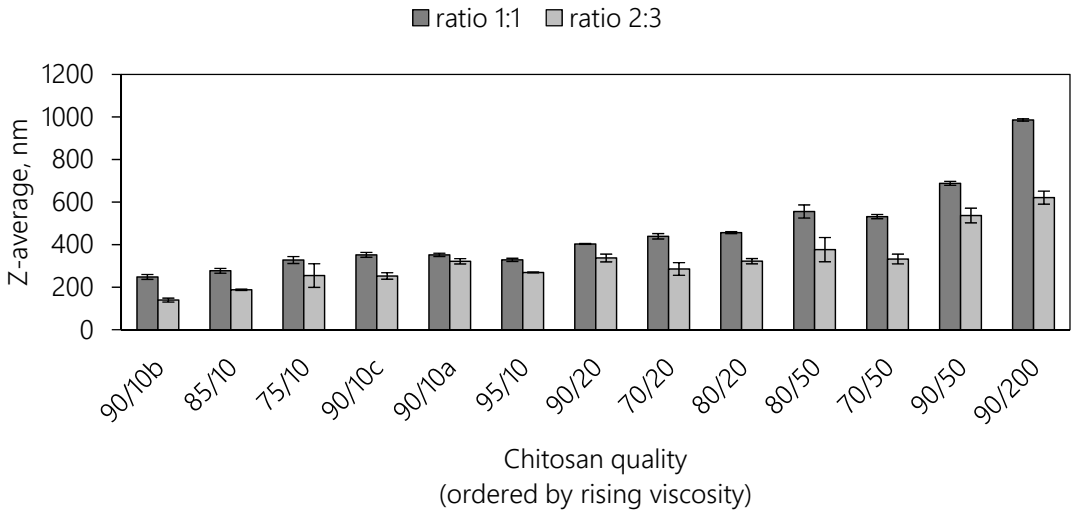

Figure 4-10. Particle sizes measured after particle formation with various chitosan qualities which are ordered by rising viscosity and CMC (n = 3, error bars = SD).

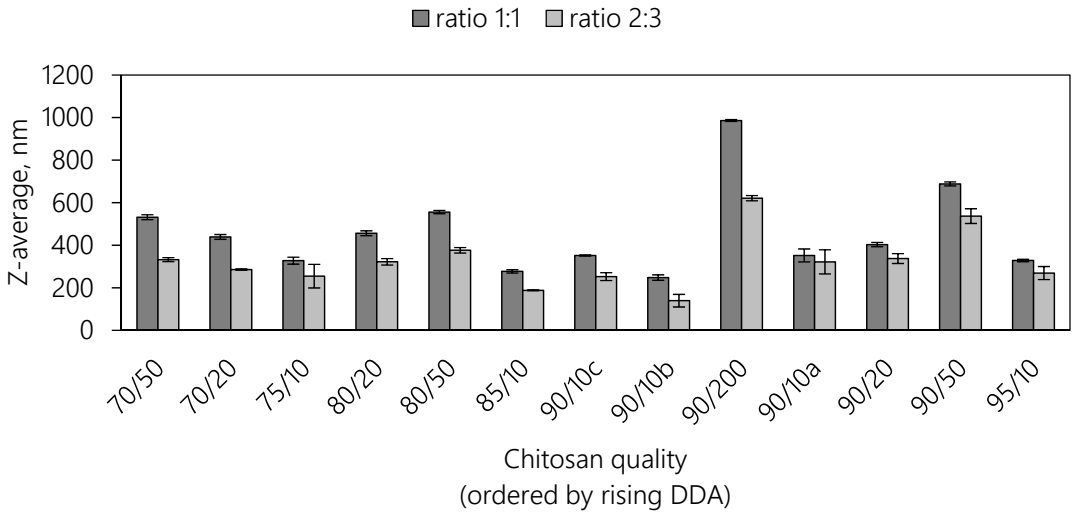

Figure 4-11. Particle sizes measured after particle formation with various chitosan qualities which are ordered by rising DDA and CMC (n = 3, error bars = SD).

4.1.5 Quantification of Nanoparticles

NPs are formed by ionic gelation in this study. Preliminary experiments showed that only a share of the particle forming excipients (chitosan and CMC) actually form NPs: If FITC-conjugated chitosan (appears yellow) is utilised for particle formation and the formed NPs were centrifuged down, the supernatant still had a yellow colour, which indicates that free chitosan is present. Thus, it is important to quantify the amount of obtained NPs to assess the impact of chitosan quality, counterion and used ratio on

particle yield and to calculate the protein to particle ratio (particle loading) if a protein is encapsulated. Another option would be to indirectly quantify the amount of NPs by quantifying the non-reacted part in the supernatant. It is, however, not only relevant to know the total particle yield but moreover the proportions of both particle forming polymers present in the NPs to further understand and optimise the particle formation process.

4.1.5.1 Ninhydrin Assay

The quantification of chitosan is challenging because it is a natural polymer exhibiting not one defined molecular weight or DDA but a distribution of both values. Furthermore, its functional groups are free amino groups which are present in proteins as well making a distinction between chitosan and protein challenging. The easiest way for quantification of a polymer is via its functional groups. Hence, within this project, it was first attempted to quantify chitosan via its free amino groups. This method however would only be suitable for quantification of chitosan in NPs produced without protein because it could not be distinguished between those two. Nonetheless, to get an idea of the amount of chitosan involved in the particle formation of placebo NPs it seems a suitable method. In literature the ninhydrin assay is mentioned as a potential method for quantification of chitosan [117–119]. Usually it is used to quantify proteins or amino acids. The reaction of ninhydrin with primary amino groups forms a purple dye, which is called Ruhemann's purple after Siegfried Ruhemann who first described it [120].

Before this assay can be used, however, it must be tested whether the DDA and molecular weight of the chitosan involved in the particle formation remain unchanged because this is crucial for the applicability of the ninhydrin assay [117]. Therefore, an experiment determining the DDA and the molecular weight before and after particle formation was conducted. Unchanged DDA and molecular weight would be taken as evidence that the assay can be applied to calculate the concentration of chitosan involved in particle formation.

For the experiment chitosan before and after particle formation was needed. For the "pre" chitosan the raw material was used. As "post" the chitosan which was present in the supernatant after NP formation was used. To obtain it, NPs with three different chitosan qualities (75/10, 90/10c and 90/50) and CMC (ratio 1:1) were produced, centrifuged and the supernatant was skimmed off. The excess chitosan in the supernatant was precipitated using NaOH. The precipitated chitosan was washed via centrifugation. Subsequently, the obtained "post" chitosan was dried for 48 h in a vacuum drier. Only if the characteristics of the "pre" and "post" chitosan stay unchanged it can be concluded that the share which formed NPs complies with the raw material. If there is any change it can be concluded indirectly which share reacted and conclusions from that include if particles preferentially form with higher or lower deacetylated and molecular weight chitosan.

The DDA was assessed by ^{1}H-NMR, examples for obtained spectra of chitosan 75/10 before and after particle formation are shown in Figure 4-12 and Figure 4-13, respectively.

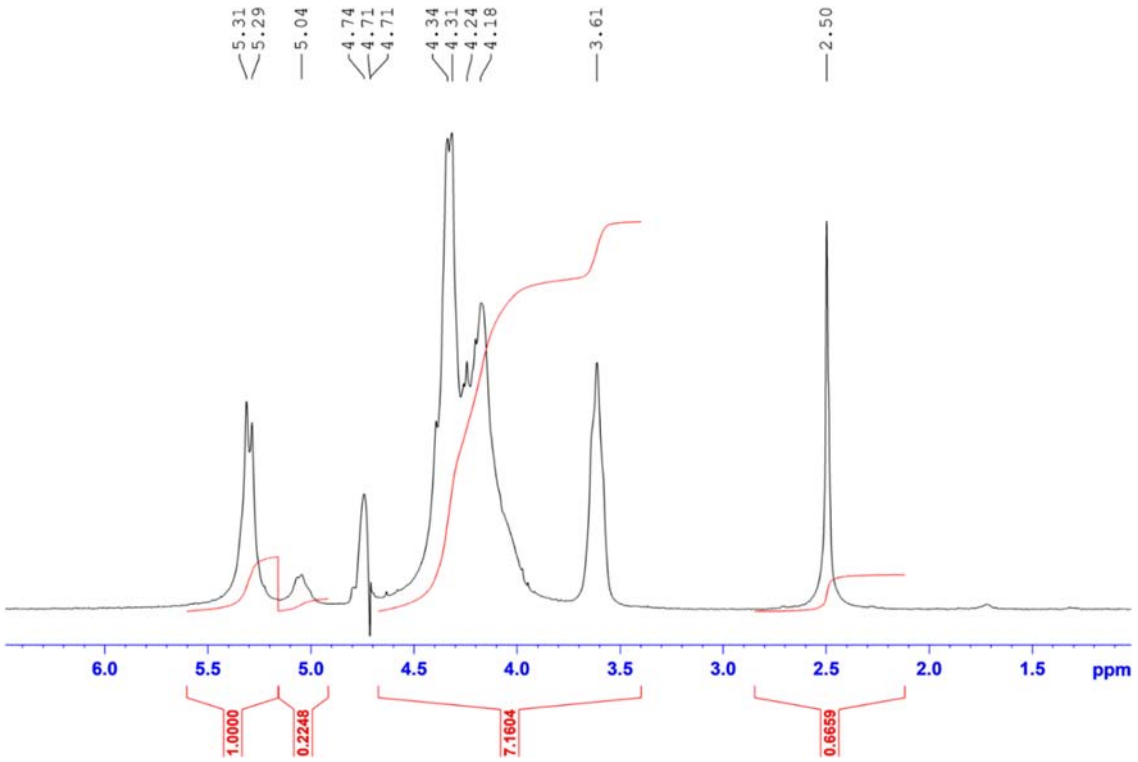

Figure 4-12. ^{1}H-NMR spectrum of chitosan 75/10 starting material with integrals of different H-Atoms. Integrals (H-$_{1}$D = 1.000 and H-Ac = 0.6659) were used to calculate the DDA.

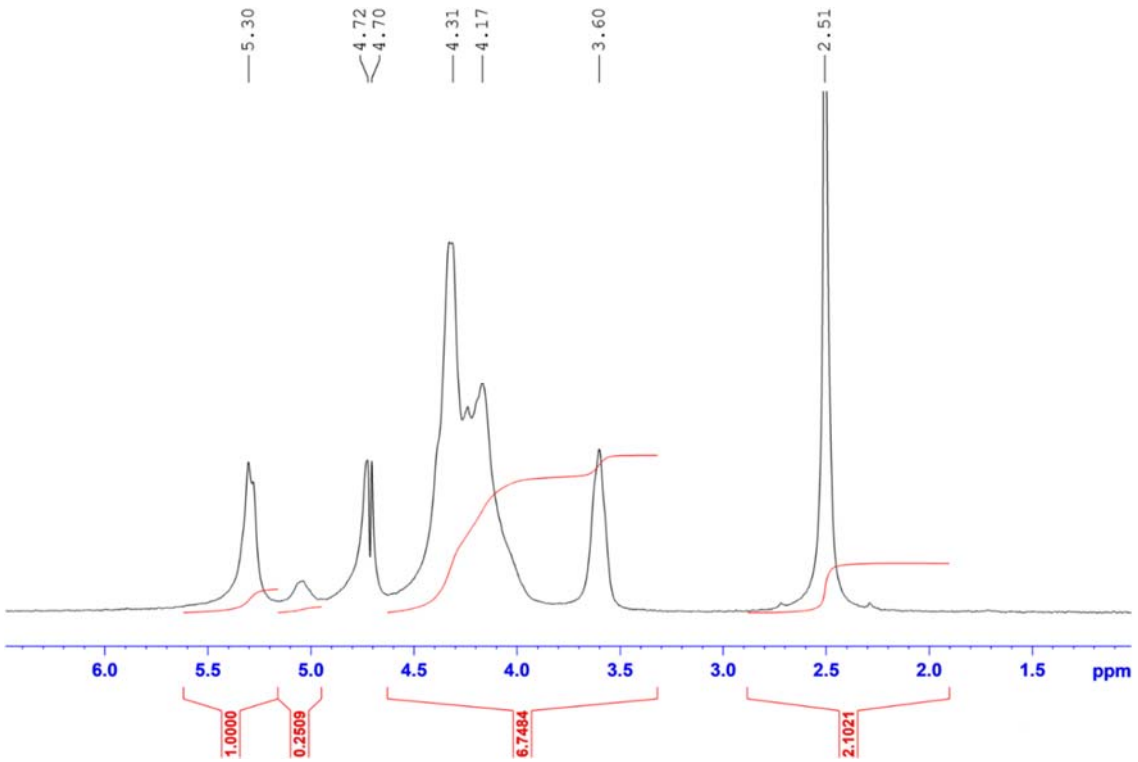

Figure 4-13. ^{1}H-NMR spectrum of chitosan 75/10 after particle formation with integrals of different H-Atoms. Integrals (H-$_1$D = 1.000 and H-Ac = 2.1021) were used to calculate the DDA.

Results for all measured samples are summarised in Table 4-3. All samples showed lower DDA values after in comparison to before particle formation.

Table 4-3. Integrals and calculated DDA for examined chitosan qualities before and after particle formation (n = 2, ± min/max, 90/10c "post" n = 1 due to experimental reasons).

Chitosan quality	*Before/after particle formation*	*Integrals*		*Calculated DDA*
		H-$_1$D	*H-Ac*	
75/10	Before	1	0.6429 ± 0.0230	82.4%
	After	1	2.4087 ± 0.3066	55.5%
90/10c	Before	1	0.2531 ± 0.0077	92.2%
	After	1	1.8388	62.0%
90/50	Before	1	0.2919 ± 0.0577	91.1%
	After	1	3.9823 ± 0.0122	43.0%

The DDA of the "post" chitosan was lower for all examined qualities. Hence, the part of the chitosan with a higher DDA reacted to form particles. The more reactive chitosan was the higher deacetylated share of the distribution probably due to the higher availability of free amino groups. This effect was independent of the absolute value of

the DDA of the “pre” chitosan. These results already show that the ninhydrin assay is not suitable for determining the amount of reacting chitosan in this NP formation method because the DDA does not stay the same which would have been a crucial prerequisite for the applicability.

However, in order to complement the determination of the DDA, the molecular weight before and after particle formation was measured as well. This addressed two questions. First, is the molecular weight after particle formation still the same as before? And second, if not is the underlying molecular weight distribution monomodal or are different fractions present that possibly disappear completely after particle formation? The same samples prepared for the determination of the DDA were used for the following experiments. SEC coupled with two different detectors was used to determine the molecular weight: a multiple angle light scattering (MALS) and an RI detector. The MALS detector does not need calibration but depending on the scattering (measured at 90°) gives the molecular weight directly. On the other hand, the RI detector must be calibrated with a standard (in our case: pullulans) and then not only gives the hydrodynamic volume, but moreover how much of the substance elutes at a given time. This becomes obvious in Figure 4-14. While the MALS detector showed different molar mass fractions, the RI detector indicated that only one fraction (retention volumes between 12 mL and 15.5 mL) corresponded to the mass of the examined chitosan. Consequently, only the MALS peak corresponding to the mass fraction was used for determination of molar mass. The other peaks probably correspond to impurities which were not further examined.

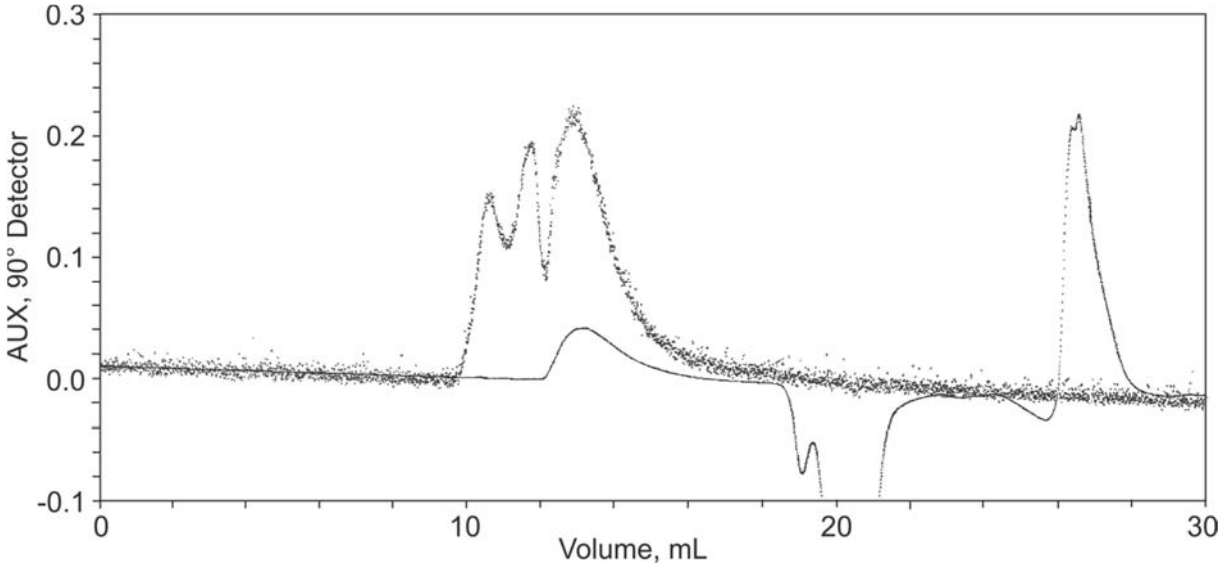

Figure 4-14. SEC chromatogram of chitosan 75/10 before particle formation. Dots indicate the scattering detection (MALS detector) at an angle of 90°, while the line depicts the mass fraction recorded by the RI detector. The MALS signal at 10.5 min and the RI signals at approximately 20 min and 26 min can be ascribed to HAc which served as solvent.

The molecular weight was either determined by taking the mean retention volume (of the complete RI peak width) and calculating the hydrodynamic volume from it or by using the scattering signals of the MALS detector for the peak corresponding to the mass fraction (RI detector). The results are given in Table 4-4. Due to time constraints, the experiments were only performed once.

Table 4-4. Molecular weight for examined chitosan qualities before and after particle formation calculated as hydrodynamic volume or molar mass (n = 1).

Chitosan quality	*Before/after particle formation*	*Hydrodynamic volume, kDa*	*Molar mass, kDa*
75/10	Before	81.4	82.3
	After	57.1	62.2
90/10c	Before	77.9	133.1
	After	60.6	71.0
90/50	Before	106.4	140.7
	After	94.2	96.5

The values for hydrodynamic volume and molar mass agree for some samples, but not for all. This is probably due to reactions with the column materials decreasing the hydrodynamic volume. Nonetheless, the overall trend is similar for both evaluation

methods: the molecular weight of “post” is lower than that of “pre” chitosan. Hence, the higher-molecular-weight-chitosan preferably reacts to particles and the lower share of the distribution remains in the supernatant. This phenomenon is, as has been seen before for the DDA, independent of the starting molecular weight. No separate fractions of molecular weight which correspond to distinguished mass fractions could be found for the examined chitosan qualities. Each sample showed one peak which simply slightly shifted to the right after in comparison to before particle formation.

Based on those experiments, the determination of DDA and molecular weight, it can be concluded that the ninhydrin assay is not suitable to calculate how much chitosan has reacted. If the amount of chitosan reacted was determined by a ninhydrin assay and would be indirectly calculated by determining the concentration in the supernatant, it would be overestimated (lower DDA than the reference would give less intensive colouring in the assay).

4.1.5.2 Anthrone Assay

The previous chapter showed that a usable assay must work independently of chitosan’s DDA and molecular weight. The anthrone assay is based on the detection of glucose units, deeming it a suitable technique to quantify chitosan regardless of DDA and molecular weight (because always the same mass instead of the same molar concentration was used). Moreover, the CMC could be quantified by this assay as well as it consists of glucose units as well.

By incubation with concentrated sulphuric acid the polymers are split into monomers which further react to form a furfural. This forms a colourant with anthrone. The underlying reaction is shown exemplarily for glucose (1) in Figure 4-15.

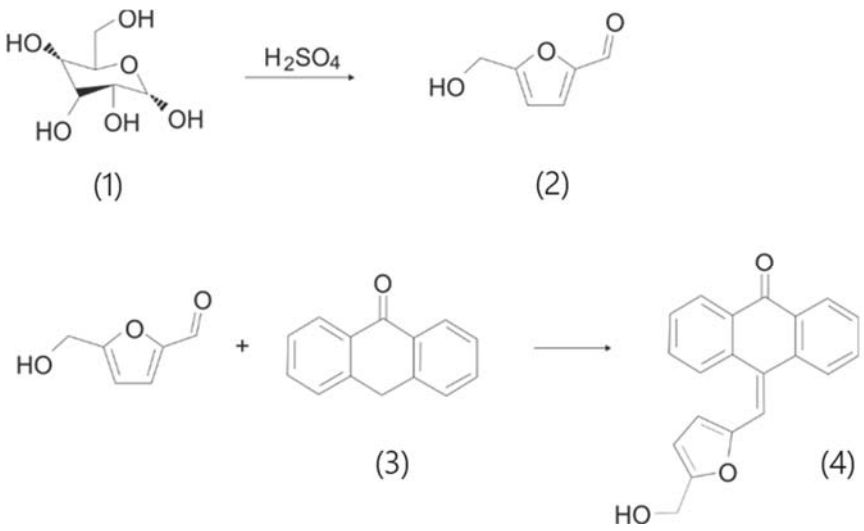

Figure 4-15. Reaction steps of the anthrone assay with glucose, taken from [121].

By incubating glucose with concentrated sulphuric acid it reacts to hydroxymethylfurfuraldehyde (2). This product condenses with anthrone (3) if heated and forms 10-[5-hydroxymethylfuranyl)methylene]-anthrone (4) which gives a green colour [121].

Different experimental conditions were tried for chitosan quantification. In the following the final conditions are briefly described: Chitosan was dissolved in 1 % HAc and mixed with the same volume anthrone reagent (0.75 g anthrone (Merck, Germany) dissolved in a mixture of 17 mL water and 83 mL of 96 % sulphuric acid (Carl Roth, Germany)) in a 2 mL-microtube and incubated for 30 min in boiling water. After cooling with ice, the absorption at 578 nm was measured. Resulting calibration curves with chitosan qualities 75/10, 90/20 and 90/50 are shown in Figure 4-16.

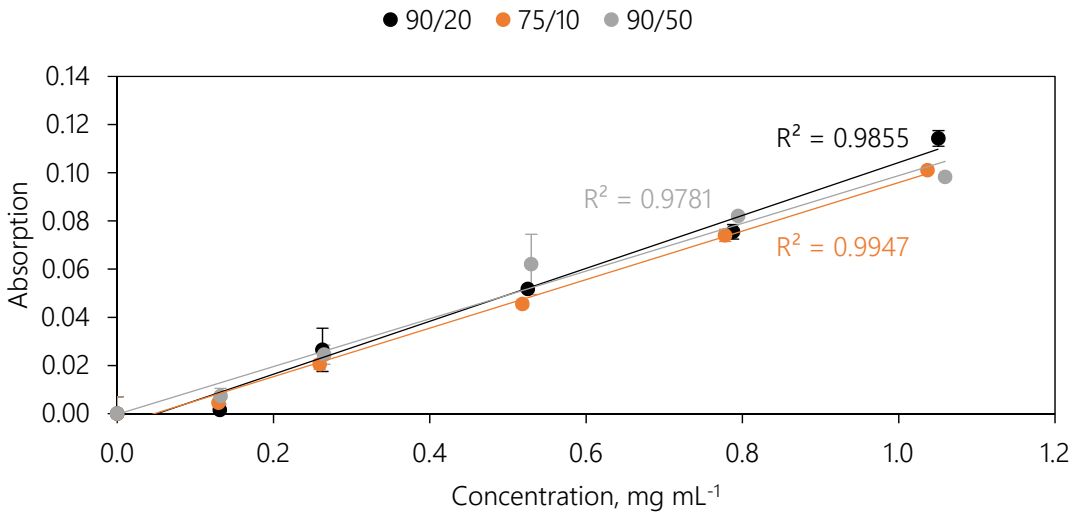

Figure 4-16. Calibration curves of chitosan qualities exhibiting various DDA values and viscosities with the anthrone assay (n = 2, error bars = min/max).

The green colour resulting with chitosan was very light as indicated by rather low absorption values between 0.005 and 0.1 for concentrations from 0.1 mg mL^{-1} to 1 mg mL^{-1}, which might possibly be due to incomplete degradation of chitosan. Nonetheless, the coefficients of correlation were satisfactory with values of 0.9855, 0.9947 and 0.9781 for chitosan qualities 75/10, 90/20 and 90/50, respectively.

As mentioned before, CMC consists of glucose units as well. Therefore, it was tried whether it reacts in the anthrone assay as well before a further look was taken into the applicability of this assay for NP/excipient quantification. The sample preparation was similar, with the exceptions that water was used as solvent for CMC and the incubation time was reduced to 7 min. The resulting calibration curve (coefficient of determination of 0.9993) is shown in Figure 4-17. As can be seen by the absolute absorption values, the colour development was more pronounced for CMC. The anthrone assay develops different colours subject to the sample, analysing CMC gave a dark blue colour.

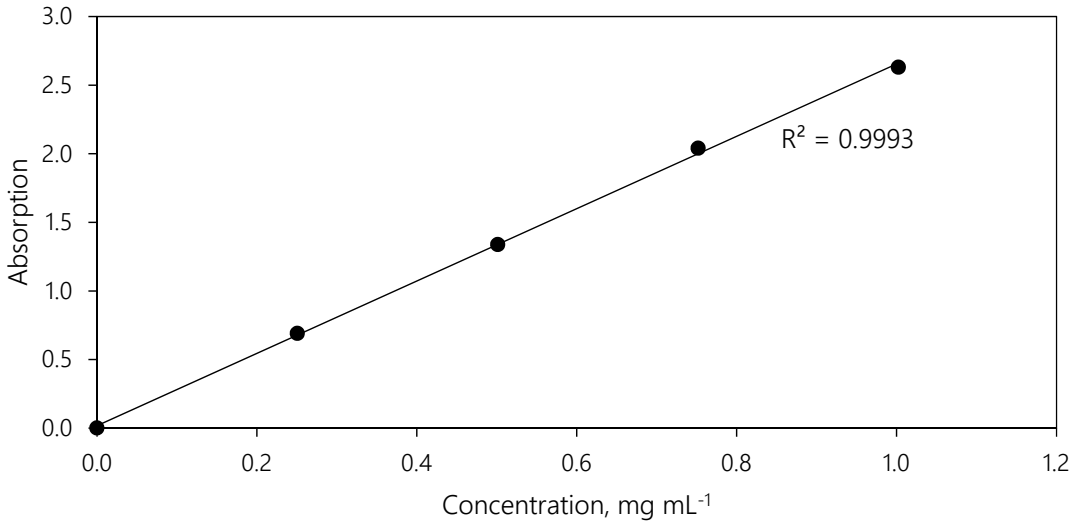

Figure 4-17. Calibration curve of CMC with the anthrone assay (n = 1).

In this chapter it was shown that both used polymers can be quantified using the anthrone assay. If they reacted similarly the assay could be used for a determination of the overall polymer in the NPs. Nevertheless, both polymers show a different behaviour in the assay. That is why they must be separated in order to quantify them correctly. For that purpose the NPs were centrifuged and the supernatant skimmed off to quantify the excess amount of chitosan and CMC in it. Chitosan was precipitated with 1 M NaOH. The supernatant still containing the excess CMC was separated from the pellet. The chitosan containing pellet should have been dissolved in dilute acetic acid prior to analysis. The CMC in the supernatant could be used directly. Two problems occurred with this procedure: The pellet could not be dissolved and the separation by centrifugation was not complete. This became obvious after performing an anthrone assay with the supernatant. Instead of the blue colour a mixed one developed indicating that chitosan was still present in the sample. Therefore, it could be concluded, that even though a method for detection of chitosan and CMC was developed, no quantification could be performed due to a lack of an efficient separation technique. Nonetheless, this method might be used to quantify NiM, chitosan and CMC combined, in aerodynamic characterisation. Please refer to chapter 4.5.2 for this.

4.1.5.3 Alternative Methods for Quantification

In the literature another method to quantify chitosan is discussed: Fluorescence measurements of excess FITC-tagged chitosan [122]. In such an experiment the chitosan would be labelled with FITC before the particle formation (described in 3.2.3). With this label the unreacted chitosan can be quantified after particle formation in the supernatant. This technique was however not used in this study because the particle formation process would have been changed. The FITC-label which would covalently bind to the amino groups of the chitosan would change the DDA of the respective quality. And changing the DDA of a chitosan alters the particle formation process (shown in 4.1.1) as a consequence. Determined chitosan concentration in NPs would only be true for particle formation with the tagged chitosan but not the raw material.

Instead of quantifying the excipients individually other papers quantify the NP together by weighing the obtained NP and comparing that mass to the originally applied mass of excipients [123]. This method was not used because of the associated high error potential: contaminants in the nanosuspension, polymer not involved in particle formation not being discarded with supernatant or loss during drying.

A potential surrogate for particle concentration might by the determination of the turbidity of the nanosuspension. This might be helpful if evaluating whether a washing step diminished the particle concentration. The turbidity primarily depends on the number of particles present, but is, in addition, also to some extent determined by their size. The size varies, as explained earlier, with the ratio between chitosan and CMC as well as the chitosan quality used. Consequently, the measurement of transmission to quantify turbidity is not a reliable parameter but can be used as an indicator to get a basic understanding of different particle yields, e.g. higher turbidity if more counterion was used signifying a higher particle yield.

This means that no method to quantify the NPs properly could be found in this project. Future projects should address this topic as it is important to know the particle yield to calculate e.g. a particle load and compare it to find the best ratio of antigen to carrier (particles).

4.1.6 Stabiliser Addition

As mentioned before, prepared NPs are only stabilised electrostatically. The following experiments tested whether the introduction of steric stabilisers further stabilises the nanosuspension which could allow the addition of even more CMC (e.g. in a ratio of chitosan to CMC of 1:2) potentially leading to higher particle yields, potentially even to a complete particle formation.

Three different chitosan qualities (75/10, 90/20 and 90/50) in three different ratios of chitosan to CMC (2:3, 2:4 and 2:5) were utilised. The different stabilisers polyvinyl alcohol (PVA), hydroxypropyl methylcellulose (HPMC), polyethylene glycol (PEG) 200, Poloxamer 188 and polysorbate 80 were dissolved to a concentration of 1 mg mL^{-1} either in the chitosan phase or in the CMC phase. The concentration of 100 wt% stabiliser in relation to the polymer concentration was chosen because it is a very high concentration under which an effect would be expected, if there was one. This has been shown in previous projects [124,125]. All other parameters were kept the same: chitosan and CMC were dissolved to a concentration of 1 mg mL^{-1} in 2 % HAc and water, respectively, and CMC was added to chitosan. Using the 2:3-ratio NPs could be formed, nonetheless, this ratio was stable without addition of stabilisers as well. Here, no substantial effect on particle size could be observed for any tested stabiliser. With the other two ratios (2:4 and 2:5) no stable nanosuspensions could be obtained at all – irrespective of the used stabiliser. Agglomeration took place for all chitosan qualities, no matter whether the stabiliser was added to the chitosan or the CMC phase (data not shown). This straightforward method of introducing the stabiliser to the particle formation process was not successful. It is likely that the stabilisers did not adsorb to the outer surface of the particles but were included in the particles during particle formation and hence not able to sterically stabilise the outer surface. The later addition of the stabiliser to previously formed particles might allow for a better stabilisation. Still, the main goal of these trials, adding more counterion to increase the particle yield, could not be achieved. Therefore, this approach was not followed up by further experiments.

If future experiments necessitated sterically stabilised particles, the potential of subsequent addition of stabiliser to a nanosuspension should be reconsidered.

4.1.7 Scalability of Batch Size

The standard batch size used in this project was 10 mL. Since this was a rather low volume and further applications of the nanosuspension (further processing to NiMs, chapter 4.4, or for *in vitro* experiments, chapter 4.6) will require larger batch sizes, the effect of batch size on resulting particle size was examined. The particle size was not strongly affected by batch size. Even relatively large batch sizes of up to 300 mL could be produced in the same size range, confer Figure 4-18. Particles consist of chitosan 90/20 and CMC in a ratio of 2:3 including 1 mg mL^{-1} OVA in the starting chitosan solution (encapsulation experiments are described in chapter 4.3).

Common to all batch sizes was the importance of slow CMC addition that was already mentioned earlier (4.1.4).

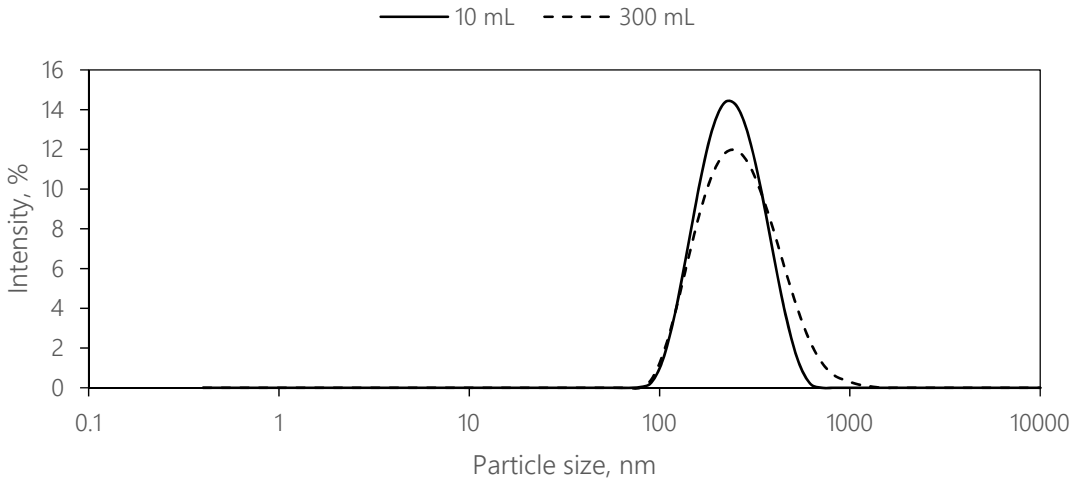

Figure 4-18. Particle size distributions resulting from two different batch sizes (as indicated in the legend) resulting in z-averages of 215 nm and 234 nm for batch sizes 10 mL and 300 mL, respectively (data of one representative experiment).

4.2 Production and Characterisation of Nanoparticles Consisting of Chitosan and Deoxycholate

In addition to CMC another counterion was used within this project for comparison: sodium deoxycholate (DOC). It was used in a previous project to form NPs as well [126]. DOC is a promising excipient for NPs as antigen carriers in vaccination because bile salts are known to interact with membranes, increasing their permeability which might lead to improved uptake of the formulation [79,127]. Within this project the goal was to compare the two counterions regarding their ability to form NPs. The most prominent differences are their molecular weight (0.4 kDa for DOC compared to approximately 90 kDa for CMC) and their amount of charges per molecule (one for DOC compared to multiple charges for CMC).

4.2.1 Development of Particle Formation Method

A particle formation method similar to that of chitosan and CMC was developed instead of utilising the one developed earlier [126] for better comparison of the utilised counterions and their effect on particle formation. The previous method was based on dissolving chitosan in acetic acid. But prior to the particle formation water and PBS buffer at pH 7.4 were added and the solution was adjusted to a pH of 5.5. DOC (dissolved in water) was subsequently added to the chitosan phase resulting in a concentration of 0.4 mg mL^{-1} of each substance in the final nanosuspension.

For the new method, the same weight concentrations of the excipients, which were used for the NPs consisting of chitosan and CMC, were tried. In first trials chitosan was dissolved in different solvents (either pure 1 % or 2 % HAc, corresponding to pH values of 2.6 and 2.7, respectively, or 1 % HAc adjusted to higher pH values (3, 4 and 4.5) with 1 M NaOH) to a concentration of 0.1 wt%. DOC was dissolved in water to 0.05 wt% and 0.1 wt%. Results are displayed in Figure 4-19 (0.1 wt% DOC) and Figure 4-20 (0.05 wt% DOC).

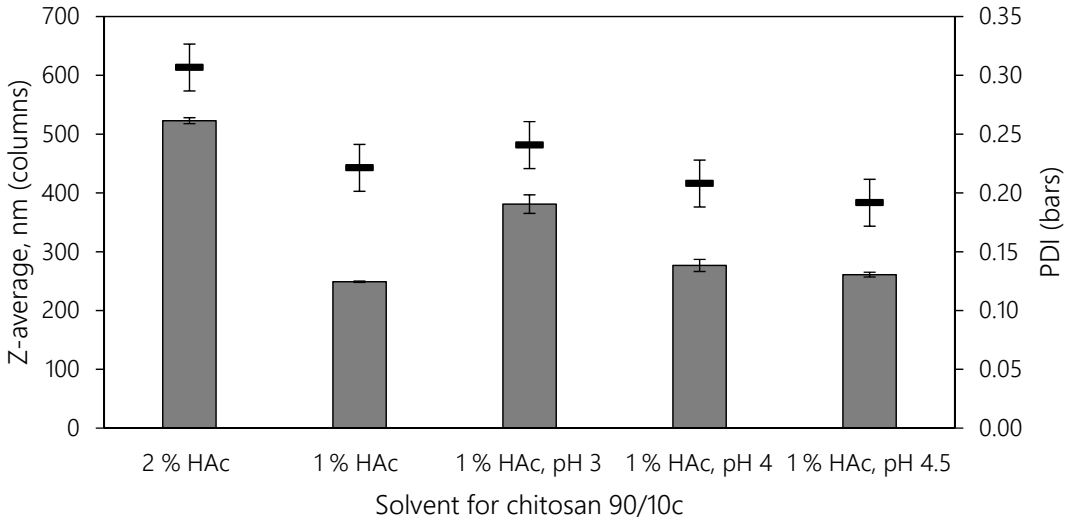

Figure 4-19. Particle size and PDI values obtained from nanosuspensions formed with chitosan 90/10c dissolved to 0.1 wt% in different solvents (indicated by column) with 0.1 wt% DOC (n = 2, error bars = min/max).

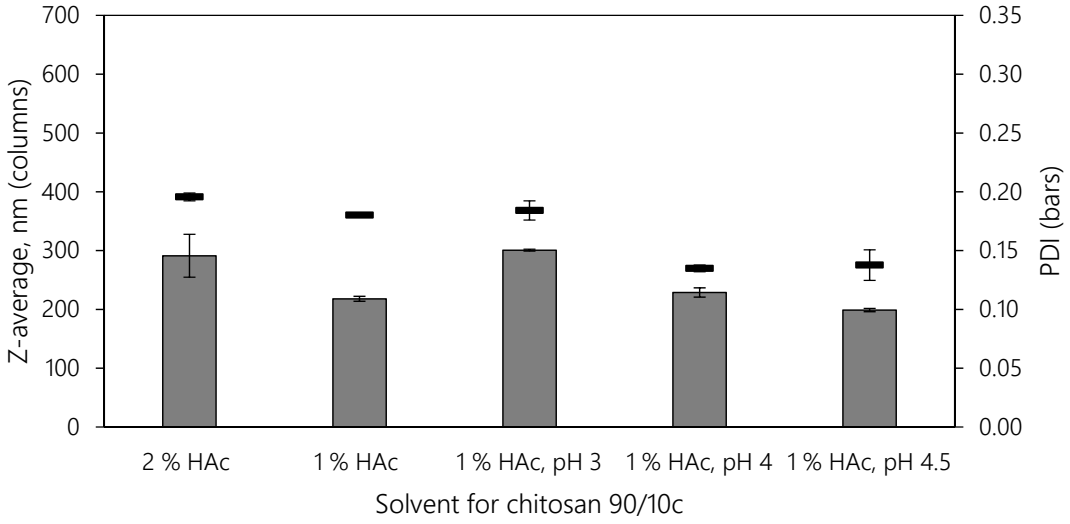

Figure 4-20. Particle size and PDI values obtained from nanosuspensions formed with chitosan 90/10c dissolved to 0.1 wt% in different solvents (indicated by column) with 0.05 wt% DOC (n = 2, error bars = min/max).

All combinations resulted in stable nanosuspensions (no agglomeration occurred after combination of the substances). Overall, the particles formed with 0.1 wt% DOC were larger (up to 500 nm) than those with 0.05 wt% DOC (up to 300 nm) but concurrently the nanosuspensions were more turbid if utilising 0.1 wt% DOC, indicating more particle formation. In between the different solvents, the same trends could be observed for both DOC concentrations. Particles formed with 2 % HAc were larger than those with

1 % HAc. And utilising a chitosan solution at pH 3 gave larger particles than those at pH 4 and 4.5 (particle sizes comparable to those produced with chitosan dissolved in 1 % HAc without further alteration of the pH).

Particle formation with DOC probably mostly relies on the charge equalisation and hence decreased solubility. DOC only has one charge per molecule, therefore effective cross-linking cannot take place. Depending on the present salts and pH values this results in differently sized particles. If more DOC was present more chitosan charges could be equalised and hence more particles could be formed. In comparison to NP formed with chitosan and CMC the turbidity was generally lower, indicating less particle formation for DOC as counterion which was probably due to the lack of cross-linking.

For further experiments 1 % HAc was chosen as best solvent and the concentration of 0.1 wt% for DOC because of the higher particle concentration.

4.2.2 Particle Stability

Similar to the experiments with chitosan and CMC the stability of NPs was determined via titration experiments. For ZP measurements a 1:2 dilution with water was chosen as well. Results are shown in Figure 4-21.

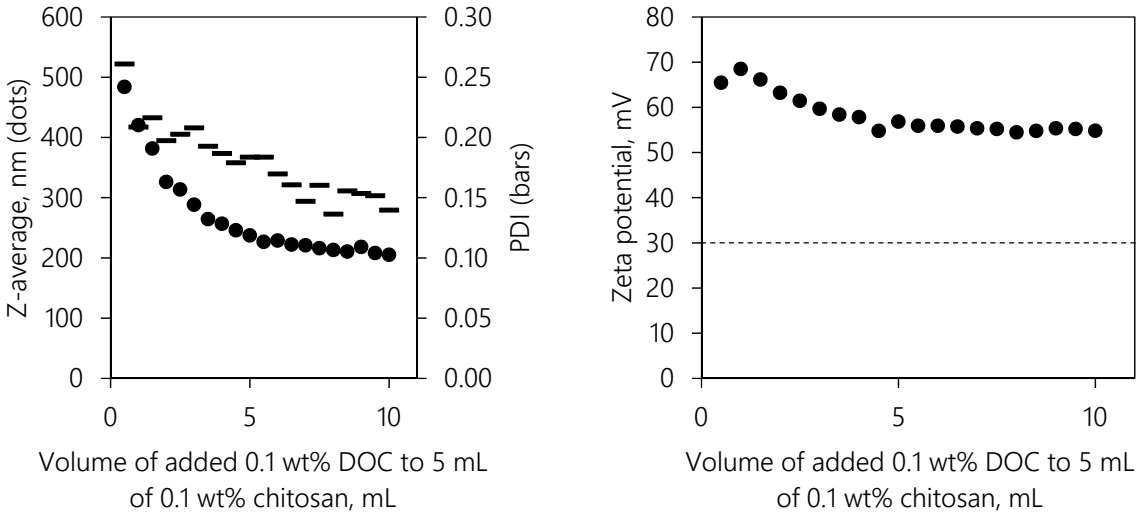

Figure 4-21. Particle size and PDI values (left) as well as corresponding ZP (right) are displayed for experiment with chitosan 90/10c (dissolved in 1 % HAc) (n = 1).

Particle size and PDI decreased when more counterion was added to the chitosan solution. In contrast to titration experiments with chitosan and CMC no size or PDI increase, that would have indicated particle instability, could be observed up to a weight ratio of chitosan to CMC of 1:2. This went along with ZP values being well above +30 mV for all nanosuspensions. To assess the particle stability limit, further experiments were performed to find the ratio of chitosan to DOC where particles become unstable. Results of those experiments are shown in Figure 4-22.

Even though the ratio of chitosan to DOC was extended from 1:2 (10 mL 0.1 wt% DOC added to 5 mL of 0.1 wt% chitosan) over 1:3 and 1:4 (7.5 mL and 10 mL 0.1 wt% DOC added to 2.5 mL of 0.1 wt% chitosan, respectively) to 1:10 (5 mL 0.1 wt% DOC added to 0.5 mL of 0.1 wt% chitosan) no instability could be observed. Particle size, PDI and ZP stayed on the same level. Only the turbidity of the nanosuspension increased with increasing DOC concentration in the final suspension.

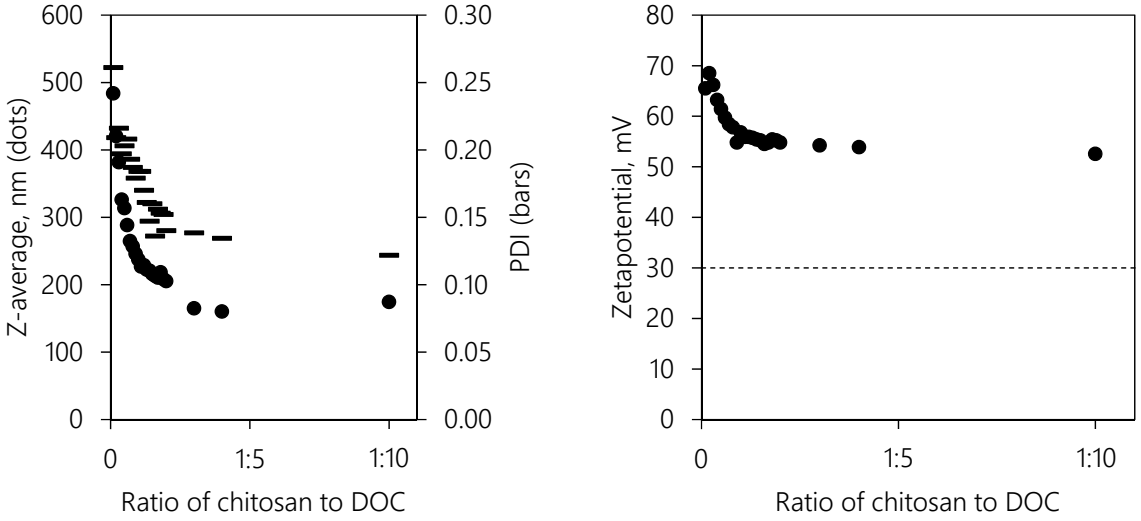

Figure 4-22. Particle size and PDI values (left) as well as corresponding ZP (right) are displayed for experiments with chitosan 90/10c (dissolved in 1 % HAc) with higher ratios of DOC to chitosan (n = 1).

Overall, particle sizes are smaller compared to particles formed with CMC which could be expected due to the much lower molecular weight of DOC and the lack of cross-linking. The particle size decrease when adding more DOC was probably due to denser packaging of chitosan strands because more precipitated simultaneously. If both

polymers were used in the same concentration of 0.1 wt% very different volumes of chitosan and DOC phase must be taken for a ratio 1:10. Hence, it was tried to use DOC in a higher concentration (e.g. 1 wt%) and reduce the volume by this. But if concentrations above 0.1 wt% were used, agglomeration occurred after addition of DOC to chitosan and no NPs could be obtained (data not shown).

No ITC measurements to study the binding between chitosan and DOC could be performed because no shared solvent (suitable for particle formation) for chitosan and DOC was found, a crucial prerequisite for this technique.

4.2.3 Particle Size

Utilising DOC as counterion it was checked as well how the particle size was influenced by different chitosan qualities used for particle formation. Particle sizes and respective PDI and ZP values obtained are shown in Table 4-5.

Table 4-5. Particle size, PDI and ZP obtained after particle formation with various chitosan qualities (n = 3, for clarity no SD values were included). The chitosan qualities are ordered from top to bottom by rising viscosity.

Chitosan quality	*Ratio 1:1*			*Ratio 1:5*		
	Z-average, nm	*PDI*	*ZP, mV*	*Z-average, nm*	*PDI*	*ZP, mV*
90/10b	204.7	0.099	51.9	148.6	0.088	47.5
85/10	195.4	0.145	49.7	158.1	0.108	47.2
75/10	270.5	0.141	53.8	177.3	0.113	50.3
90/10c	235.2	0.147	52.2	165.7	0.120	48.4
90/10a	207.3	0.162	52.5	168.6	0.128	48.8
95/10	216.6	0.140	53.9	159.6	0.120	51.9
90/20	255.8	0.145	53.1	167.7	0.124	48.2
70/20	327.0	0.189	57.7	207.3	0.157	51.9
80/20	325.8	0.194	54.2	198.3	0.160	53.2
80/50	313.2	0.284	56.3	198.9	0.194	50.1
70/50	404.7	0.266	61.7	225.0	0.218	51.5
90/50	320.2	0.285	56.5	195.5	0.205	51.4
90/200	391.6	0.489	60.6	215.0	0.270	59.1

Again, two different ratios were used: 1:1 (comparison to particle sizes achieved after particle formation with CMC) and 1:5 (stable ratio in particle formation with chitosan and DOC). All obtained nanosuspensions showed ZP values well above +30 mV, indicating stability. The particle size, PDI and ZP values were lower if more counterion was used, this was consistent with the effect seen for NPs consisting of chitosan and CMC. Size however was not predominantly governed by molecular weight as it was the case for particle formation with CMC. Rather, it depended on the DDA as well. Particle size was positively correlated with molecular weight and negatively correlated with DDA. Accordingly, ordering the chitosan qualities by either characteristic did not result in a clear trend (Figure 4-23 by rising viscosity, Figure 4-24 by rising DDA). Nevertheless, the size was more strongly influenced by the molecular weight (or corresponding viscosity) than by the DDA.

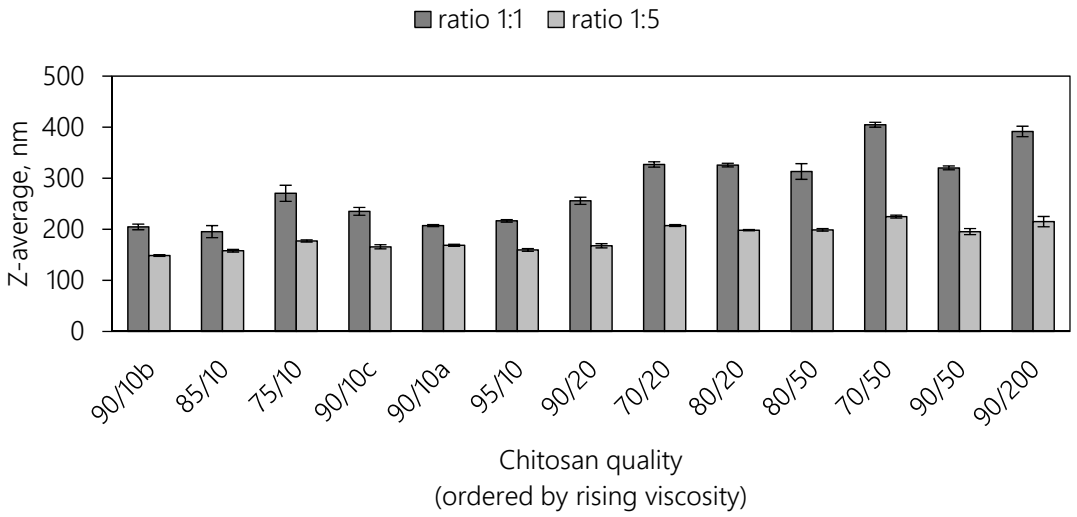

Figure 4-23. Particle sizes measured after particle formation with various chitosan qualities which are ordered by rising viscosity and DOC (n = 3, error bars = SD).

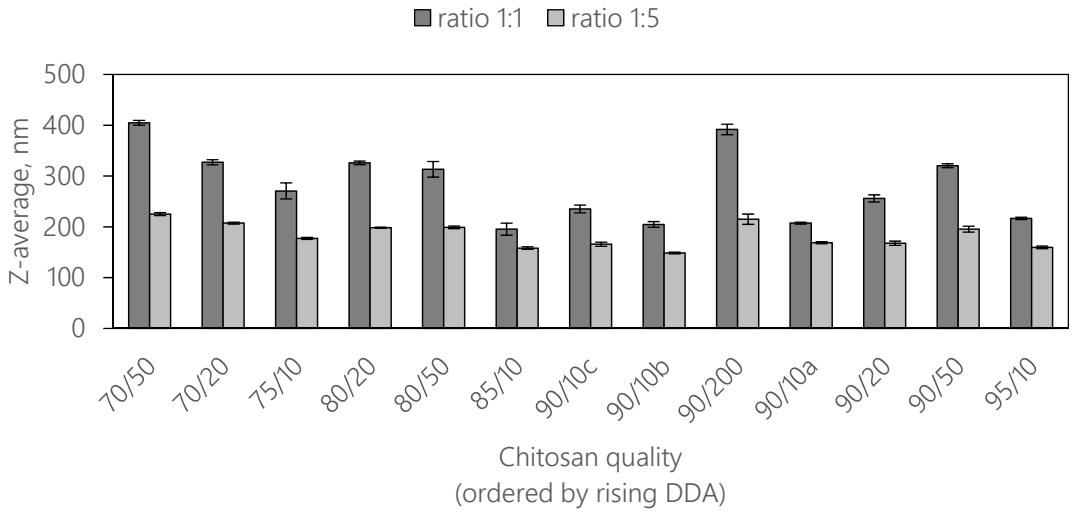

Figure 4-24. Particle sizes measured after particle formation with various chitosan qualities which are ordered by rising viscosity and DOC (n = 3, error bars = SD).

4.2.4 Comparison of Nanoparticles Consisting of Chitosan and as Counterion Carboxymethylcellulose or Deoxycholate

In general, particles formed with DOC were smaller than those formed with CMC, shown in Figure 4-25. To reach the targeted particle size of a maximum of 500 nm all available chitosan qualities can be used. Using DOC could rather result in particles too small to be recognised as particles by cells (below 100 nm). To meet the size requirements, a higher molecular weight chitosan would have to be used. Whether this higher molecular weight would have an impact on the adjuvant potential of chitosan would be interesting to test. Scherließ et al. did measurements on that topic finding a comparable or even better immune response if a higher molecular weight chitosan was used. Nonetheless, these authors also varied the DDA and particle size of the chitosan. Hence, those results cannot be fully ascribed to the molecular weight and further tests to distinguish the effect are needed [128]. And if working with higher molecular weight chitosan, it must be kept in mind that the PDI rises (broader size distribution) as well.

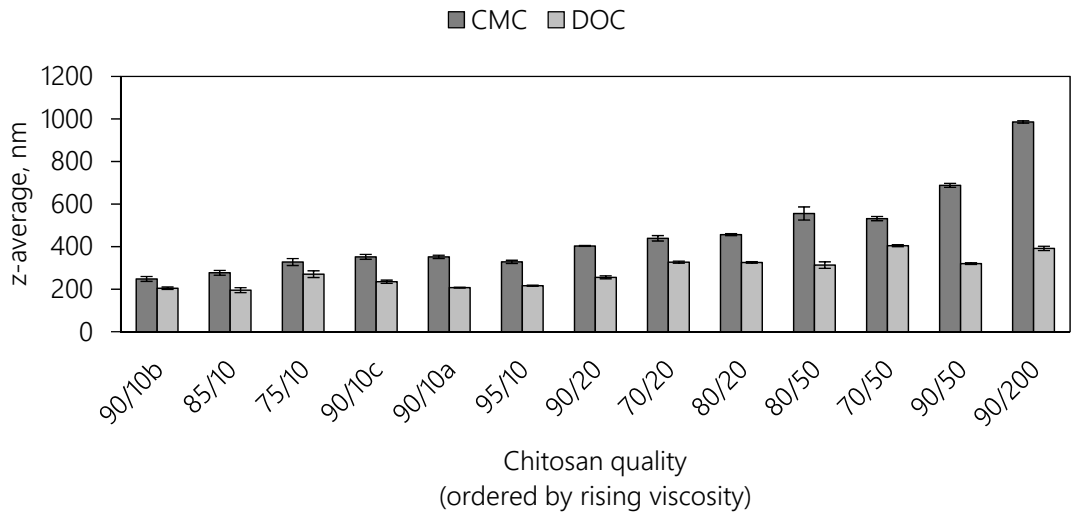

Figure 4-25. Particle sizes measured after particle formation with various chitosan qualities which are ordered by rising viscosity and different counterions in a weight ratio of 1:1 (n = 3, error bars = SD).

Overall, the turbidity of nanosuspensions formed with chitosan and DOC was lower compared to particle formation with chitosan and CMC indicating less particle formation. This was backed up by other trials: If NPs were centrifuged, the remaining pellet was smaller than after comparable particle formation with CMC or if FITC-tagged chitosan was utilised for particle formation almost no colour was visible in the resulting NPs. An explanation for this might be the low molecular weight in combination with the low charge density of DOC. The low charge density could not saturate chitosan (indicated by ZP plateau contrary to ZP drop when CMC was used) and hence could not form particles as efficiently. Figure 4-26 shows the resulting different particle sizes and ZP values subject to different ratios of chitosan to CMC. Chitosan 90/10c was utilised for these experiments.

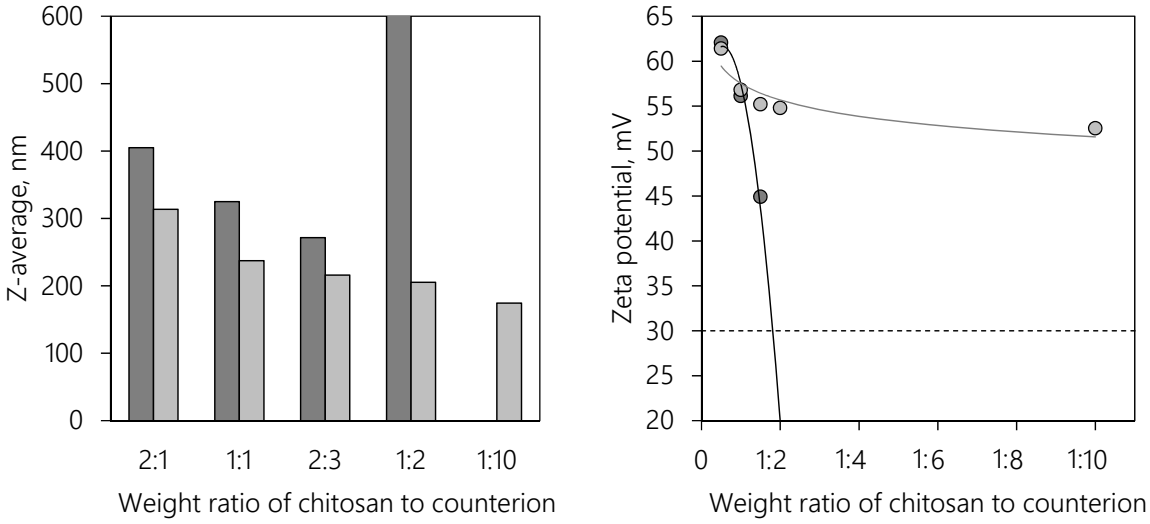

Figure 4-26. Differences in size (left) and ZP (right) subject to utilised counterion: CMC (dark grey) or DOC (light grey). NPs consisting of chitosan 90/10c and CMC were not stable at a weight ratio of 1:2 and formed large agglomerates (above 1 µm), this is indicated by the truncated bar (n = 1).

Particle sizes were generally higher and ZP values lower if CMC was utilised as counterion in comparison to DOC, irrespective of the utilised amount of the counterion. The ZP drop below +30 mV (if utilising CMC as counterion) and concurrent agglomeration of particles could not be observed if utilising DOC as counterion. This difference in ZP was probably a consequence of the lower charge density of DOC. A single charge per molecule is not sufficient to promote cross-linking, which resulted in a generally higher ZP because chitosan's free amino groups could not be cross-linked as effectively. The particle formation probably solely relies on the charge equalisation and following precipitation of chitosan strands that coil up only coincidentally. In contrast, CMC can promote cross-linking due to multiple charges per molecule.

4.3 Loading of Nanoparticles with Protein

In the following chapter the loading of the NPs with proteins will be presented. OVA has been used as model antigen for all experiments performed in this project. Experiments examining the protein load of NPs were solely conducted with NPs consisting of chitosan and CMC because this combination results in more promising particles (especially higher particle yield) compared to particles formed with chitosan and DOC.

Preliminary ITC measurements showed that the particle formation process is affected by the addition of OVA to the chitosan phase. This difference is displayed in Figure 4-27.

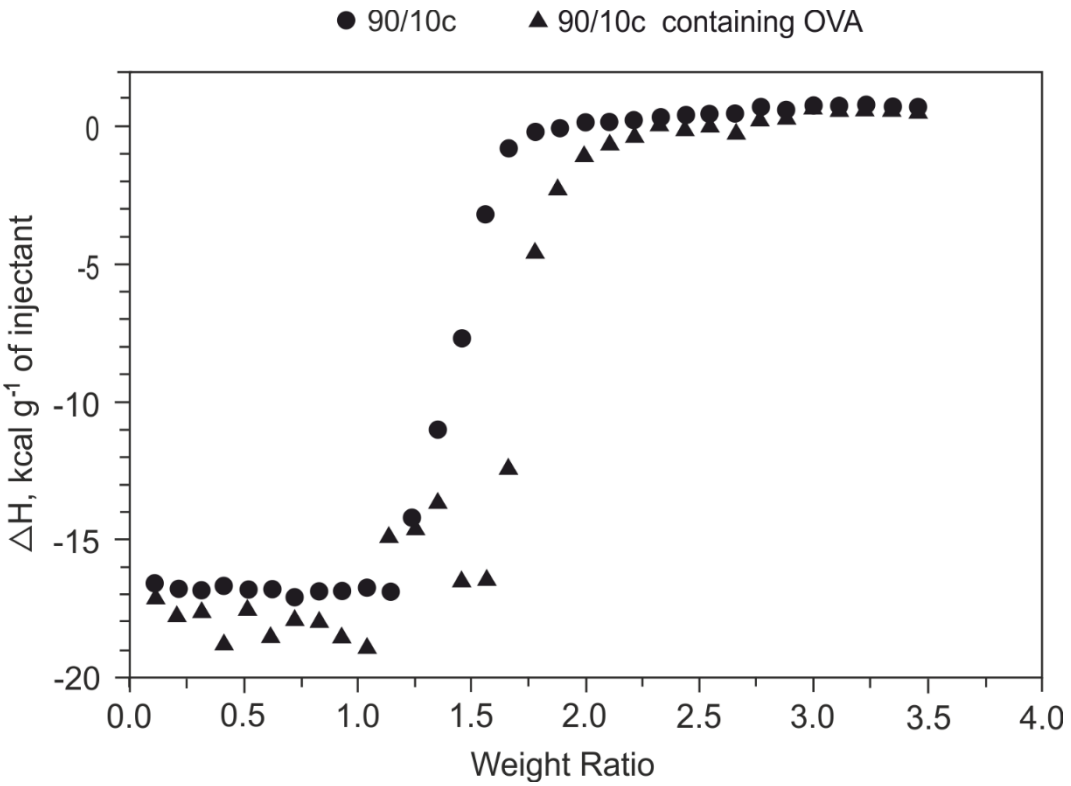

Figure 4-27. Binding curves for titration experiment with CMC (syringe) and chitosan 90/10c containing or not containing OVA (concentration not considered in weight ratio) in the cell (n = 1).

In case of OVA addition to the chitosan phase, a higher amount of CMC addition was necessary for the complete reaction (slight curve shift to the right). This could be ascribed to OVA because, by being dissolved in acetic acid, it was positively charged (pH below IEP of pH 4.5) and could participate in the particle formation process with CMC. The titration curve fluctuated more when OVA was included. A possible explanation for this could be more agglomeration due to the high stirring speed which the OVA did not tolerate as well as the chitosan and CMC. A lower stirring speed was however not utilised because this was necessary to ensure an instant mixing of all components. Evidence of OVA's participation in the particle forming process could be provided by measuring a reduction in particle size compared to OVA-free counterparts. This is illustrated in Figure 4-28. The difference in particle size was more pronounced if a higher molecular weight chitosan quality was used.

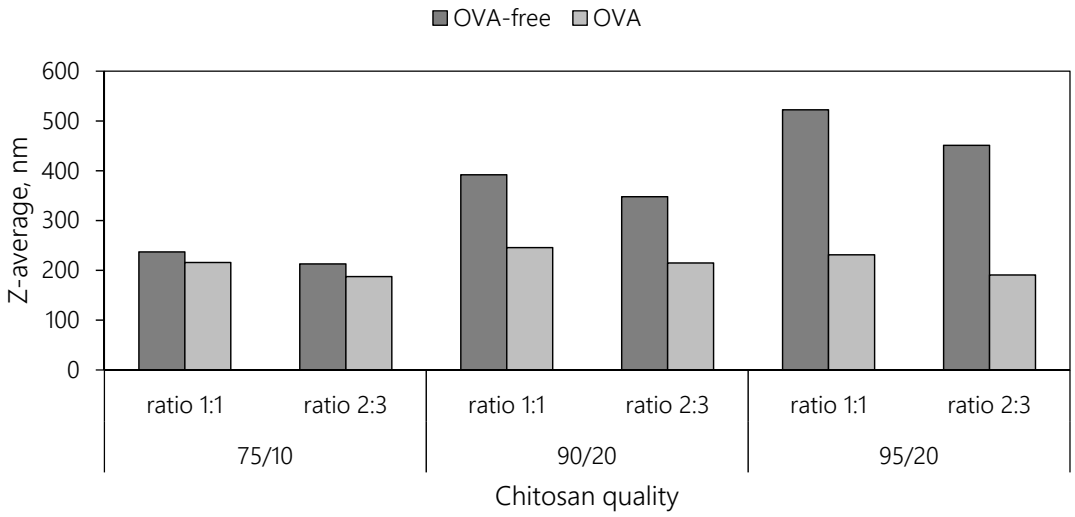

Figure 4-28. Particle sizes of NPs formed with different chitosan qualities (using 2 % HAc as solvent for chitosan) and containing or not containing OVA (n = 1).

4.3.1 Influencing Factors on Protein Loading

In the following subchapters different aspects that could potentially influence the protein load were examined. Two different possibilities to describe the protein load are the determination of the loading efficiency (LE, relating to the amount of OVA used) or the loading capacity (LC, relating to the amount of particle forming polymer used). While the LE rather gives information about the efficiency of the process, the LC gives information about the obtained product. Hence, this value will be used primarily in the following chapter. Nonetheless, as described in chapter 4.1.5 the particle forming excipients do not completely react to form particles. As a consequence, this value cannot be taken as loading capacity per nanoparticle mass but per excipient mass (related to polymer mass in the preparation process).

If not indicated otherwise, OVA was used in a concentration of 1 mg mL^{-1} in the following experiments.

4.3.1.1 Solvent

The effect on protein load by using different solvents was studied. Chitosan 90/10a was thus dissolved in different acidic media, OVA was dissolved shortly before the experiment in the chitosan solution. HCl was tried as an alternative acid to HAc. NPs could only be formed if HCl was used in a concentration of 0.01 M or lower. If a higher concentration, e.g. 0.1 M, was used, no NP formation with chitosan (no OVA included) and CMC could be observed. This was due to the very low pH of below 2 of the resulting mixture, preventing particle formation because all polymers (including CMC) were positively charged and no negatively charged counterpart for particle formation was available. As mentioned earlier, the used acetic acid concentrations resulted in pH values of 2.6 and 2.7 for 2 % HAc and 1 % HAc, respectively. Moreover, an acidic buffer system was used for comparison, namely acetate buffer with pH values of 3.7, 4.0 and 4.5. When using the buffer at pH 4.5, no stable nanosuspensions could be obtained (ZP of 29.3 mV and 15.8 mV for ratios 1:1 and 2:3, respectively), hence no LC was determined. Moreover, no LC could be determined for acetate buffer at pH 4.0 in the 2:3 ratio because no stable NPs could be produced here as well (ZP of 25.0 mV). Resulting LCs are displayed in Figure 4-29 for different chitosan solvents.

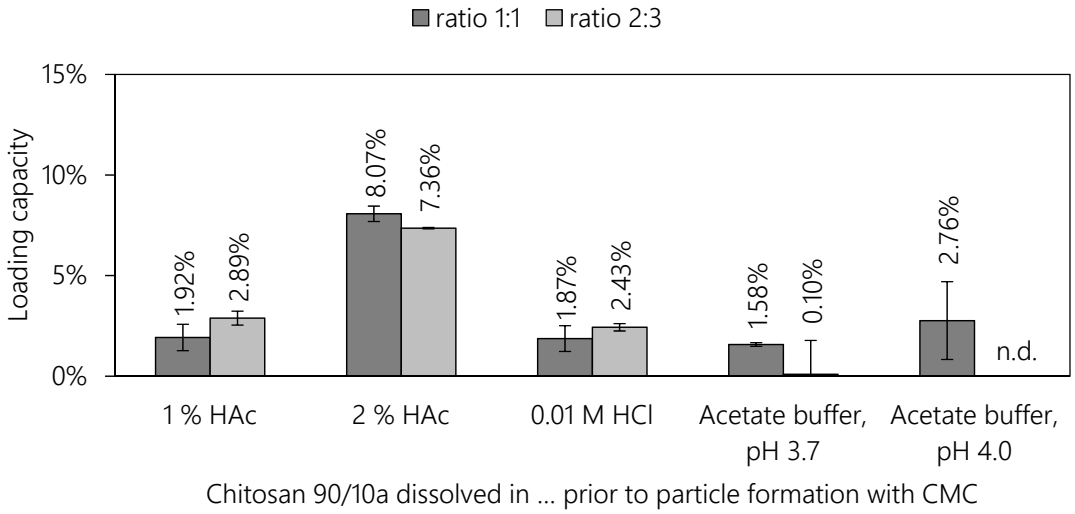

Solvent	*Ratio 1:1*			*Ratio 2:3*		
	Z-average, nm	*PDI*	*ZP, mV*	*Z-average, nm*	*PDI*	*ZP, mV*
1 % HAc	169.6	0.140	43.2	142.4	0.134	36.9
2 % HAc	168.8	0.169	45.1	148.2	0.143	37.1
HCl 0.01 M	172.8	0.169	38.1	143.1	0.133	31.6
Acetate buffer, pH 3.7	173.5	0.142	32.6	504.3	0.355	29.1
Acetate buffer, pH 4.0	263.0	0.180	34.9	n.d.	n.d.	25.0

Figure 4-29. Protein LC depending on solvent for chitosan (top, n = 2, error bars = min/max) and respective particle size, PDI and ZP values (bottom). Parameters were not determined (n.d.) if agglomeration occurred.

LC was highest for 2 % HAc with 8.07 % and 7.36 % for ratios 1:1 and 2:3, respectively. The values for LC are comparable for both utilised ratios of chitosan and CMC even though less OVA (corresponding to a lower share of chitosan starting solution in the final nanosuspension) was used for the ratio 2:3. Because of this, calculating the LE gives a slightly different result. Here, values of 16.14 % and 18.40 % for ratios 1:1 and 2:3, respectively, were determined. Those trends were not only true if 2 % HAc was used as solvent, but also for the other solvents (1 % HAc and 0.01 M HCl) as well.

Thereupon, utilising more CMC for particle formation resulted in a higher share of encapsulated OVA. This was probably due to a higher share of polymers forming particles utilising the 2:3 ratio which were then able to encapsulate more OVA. This

trend could not be observed for acetate buffer at pH 3.7. Here, the NP size was increased substantially for the 2:3 compared to the 1:1 ratio, indicating unstable NPs. Hence, the calculated LCs could not be regarded as reliable. Compared to 2 % HAc, all other solvents gave substantially lower LCs. Consequently, this solvent was used for subsequent experiments.

4.3.1.2 Stirring Time

Another parameter to be investigated was stirring time, more precisely the time the nanosuspension was stirred after adding CMC and prior to refrigeration. OVA was dissolved shortly before the particle formation in chitosan 90/10a solution (2 % HAc). The respective particle sizes and PDI obtained after different stirring times only varied between 173 nm and 183 nm and 0.156 and 0.180, respectively. Thus, no substantial effect of stirring time on particle size could be observed. The resulting LCs after different stirring times are shown in Figure 4-30.

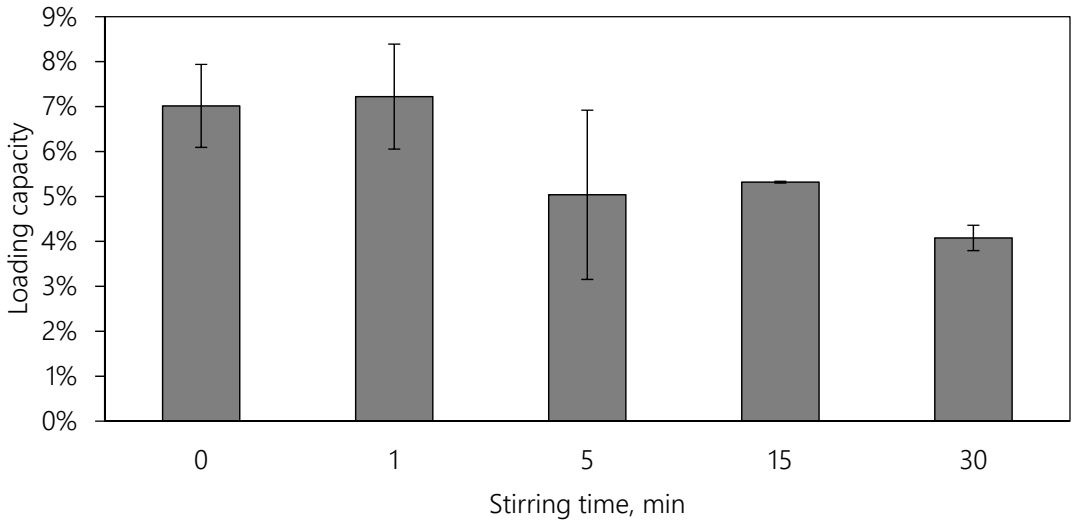

Figure 4-30. Protein LC depending on the stirring time following mixing of components (n = 2, error bars = min/max).

The LC decreased with increasing stirring time, from 7.01 % with no stirring after CMC addition to 4.08 % after 30 min stirring. This might be due to the rearrangement of the polymers and the protein within the NPs during stirring, excluding the OVA more and more over time, even though it was encapsulated during the initial particle formation.

The results showed no advantage of additional stirring after the mixing of the components. Therefore, the nanosuspensions were not stirred after addition of the CMC was completed.

4.3.1.3 Temperature

Experiments to study the influence of temperature on the protein load and, concurrently, on the particle size were performed with chitosan 90/10a. The chitosan and the CMC starting solutions (OVA was dissolved shortly before the experiment in chitosan solution which was prepared with 2 % HAc) were brought to 6, 21, 25, 30, 40 or 50 °C, respectively. The particle formation itself was performed at room temperature. Results for LC and particle size are depicted in Figure 4-31.

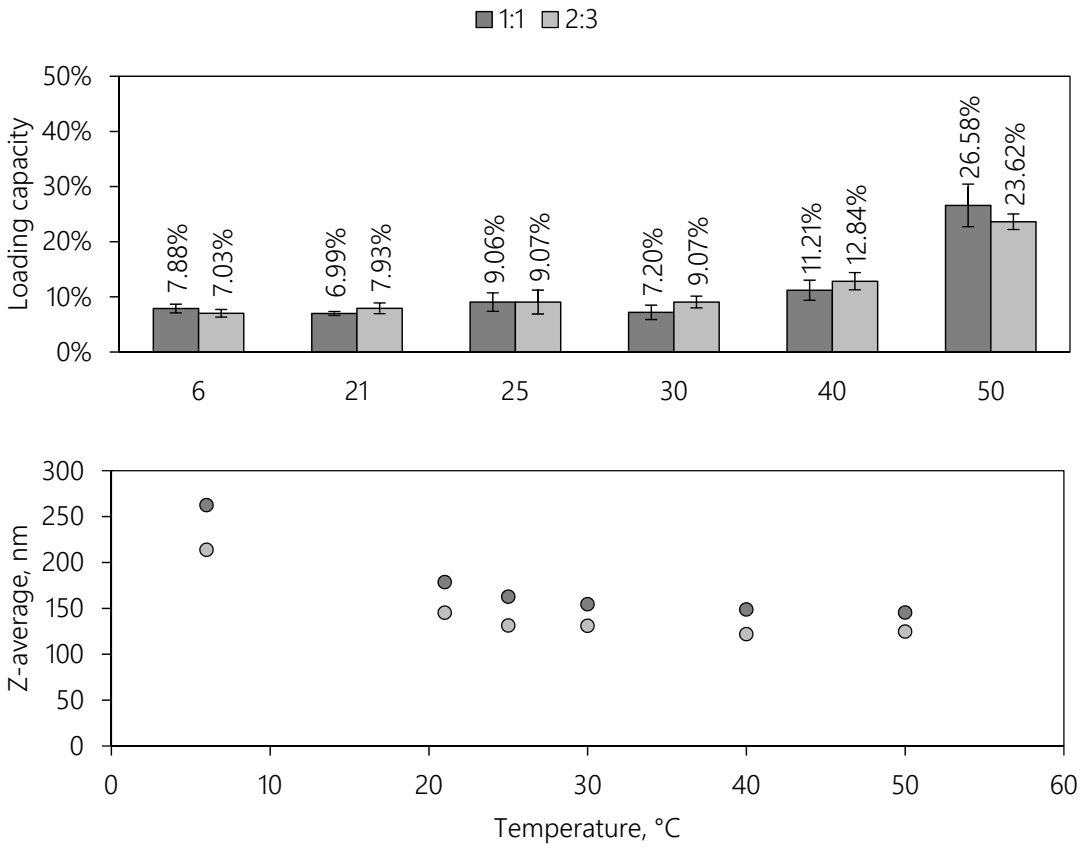

Figure 4-31. Protein LC depending on temperature (top, n = 3, error bars = SD) and respective particle size (bottom, n = 1).

PDI values were all below 0.2 for ratio 1:1 and below 0.15 for ratio 2:3 with the only exception of the particles formed with solutions at 6 °C. Here, PDI values of 0.236 and 0.204 were measured for ratios 1:1 and 2:3, respectively. All ZP values indicated stable nanosuspensions giving lower values for ratio 2:3 in comparison to 1:1. Particle size decreased with increasing temperature probably due to lower viscosity of the solution and higher mobility of the polymer strands resulting in denser and smaller particles. The LC was positively correlated with temperature. Especially a temperature of 50 °C proved to be favourable. Nonetheless, for subsequent experiments ambient conditions were maintained, on the one hand because of practicability and on the other for protein stability reasons (temperature closer to melting temperature, longer residence time of OVA in starting acidic solution during heating). If a higher LC for a NP formulation however would be needed, the elevation of temperature in consideration of the stability of the utilised protein should be kept in mind.

4.3.1.4 Chitosan Quality

The effect of chitosan quality on protein load was studied in this trial. Chitosan phase with 2 % HAc as solvent was prepared with qualities varying in molecular weight and DDA (ranging between 75 % and 95 %). The previously used batch of chitosan 90/10 (chitosan 90/10a) was used up. For this reason a quality with comparable characteristics was utilised for further experiments: chitosan 90/20. Even though the nominal viscosity differs, the determined values for viscosity (given by the supplier) were rather similar with 15 mPa s and 18 mPa s, respectively. Figure 4-32 shows the results for LC as well as particle size, PDI and ZP.

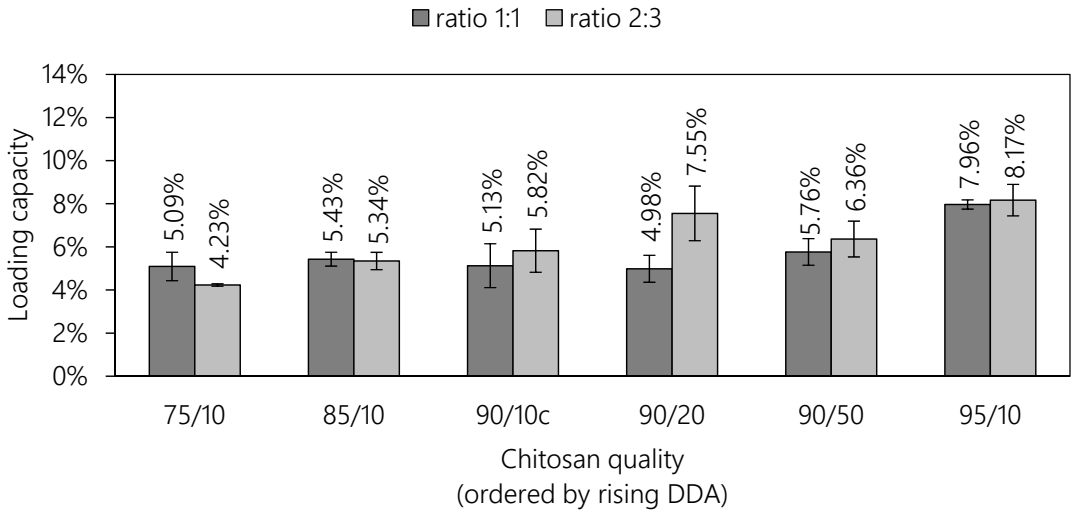

Chitosan quality	*Ratio 1:1*			*Ratio 2:3*		
	Z-average, nm	*PDI*	*ZP, mV*	*Z-average, nm*	*PDI*	*ZP, mV*
75/10	207.0	0.148	46.0	185.5	0.121	36.7
85/10	185.0	0.158	48.2	181.8	0.114	37.9
90/10c	218.3	0.178	52.0	187.7	0.144	43.4
90/20	215.1	0.153	51.3	219.4	0.145	43.9
90/50	343.3	0.243	57.4	268.8	0.160	46.4
95/10	158.3	0.161	45.3	135.2	0.137	39.7

Figure 4-32. Protein LC depending on chitosan quality used (top, n = 2, error bars = min/max) and respective particle size, PDI and ZP values (bottom, n = 1).

The effect on LC by the different weight ratios of chitosan to CMC for particle formation which was observed earlier could be confirmed. While the DDA of chitosan did not have a substantial effect on the particle size of particles formed with CMC (section 4.1.4) it did have an influence on LC. The DDA was positively correlated with the LC. An explanation for this might be the presumptive higher particle yield if utilising a higher deacetylated chitosan quality (as presented in chapter 4.1.2) which can bind more CMC. This higher particle amount probably leads to higher encapsulation opportunities for the OVA, not only leading to a comparable LC despite the lower amount of utilised OVA but for most qualities even to an increased LC. All the while, no consistent effect of molecular weight on LC could be identified.

4.3.1.5 Protein starting concentration

Based on the previous results, a new chitosan quality with favourable DDA (as high as possible) and viscosity (approximately 20 mPa s to meet the size requirements of maximal 500 nm) was purchased: chitosan 95/20. This chitosan was compared to qualities 75/10 and 90/20 in terms of size and protein load. All qualities exhibit a comparable viscosity and differ in DDA. As this was shown to influence the LC in previous experiments (chapter 4.3.1.4) utilising those qualities gives an overview over achievable LCs depending on the DDA of the starting material. The aim of these experiments was to assess whether the amount of OVA in the starting solution influenced the protein load.

As mentioned before, the particle size depended on the protein addition. Resulting sizes of NPs produced with the three chitosan qualities as a function of the OVA addition (0 - 4 mg mL^{-1}) are depicted in Figure 4-33.

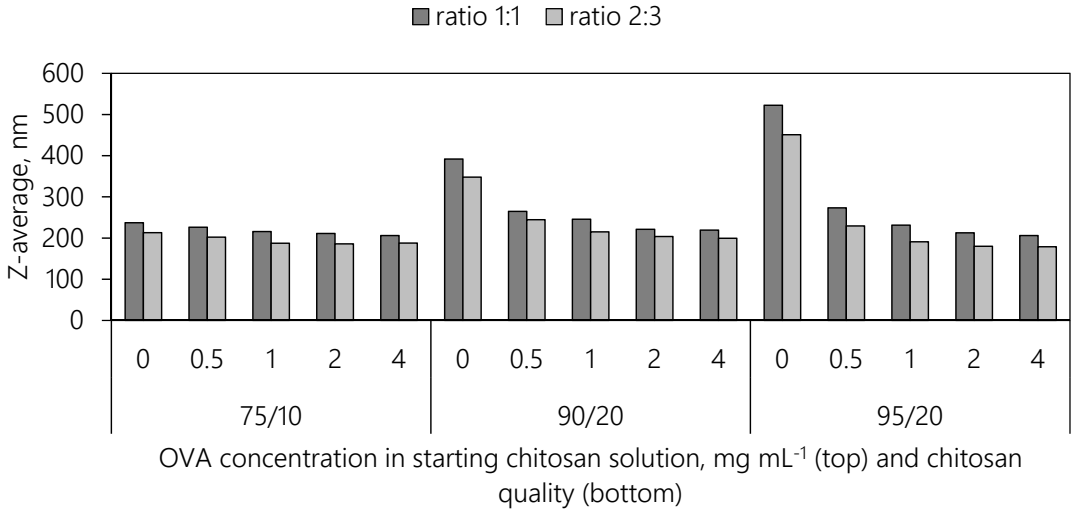

Figure 4-33. Particle sizes depending on chitosan quality used and OVA concentration (0 - 4 mg mL^{-1}) in the starting solution (n = 1).

Measured sizes for NPs made with chitosan 95/20 were approximately 250 nm if OVA was added. The OVA-free particles exhibited a particle size of 523 nm and 451 nm for ratios 1:1 and 2:3, respectively. Hence, the addition of OVA had a substantial impact on particle size. This impact was lower for particles formed with chitosan 90/20 and even less for those formed with the 75/10-quality. This effect is probably due to the varying

DDA and viscosity of the three chitosan qualities. The effect of particle size reduction was more pronounced for a higher deacetylated and more viscous chitosan. Results for the respective LCs can be seen in Figure 4-34.

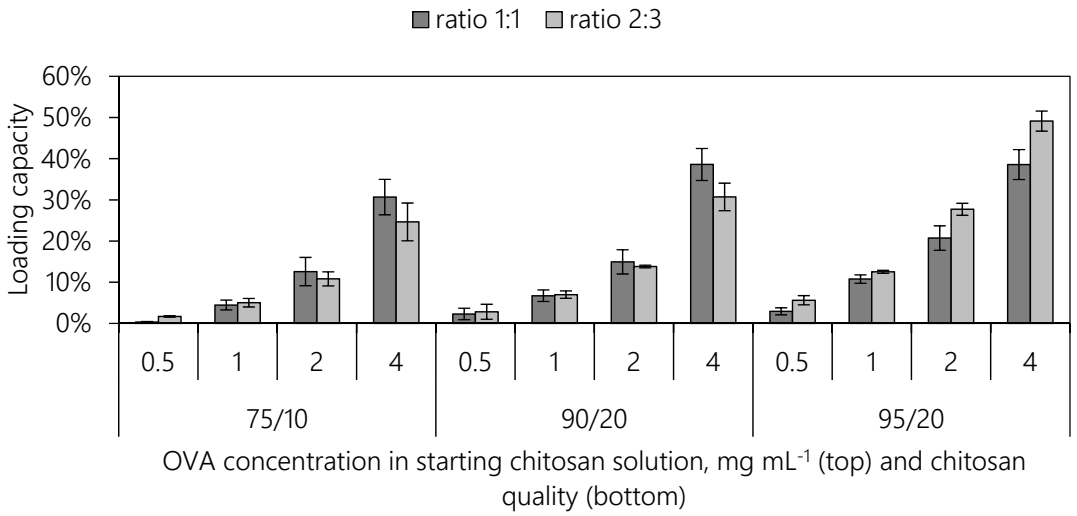

OVA concentration in starting solution, mg mL^{-1}	*Ratio 1:1*			*Ratio 2:3*		
	75/10	*90/20*	*95/20*	*75/10*	*90/20*	*95/20*
0.5	0.35 %	2.30 %	2.94 %	1.70 %	2.84 %	5.64 %
1	4.47 %	6.73 %	10.78 %	5.03 %	7.01 %	12.53 %
2	12.60 %	14.94 %	20.73 %	10.82 %	13.82 %	27.72 %
4	30.69 %	38.60 %	38.57 %	24.65 %	30.71 %	49.14 %

Figure 4-34. Protein LC depending on chitosan quality used and OVA concentration (0 - 4 mg mL^{-1}) in the starting solution (n = 3, error bars = SD).

Earlier results (comparable/higher LC/LE for ratio 2:3 compared to 1:1, higher protein load if higher DDA) were confirmed with this trial. For all chitosan qualities the utilisation of higher OVA concentrations in the starting solution resulted in higher values for the LC, going up to almost 50 %. This effect was mostly due to the rising amount of utilised OVA which is not taken into account when determining the LC. It is, if calculating the LE. Therefore, Figure 4-35 shows the corresponding LEs.

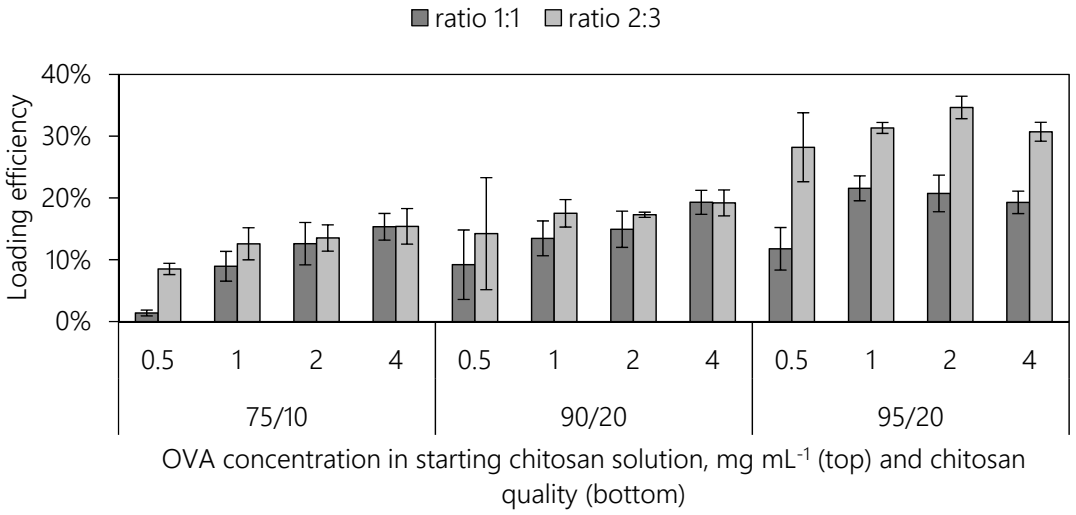

Figure 4-35. Protein LE depending on chitosan quality used and OVA concentration (0 - 4 mg mL^{-1}) in the starting solution (n = 3, error bars = SD).

Utilisation of 1 mg mL^{-1} OVA in the starting solution seemed favourable over 0.5 mg mL^{-1}. However, for the higher concentrations no further increase in LE could be measured for chitosan 95/20. For the other two qualities (75/10 and 90/20) a minor tendency of rising LE can be observed. The absolute amount of OVA encapsulated was increased for all qualities but most of the utilised OVA could not be loaded in the NPs. Therefore, if only absolute encapsulation was taken into account a higher initial concentration is reasonable. But, many proteins are very expensive and therefore should be encapsulated more efficiently.

4.3.2 Alternative Addition Sequence

In all experiments examining the encapsulation of OVA in NPs, the highest LC was achieved with chitosan 95/20 dissolved in 2 % HAc, giving a value of approximately 50 % (starting OVA concentration of 4 mg mL^{-1}). As mentioned afore, the LE was lower with approximately 35 %. As an LE of 35 % means that 65 % of the utilised protein does not associate with particles and is discarded, this would probably not be affordable in many cases. Therefore, another method by which the protein is encapsulated more efficiently was developed.

This new method consisted of two steps. In the first step the CMC phase (0.2 wt% in water) was slowly added to the OVA phase (10 µg mL^{-1} - 1 mg mL^{-1} in 2 % HAc), resulting in a ratio of 1:1 of the two solutions. This mixture already formed NPs because of the contrarily charged substances. Resulting particle sizes and corresponding LEs are given in Figure 4-36. Here, LEs rose with rising OVA concentration. It should however be noted, that the LE was not decisive here because the complete OVA-CMC mixture was used for particle formation, thus, the not encapsulated OVA was added to chitosan as well. Resulting ZPs for all OVA-CMC mixtures were approximately -14 mV.

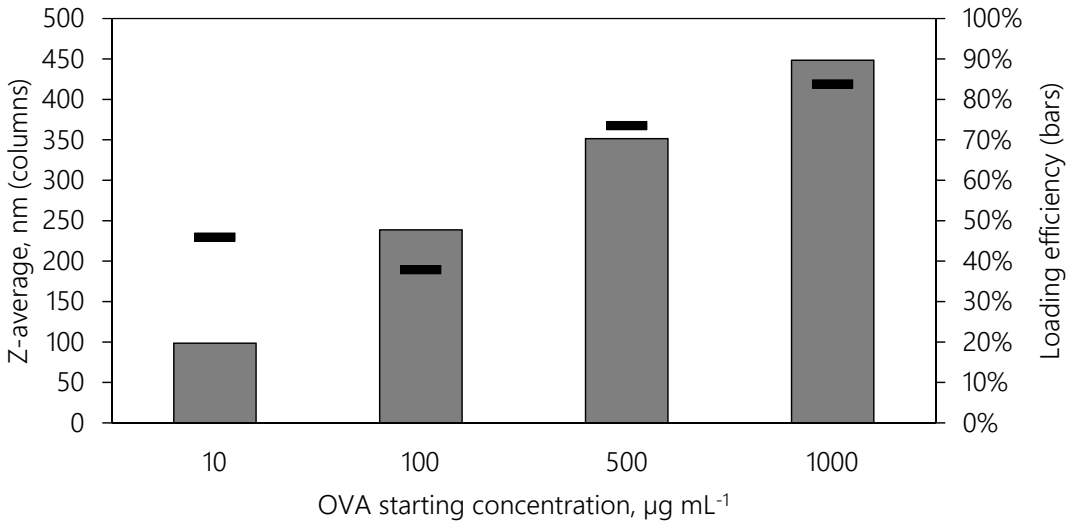

Figure 4-36. Size and LE of starting OVA-CMC mixture.

In the second step, this OVA-CMC mixture (containing 0.1 wt% CMC and 5 - 500 µg mL^{-1} OVA) was added to the chitosan phase (0.1 wt% in 2 % HAc) for final NP formation in ratios of 1:1 and 2:3. Not all nanosuspensions were stable. When the highest OVA concentration was used, NPs agglomerated regardless of which chitosan quality was utilised. Hence, those NPs were not further analysed.

Figure 4-37 gives the resulting LEs for the alternative addition sequence. For the starting concentration of 5 µg mL^{-1} no reliable LE could be measured because the resulting OVA concentrations were below the detection limit (2 µg mL^{-1}) due to encapsulation in the particles and dilution. Accordingly, if such low amounts of protein were to be determined another technique for quantification needed to be applied. LEs after particle formation with the other OVA-CMC mixtures with OVA concentrations of 50 µg mL^{-1}

and 250 µg mL^{-1}, respectively, looked very promising with values of up to 60 % or even 70 %.

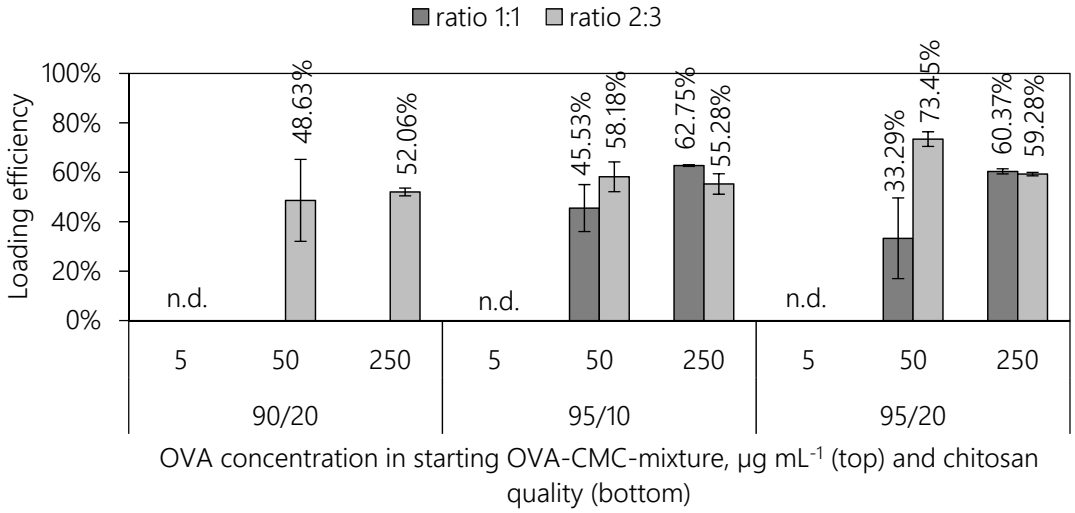

Chitosan quality	*OVA conc., µg mL^{-1}*	*Ratio 1:1*			*Ratio 2:3*		
		Z-average, nm	*PDI*	*ZP, mV*	*Z-average, nm*	*PDI*	*ZP, mV*
90/20	5	365.6	0.192	52.2	320.9	0.263	43.3
	50	330.3	0.200	51.8	293.9	0.230	42.7
	250	353.1	0.224	49.5	290.3	0.234	38.9
95/10	5	376.5	0.285	46.6	319.9	0.348	38.4
	50	352.5	0.255	46.9	276.5	0.282	37.7
	250	319.5	0.238	43.5	249.1	0.261	37.8
95/20	5	437.2	0.277	50.7	476.2	0.303	42.1
	50	425.7	0.294	50.4	365.6	0.296	42.9
	250	399.7	0.274	49.1	336.3	0.280	41.8

Figure 4-37. Protein LE depending on chitosan quality used and OVA concentration in the OVA-CMC mixture (top, n = 3, error bars = SD) and respective particle size, PDI and ZP values (bottom, n = 1).

Those values could not be compared to the previously used method because the highest concentration of 500 µg mL^{-1} OVA in the starting solution, which simultaneously was the lowest concentration used in previous experiments, did not result in stable NPs. Particle sizes measured were generally higher using the new addition sequence in comparison to the standard method described in chapter 4.3.1. This might be a consequence of the lower OVA concentration (confer Figure 4-33). Another explanation may be the sequential addition of first CMC to OVA and then OVA-CMC mixture to

chitosan, which completely changes the interactions during particle formation. The two-step addition could lead to a looser binding between the polymers because many ionic interactions were already saturated when chitosan comes into play.

Generally, it can be said for this trial (and the same was true for the standard method) that particle size decreased with increasing concentration of OVA and that particle sizes were lower if more CMC was utilised for particle formation (2:3 ratio instead of 1:1 ratio). From this trial it could be concluded that the alternative addition sequence was a promising approach to encapsulate OVA more efficiently. Corresponding LC values for the NPs are shown in Figure 4-38.

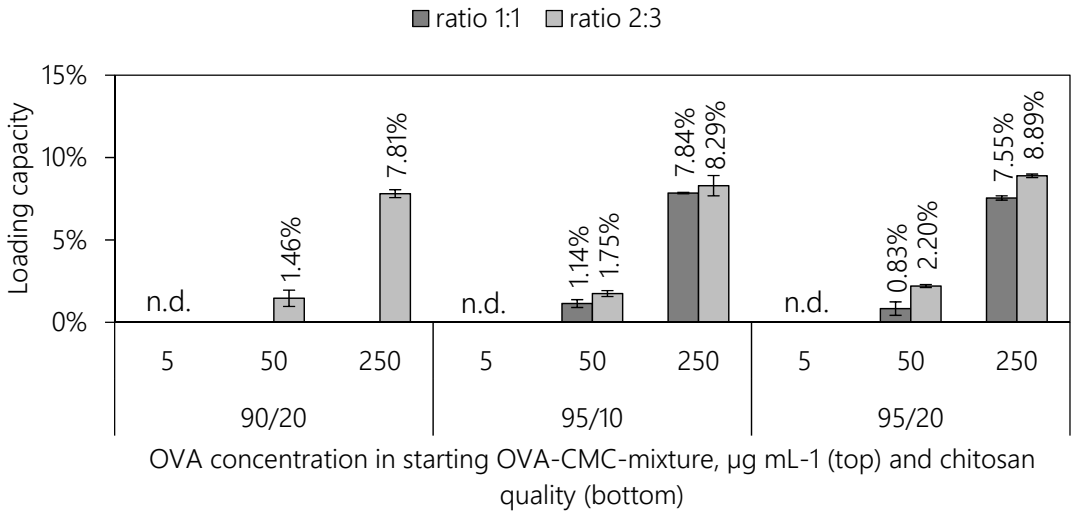

Figure 4-38. Protein LC depending on chitosan quality used and OVA concentration in the OVA-CMC mixture (n = 3, error bars = SD).

The LC values for a starting concentration of 250 µg mL^{-1} were comparable to those achieved with a starting concentration of 1 mg mL^{-1} of the standard method. Hence, less OVA is needed for similar LCs deeming this method promising for the efficient encapsulation of OVA. Future experiments need to verify whether this method can be transferred to other proteins. Nonetheless, as the protein is bound via ionic interactions to the CMC first, it will probably be transferable to other proteins as the standard method was transferable to other proteins, shown by Diedrich [92].

4.4 Development and Characterisation of Nano-in-Microparticles

The developed nanosuspensions were not stable for a long time und could therefore not be used as an application form. The stabilisation of NPs was realised by spray drying of the nanosuspension with a matrix (mannitol was used for this purpose) in this project. It led to the formation of a dry powder, which encapsulates and stabilises the NPs. The resulting particles were named Nano-in-Microparticles (NiM). As the powder was intended for nasal application, the particles must be large enough (above 10 µm) to deposit in the nose [31]. Hence, the fraction of particles below 10 µm should be kept as small as possible and the share of particles below 5 µm should be absolutely minimal because these particles could potentially reach the lung. To assess the aerodynamic behaviour of the developed formulation impaction experiments were performed (see chapter 4.5).

The development of the NPs was described in the previous chapters (4.1 - 4.3). This chapter focusses on the development of a microparticulate dosage form. The aim was to develop a dosage form that can embed all different kinds of chitosan NPs.

4.4.1 Design of Experiments with Mannitol

Instead of developing a NiM formulation directly, this project focussed on the development of pure mannitol microparticles suitable for nasal deposition in the beginning due to much easier experimental conditions. In this case water could be used as solvent in place of a washed nanosuspension. In later experiments the transferability to using a nanosuspension as solvent was tested.

The droplet size after dispersion of the fluid in the spray dryer is crucial for resulting particle sizes as particles will not be larger than the original droplet. To obtain particles suitable for nasal deposition, it is necessary to apply the ultrasonic nozzle when working with the lab spray dryer B-290. Using the ultrasonic nozzle larger droplets and subsequently larger particles (potentially suitable for nasal deposition) compared to the also available two-fluid nozzle could be obtained. Another advantage of the ultrasonic

over the two-fluid nozzle is a narrower droplet size distribution resulting in a narrower particle size distribution. A DoE was utilised to identify the parameters that significantly influence the outcome when spray drying with the B-290 in combination with the ultrasonic nozzle. Varied factors and measured responses of this DoE are shown in Table 4-6.

Table 4-6. Factors varied in DoE and measured responses.

Factors	*Responses*
Inlet temperature (110 - 150 °C) Feed rate (5 - 15 %) Mannitol concentration (5 - 20 %)	Outlet temperature Particle size Span Yield

The volume flow was not changed; it was set to 20 $m^3 h^{-1}$ (corresponding to 50 % aspirator rate), as recommended by the supplier for the ultrasonic nozzle. This rather low volume flow was necessary to allow a longer drying time for the larger droplets (in contrast to smaller droplets created with the two-fluid nozzle). Another opportunity would be to increase the length of the drying chamber. As this was not possible with the B-290, the volume flow was reduced. This simultaneously lowered the separation capacity of the cyclone. Smaller particles will not be separated as effectively from the air stream and therefore will not be collected. This reduces the yield, but it was no drawback within this project. It should rather be seen as a beneficial feature because, as explained above, the share of small particles (especially below 5 µm) should be kept as low as possible. The results of the DoE are given in Table 4-7.

Table 4-7. Varied factors and corresponding particle characteristics of powders produced within the framework of the DoE.

Experiment name	*Run order*	*Inlet temp., °C*	*Feed rate, %*	*Conc., %*	*Outlet temp., °C*	*Particle size, µm*	*Span*	*Yield, %*
N1	14	110	5	5	53	15.5	1.04	47.4
N2	6	150	5	5	69	16.9	1.04	59.4
N3	4	110	15	5	42	14.7	1.02	27.6
N4	19	150	15	5	48	17.0	1.00	39.1
N5	16	110	5	20	52	33.6	1.33	68.1
N6	7	150	5	20	74	25.1	1.11	59.8
N7	10	110	15	20	42	30.1	1.21	39.3
N8	18	150	15	20	49	33.1	0.98	50.5
N9	2	110	10	12.5	50	26.7	1.38	46.7
N10	13	150	10	12.5	55	22.4	1.07	56.5
N11	12	130	5	12.5	64	21.1	1.05	64.7
N12	15	130	15	12.5	44	24.0	1.27	36.9
N13	8	130	10	5	54	15.2	1.03	52.3
N14	5	130	10	20	53	24.8	1.08	53.6
N15	11	130	10	12.5	56	24.1	1.18	56.4
N16	17	130	10	12.5	47	22.6	1.08	54.6
N17	3	130	10	12.5	53	21.3	1.08	52.4
N18	9	130	10	12.5	59	23.4	1.08	50.9
N19	1	130	10	12.5	53	21.3	1.05	52.8

SEM pictures of selected experiments are shown in Figure 4-39. All pictures show spherical, partially indented and partially broken particles. The breakage increased with increasing mannitol concentration. Moreover, the surface of the particles changed with increasing mannitol concentration to a needle-shaped rather than a smooth surface.

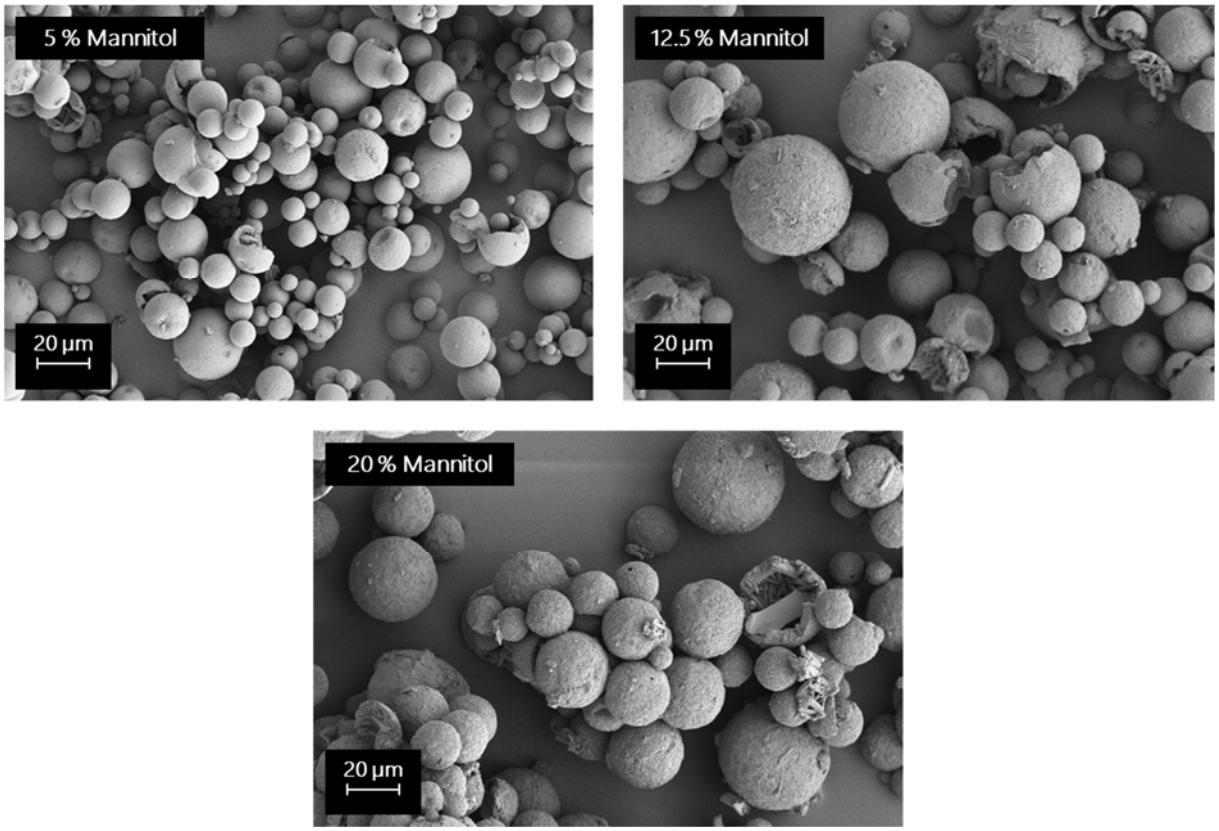

Figure 4-39. SEM images of particles created with a mannitol concentration of 5 % (N3), 12.5 % (N15) and 20 % (N7) at 500-fold magnification.

Model fit with values for R2 and Q2 above 0.5, model validity above 0.25 and reproducibility above 0.5 suggested a significant model. In line with theory, the outlet temperature was found to depend on inlet temperature (positively correlated) and feed rate (negatively correlated). Only a very slight effect of the inlet temperature (negatively correlated) on span could be found. The yield was generally low which could be ascribed to droplets sticking to the surfaces of the spray dryer instead of being dried and then collected in the product vessel. Because of this low yield, it was interesting to take a closer look at the factors that were identified to be significantly influencing product yield and which might change the process based on the findings. As depicted in Figure 4-40, it was found that all three varied factors, inlet temperature, feed rate and concentration, had an effect.

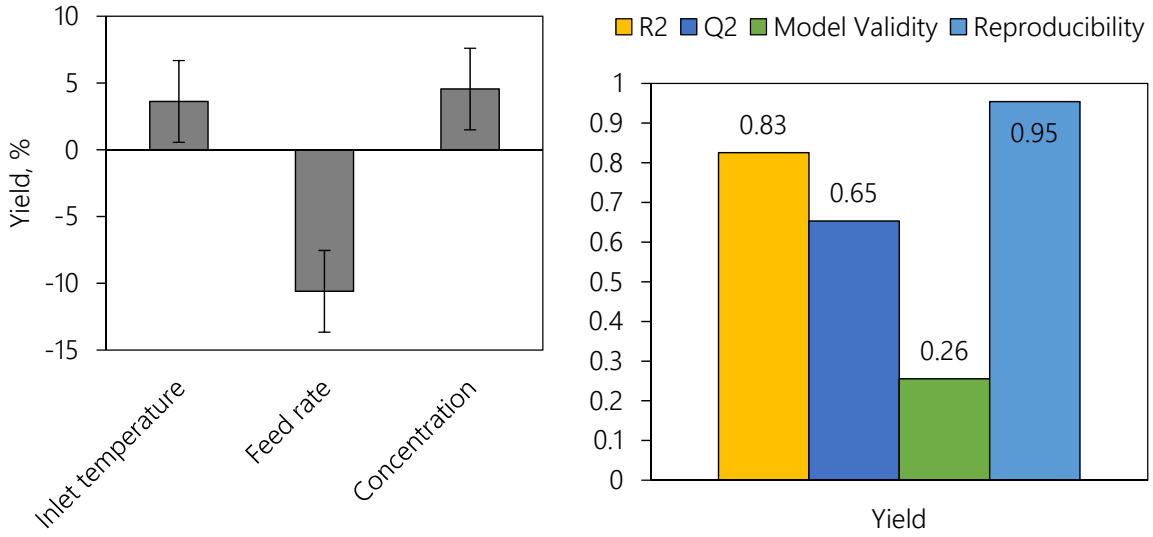

Figure 4-40. Significant coefficients (left) and model fit (right) for particle yield.

While increasing the inlet temperature and concentration increased particle yield, it was reduced by raising the feed rate. This was plausible, as an increased feed rate potentially leads to more sticking on the surfaces a higher inlet temperature and a higher concentration (hence, less solvent) lead to an improved drying leading then to particles which can be collected. However, those parameters influencing the yield had a significant influence on other outcomes as well. The concentration was positively correlated with the particle size. The outlet temperature was significantly influenced by inlet temperature (positive correlation) and feed rate (negative correlation).

The responses particle size and outlet temperature must be ranked as more important for the formulation than the yield. For this reason, a potentially low yield was accepted if the other responses were influenced favourably by a factor. The particle size was found to only significantly depend on the used concentration (Figure 4-41). Within this DoE particle sizes of up to 33 µm could be generated. The corresponding contour plot is given in Figure 4-42.

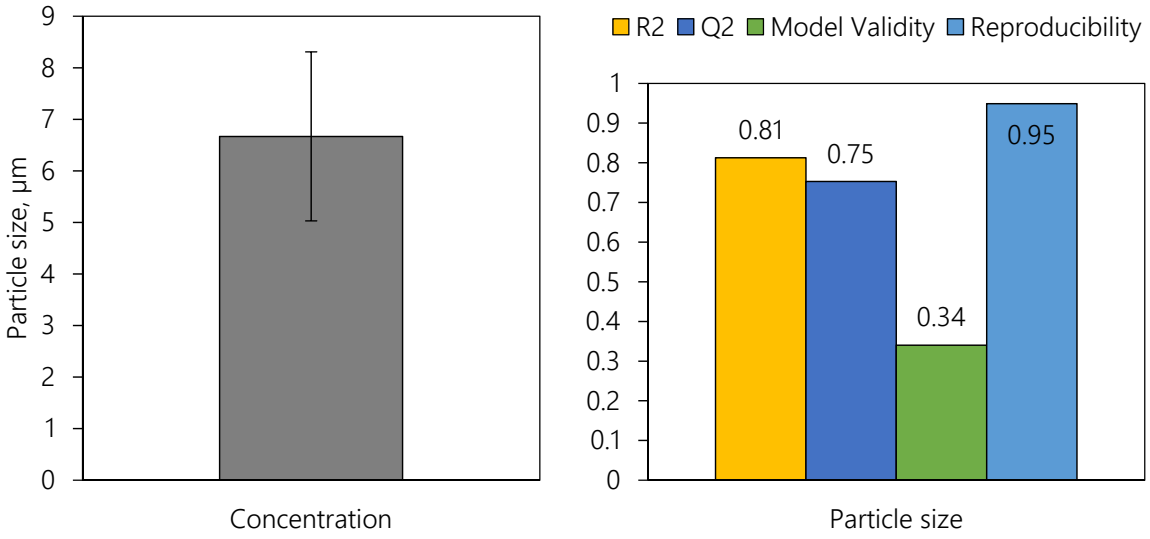

Figure 4-41. Significant coefficient (left) and model fit (right) for particle size.

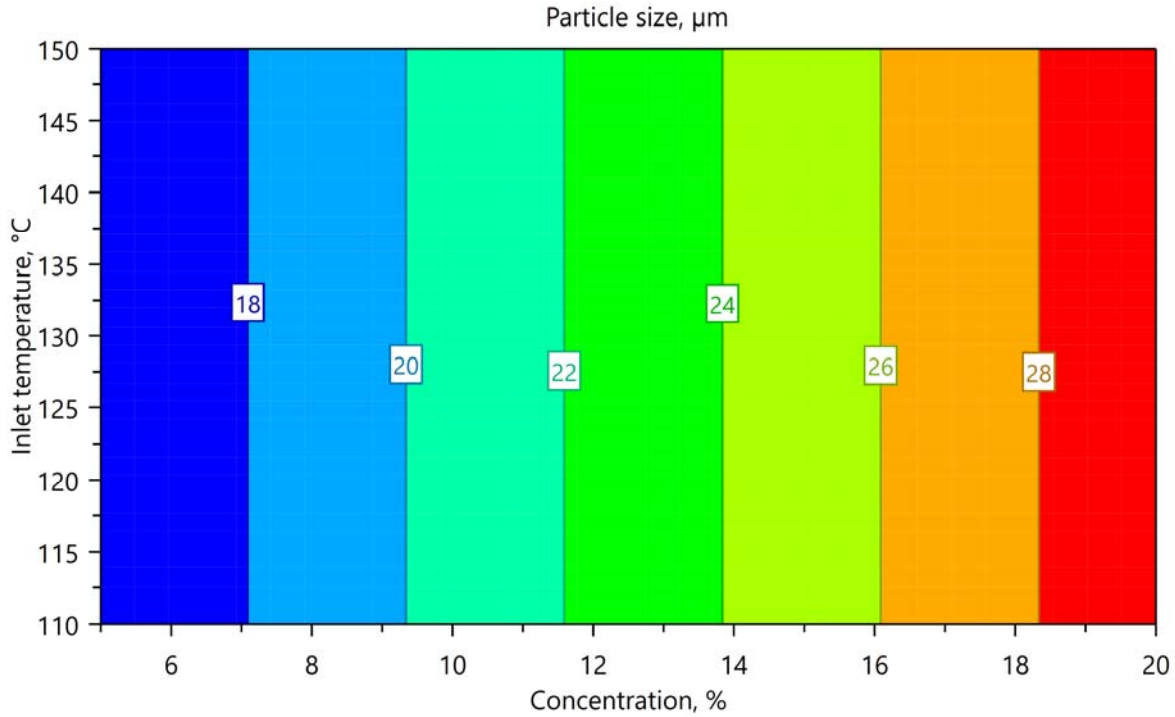

Figure 4-42. Contour plot of the mean particle size as a response of the significant factor concentration.

All produced microparticles met the criterion of exhibiting a mean particle size above 10 µm. Hence, the decision which concentration to use for further experiments was based on the share of particles below 10 µm. When a concentration of 20 % was used this value was below 3 % on average. For concentrations 5 % and 12.5 % the share was below 15 % and 5 %, respectively. Hence, a concentration of 20 % was used for the following experiments.

4.4.2 Spray Drying Large Nano-in-Microparticles

Having obtained the results from the DoE, the development of a spray drying process suitable for producing NiM was the next step. Previous work showed the necessity of keeping the outlet temperature below 40 °C when producing NiM in order to be able to redisperse the incorporated NPs from the matrix upon dissolution [92]. Hence, a spray drying experiment with rather low inlet temperature (110 °C) at a high feeding rate (15 %) was taken (N7, chapter 4.4.1) and used as basis for the development of the NiM formulation. It exhibited an outlet temperature of 42 °C which was rather close to 40 °C. Repeating this experiment, moisture deposition was observed in the product vessel. This was due to very short drying time in the B-290. For final drying, the product was thus placed in a drying chamber for 5 min at 30 °C. To destroy any agglomerates, the powder was gently sieved through a 355 µm-sieve. Depending on the ambient moisture and the batch size it was possible to maintain outlet temperatures below 40 °C even if a feed rate of as low as 12 % was used. However, at high relative humidity in the environment and large batch sizes this could not be achieved.

To obtain NiM, mannitol was dissolved in a washed nanosuspension (produced with chitosan 90/10a and no protein, weight ratio 1:1 of chitosan to CMC). Because of the high concentration of 20 % mannitol, the nanosuspension was not refilled to its original volume after washing but only to a tenth of it, increasing the NP concentration by the factor 10. Assuming a quantitative NP formation, this gave a weight ratio of mannitol to NP of 20:1. Obtained particles exhibited comparable morphology compared to pure mannitol microparticles as depicted in Figure 4-43. Only the size was decreased, probably due to the presence of surface active substances (chitosan, CMC) in the NPs. Furthermore, less breakage of particles could be seen in the SEM images for the NiMs.

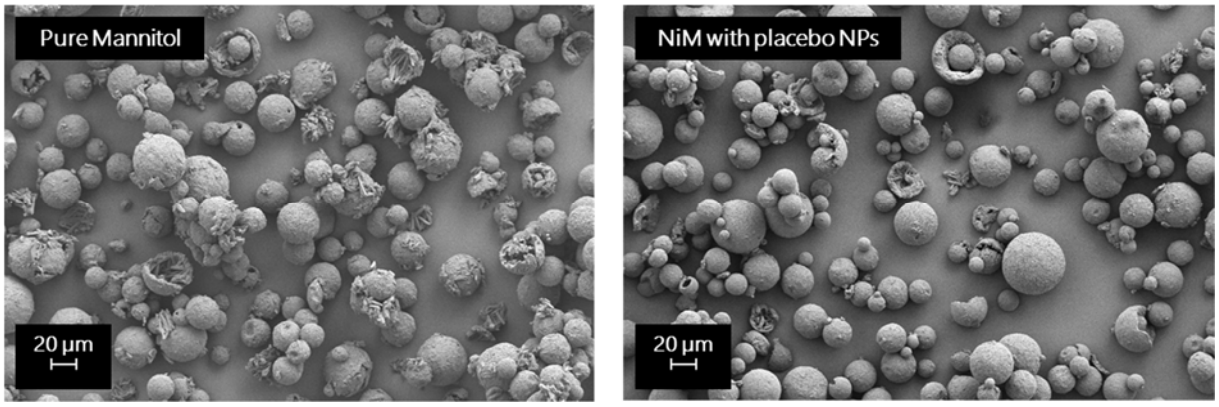

Figure 4-43. SEM images of particles produced with a mannitol concentration of 20 % which was either dissolved in water (pure mannitol) or in nanosuspension (NiM with placebo NPs) with mean particle sizes of 36.8 ± 0.0 µm and 26.6 ± 0.1 µm, respectively, at 250-fold magnification.

The incorporation of placebo NPs in the microparticle matrix resulted in slightly altered surface morphology and size. Particles were still spherical and hollow but their surface appeared smoother for NiM compared to pure mannitol microparticles. This change in surface morphology and size was more pronounced if a protein was loaded in the NPs (Figure 4-44). While the surface of the pure mannitol particles appeared needle-like, the NiM including OVA-loaded NPs appeared smoother. However, the NiM particles were generally more strongly indented which is probably due to the surface activity of all substances that formed the NPs (chitosan, CMC and OVA).

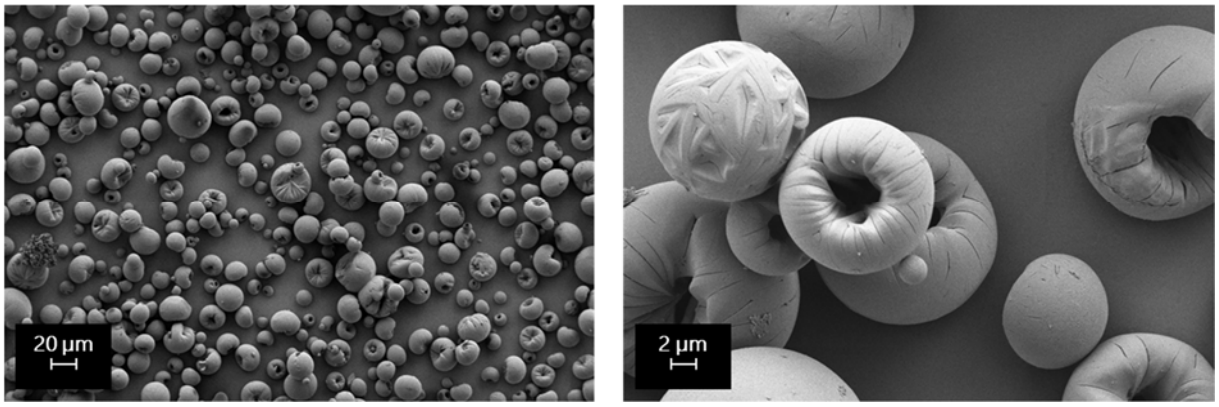

Figure 4-44. SEM images of NiM particles containing OVA with a mean particle size of 21.1 ± 0.3 µm, at 250- (left) and 2 500-fold magnification (right).

Overall, the particle size distribution is narrower when NPs are incorporated as can be seen in Figure 4-45.

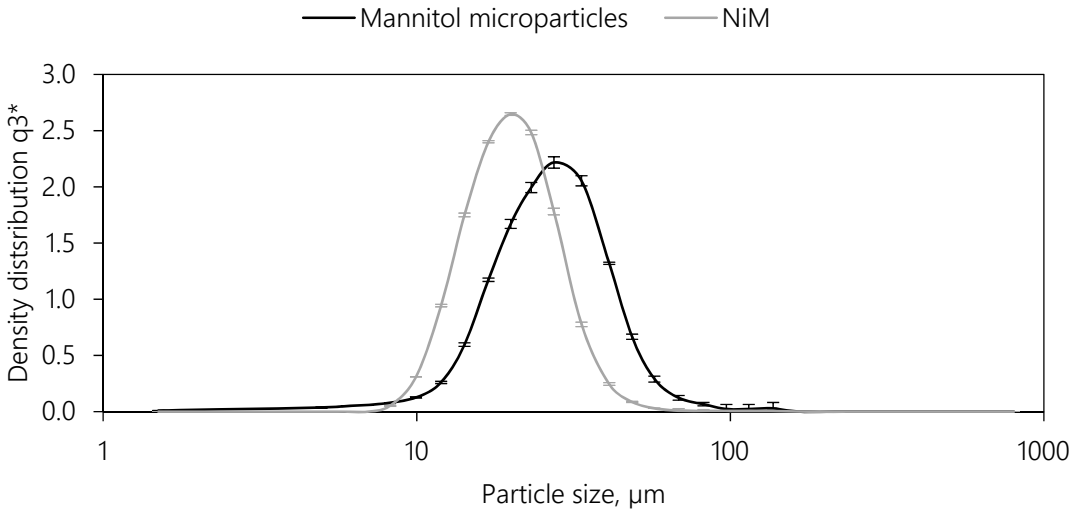

Figure 4-45. Particle size distributions of pure mannitol microparticles and NiM (chitosan 90/20, ratio 2:3, with OVA) exhibiting mean particle sizes of 26.9 ± 0.2 µm and 19.9 ± 0.1 µm and shares below 10 µm of 3.3 % and 2.6 %, respectively.

Respective span values for pure mannitol microparticles and NiM are 1.07 ± 0.04 and 0.88 ± 0.02. Incorporating different kinds of NPs (chitosan 90/10c or 90/20 in a weight ratio of either 1:1 or 2:3) did not result in changed surface morphology or particle size of NiM (data not shown).

As indicator for storage stability (in terms of endurance against elevated humidity) the hygroscopicity of this formulation was tested by DVS exemplarily. Figure 4-46 shows the resulting change in mass plot.

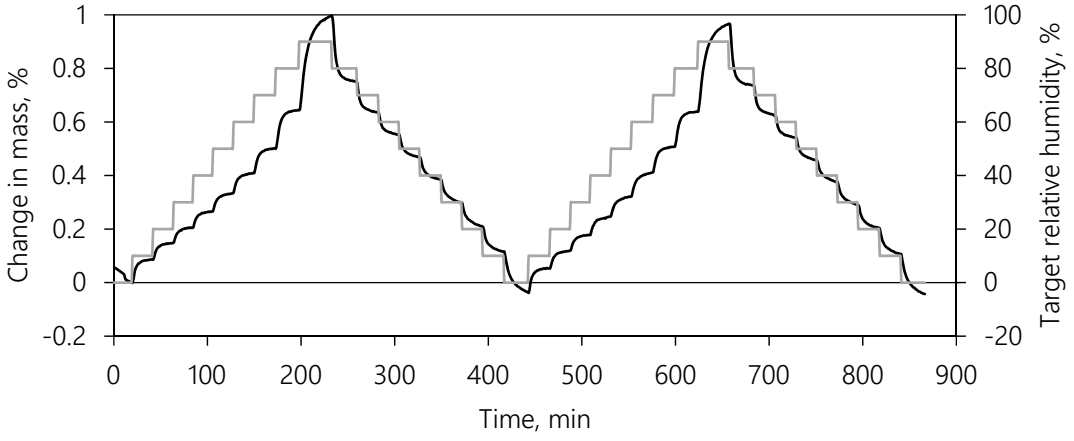

Figure 4-46. DVS change in mass plot of NiM powder as function of changing relative humidity (water) in two cycles. Change in mass is depicted in black and the target relative humidity in grey (n = 1).

The NiM powder showed a mass change of +1.00 % in the first cycle if the relative humidity was raised to 90 %. When lowering the relative humidity, the formulation lost mass, falling even a little below its initial mass which means that the powder was not completely dry in the beginning. The second cycle was performed to assess any permanent changes in the powder by the first cycle. The powder showed a similar curve (maximum mass change of +0.97 %) for the second cycle indicating no changes in the powder.

At 80 % rH the powder showed a mass change of +0.64 %. This can be classified as slightly hygroscopic (mass change of 0.2 - 2 %) according to the Ph. Eur. [129]. From this experiment, it could be concluded that the formulation was not sensitive towards air humidity.

The obtained NiM powder appeared to be a suitable formulation in terms of particle size for nasal deposition and stability against humidity. Hence, follow-up experiments to further characterise it, regarding the redispersibility of NPs and the aerodynamic behaviour, were performed.

4.4.3 Redispersibility of Nanoparticles from Nano-in-Microparticles

The redispersibility of NPs from the NiM formulation is crucial for subsequent uptake in immune competent cells. To achieve this, not only a mild spray drying process but a mild washing procedure to eliminate any free excipients or protein in the supernatant after NP formation was conducted. If those substances were still present in the nanosuspension while spray drying they would probably lead to sticking of the NPs upon dissolution of obtained NiMs. In this project, particles were centrifuged for washing. Depending on the volume of the nanosuspension that was supposed to be washed, the centrifugation could be performed with one centrifugation step (10 mL). If higher volumes were to be washed (50 mL), a multiple step regime was necessary to avoid irreversible particle agglomeration upon redispersion.

Figure 4-47 provides an example data set of the washing procedure of a 10 mL batch produced in a 1:1 ratio of chitosan 90/10c to CMC indicating no substantial size increase before and after the washing procedure.

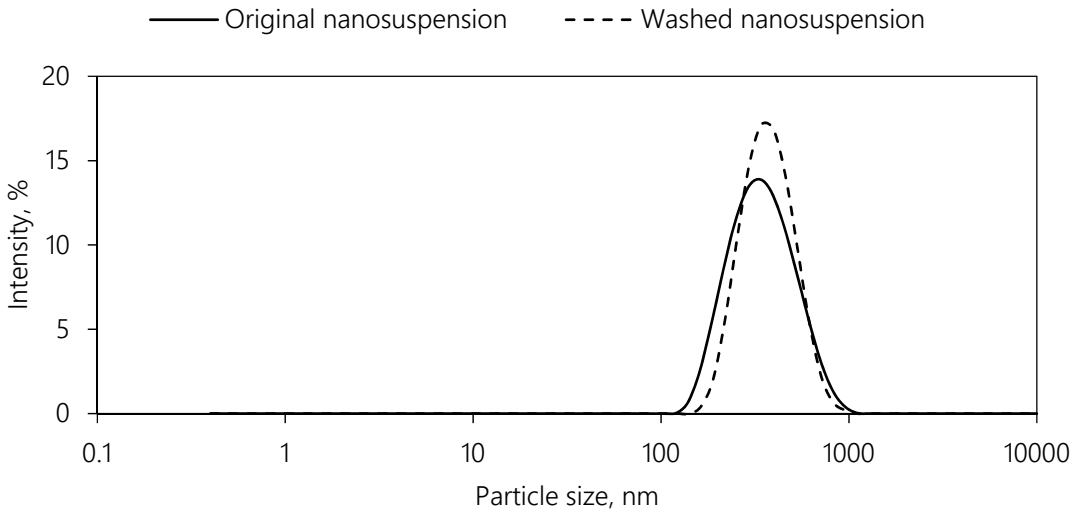

Figure 4-47. Particle size distributions of original and washed nanosuspension exhibiting z-averages of 308 nm and 341 nm, respectively.

As mentioned earlier, keeping the outlet temperature during spray drying at a maximum of 40 °C was necessary to maintain the redispersibility of the NPs from the dry powder (confer chapter 4.4.2). Figure 4-48 gives an example for NPs redispersed from NiM powder (300 mL batch, centrifuged as 6x 50 mL and reunited).

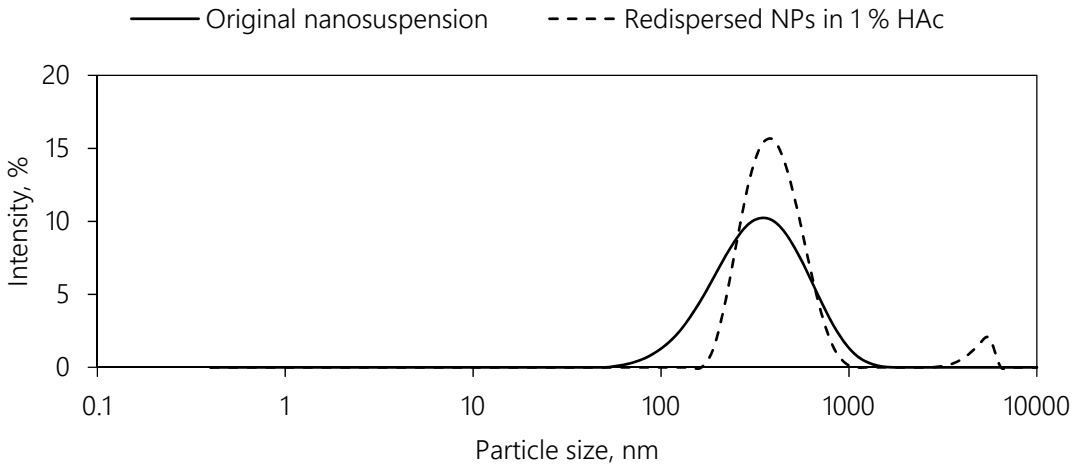

Figure 4-48. Particle size distributions of original nanosuspension and redispersed NPs from NiM formulation in 1 % HAc exhibiting z-averages of 291 nm and 403 nm, respectively.

The NPs were produced with chitosan 90/20 and CMC in a 2:3 ratio. They were redispersed by adding 1 % HAc to the powder followed by gentle shaking. It was not necessary to apply strong shear forces for redispersion of NPs. An increase in z-average could be observed for redispersed NPs: 403 nm as opposed to 291 nm (PDI values were 0.24 and 0.25, respectively). The particle size distribution of the redispersed NiM showed a second peak between 1 000 nm and 10 000 nm. In this size range the measurement cannot be regarded as reliable. Moreover, an intensity distribution is influenced by large particles particularly strongly. Therefore, it is likely that this peak is not related to any substantial amount of particles, but alters calculation of z-average. This increase in z-average was still acceptable, but future experiments should also address the optimisation of the washing process, especially if the 2:3 ratio is utilised for particle formation. Due to the higher particle yield, which probably resulted in a higher extent of sticking between the NPs, the washing process was not as appropriate as for the 1:1 ratio.

Another thing that has to be kept in mind if it comes to *in vitro* uptake experiments of the developed NPs or rather to the NiM formulation is the redispersibility of the NPs in a buffer/medium suitable for the use in cell culture. If particles were redispersed in diluted HAc and given onto the cells the pH value would probably harm the cells. If particles are redispersed in a more physiological medium (PBS), in contrast to diluted HAc, a slight swelling of particles (probably due to the higher pH and salt concentration) can be observed as an increased z-average, shown in Figure 4-49 (300 mL batch, centrifuged as 6x 50 mL and reunited). NPs for this experiment were produced in a 1:1 weight ratio of chitosan 90/10a and CMC. This increase must be kept in mind when producing NPs because it cannot be eliminated if utilising NPs obtained via ionic gelation from chitosan and CMC.

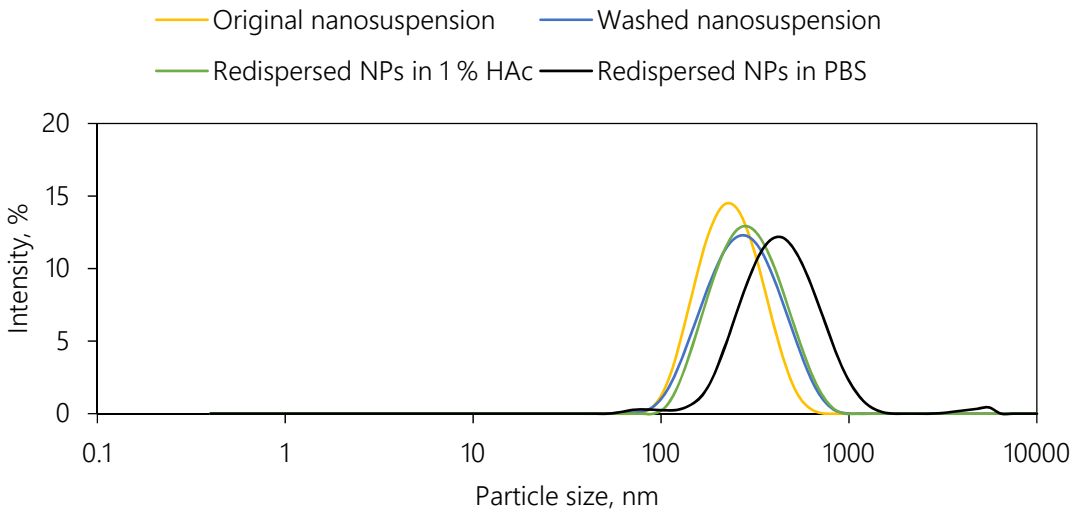

Figure 4-49. Particle size distributions of original and washed nanosuspension, redispersed NPs from NiM formulation in 1 % HAc and in PBS exhibiting z-averages of 210 nm, 241 nm, 258 nm and 378 nm, respectively.

4.5 Aerodynamic Characterisation of Developed Nano-in-Microparticles

The potential of a formulation to deposit in the nose cannot necessarily be assessed by using the geometric particle size, determined by laser diffraction. Utilising an impaction analysis which takes characteristics such as density and morphology into account is more suitable. For example, needle-like shaped particles with a low density exhibit a higher geometric than aerodynamic size and hence, are less likely to deposit in the nose than suggested by their geometric diameter. The developed NiM formulation consisted of hollow particles. Consequently, the aerodynamic particle size might be lower than the geometric one. Potentially it could even be too low to ensure nasal deposition. Immune competent cells that could take up the NPs are situated throughout the mucosa of the respiratory tract. Hence, particles deposited in the lower respiratory tract could still be effective, but, for regulatory reasons, a formulation must be deposited either in the nose or in the lung. Accordingly, the developed formulation should deposit quantitatively in the nose.

All experiments that were performed in the context of the aerodynamic characterisation were performed with NiM including OVA.

4.5.1 Dispersion from a Nasal Powder Device

At first, the eligibility of a nasal powder device, namely the UDS powder, was tested regarding its dispersion ability for the powder and the powder retention in the device. The formulation showed no device retention which was determined by weighing the device before and after the shot. The resulting particle size distributions are depicted in Figure 4-50.

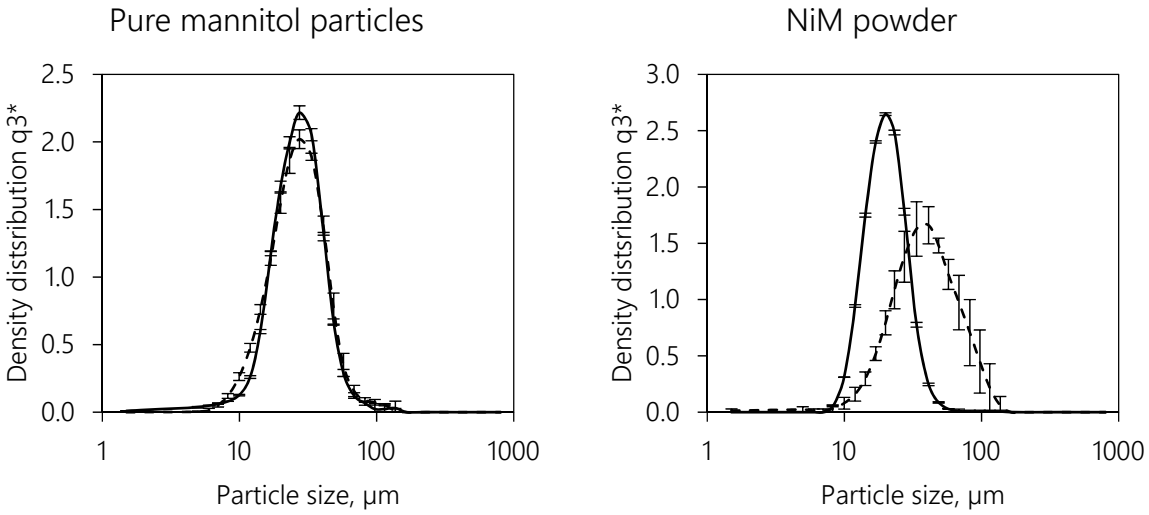

Figure 4-50. The particle size distribution after dispersion via the RODOS (solid lines) and the SPRAYER module (dashed lines) on the left of pure mannitol particles (RODOS: x_{50} = 26.9 ± 0.2 µm, SPRAYER: x_{50} = 26.8 ± 0.7 µm) and on the right the corresponding size distributions for the NiM powder are shown (RODOS: x_{50} = 19.9 ± 0.1 µm, SPRAYER: x_{50} = 31.6 ± 6.7 µm) (n = 3, error bars = SD).

The particle size distributions from dispersion via the RODOS (pressurised air, full dispersion) and the SPRAYER module (dispersion from device) for pure mannitol microparticles and NiM formulation are shown in Figure 4-50, depicting a difference between the two dispersion mechanisms for the NiM powder but not for the pure mannitol particles. This is probably due to different cohesion behaviour of the particles. While the spherical pure mannitol particles with a slightly rough surface were easily separated, the NiM could not be dispersed by the UDS powder as easily. This was because of indentions in the overall smooth surface which could get interlocked and hence are characterised by a particle size distribution which was shifted towards larger particle sizes showing a mean particle size of 31.6 ± 6.7 µm with a span of 1.4 ± 0.2. This

shift towards a larger mean particle size made the NiM powder even more suitable for nasal deposition. It could hence be concluded that the UDS powder device was suitable for the application of the developed formulation.

4.5.2 Development of a Method for Quantification of Nano-in-Microparticles in Deposition Studies

To assess the nasal deposition of the NiMs, a quantification method was needed. As usually done, it was tried to develop a method to quantify the active ingredient (in this case: OVA). However, no reliable quantification method could be developed. The first problem was the compatibility of the BCA assay (which was used for protein quantification before within this project) with the stage coating, which was applied to each stage of the NGI and the nasal expansion chamber or the nasal cast prior to each experiment in order to avoid particle bouncing on the hard surfaces. Depending on the utilised quality of 1,2-propanediol, which was used as component in the stage coating, it interfered with the BCA assay, probably due to impurities (reducing shares) that react with the BCA themselves. The problem with reducing impurities exists for mannitol, too. The second problem was the pH or the salt concentration of the samples. In order to dissolve the NPs either a strong acid (citric acid) or a high salt concentration (10 % NaCl in 10x PBS) was necessary. If citric acid was used, the resulting pH of the samples would have been too low to allow a reduction of copper by the protein. Concentrations of sodium chloride above 1 M (corresponding to 6 %) are not compatible with the BCA assay, as specified by the manufacturer. To conclude, the BCA assay could not be used for quantification of the protein content.

Instead of quantifying the protein, it was tried to quantify the carbohydrate part of the NPs with the anthrone assay. The method developed for determining chitosan and CMC individually could be adapted (increased incubation time) to quantify NiM powder in a concentration between 0.25 mg mL^{-1} and 2 mg mL^{-1} (coefficients of determination above 0.98). However, the assay was also not compatible with the stage coating

resulting brownish colours. Figure 4-51 displays the calibration (top row) and the samples (rows 2 - 3).

Figure 4-51. Image of microplate after performed anthrone assay showing an incompatibility between the assay and the stage coating resulting in brownish colours (rows 2 - 3) instead of light yellow-green ones (row 1).

To overcome the challenges associated with quantifying the protein and the NPs within the formulation, another approach was chosen. The NiM formulation mostly consisted of mannitol as described earlier. Thus, it was tested to quantify the mannitol in the formulation by a commercially available assay that works enzymatically. Hence, no interferences were to be expected due to high specificity. Instead of utilising mannitol as calibration substance, the NiM powder was used because the exact ratio of mannitol to NPs was unknown because neither the concentration of excipients involved in particle formation nor NPs in total could be determined (please refer to chapter 4.1.5 for more information on this topic). The calibration in the range of 0.25 - 2 mg mL^{-1} gave coefficients of determination above 0.99.

4.5.3 Nasal Deposition of NiM Formulation

For assessment of the nasal deposition an NGI in combination with a nasal expansion chamber or a nasal cast was used. Usually, the NGI is used to determine the fine particle fraction (particles below 5 µm) in formulations intended for pulmonary delivery [113]. In this project it was used to show that (preferably) no fine particle fractions can be measured.

The nasal deposition profile of the NiM formulation was investigated with and without applied airflow. If the NGI was used, the airflow was set to 15 L min^{-1} (impaction analysis

is only feasible with an applied airflow, this volume flow corresponds to normal breathing rate of an adult). With this airflow the cut-off diameter for the FPF of 5 µm lies between stage 4 (cut-off diameter 5.64 µm) and stage 5 (cut-off diameter 3.18 µm) and was calculated by interpolation between those two stages according to the Ph. Eur. [113].

In a first setting the deposition profile of the NiM powder in a 2 L nasal expansion chamber was examined. This adapter is recommended for deposition profile assessment of nasal sprays by the FDA [130]. The resulting deposition profile is displayed in Figure 4-52.

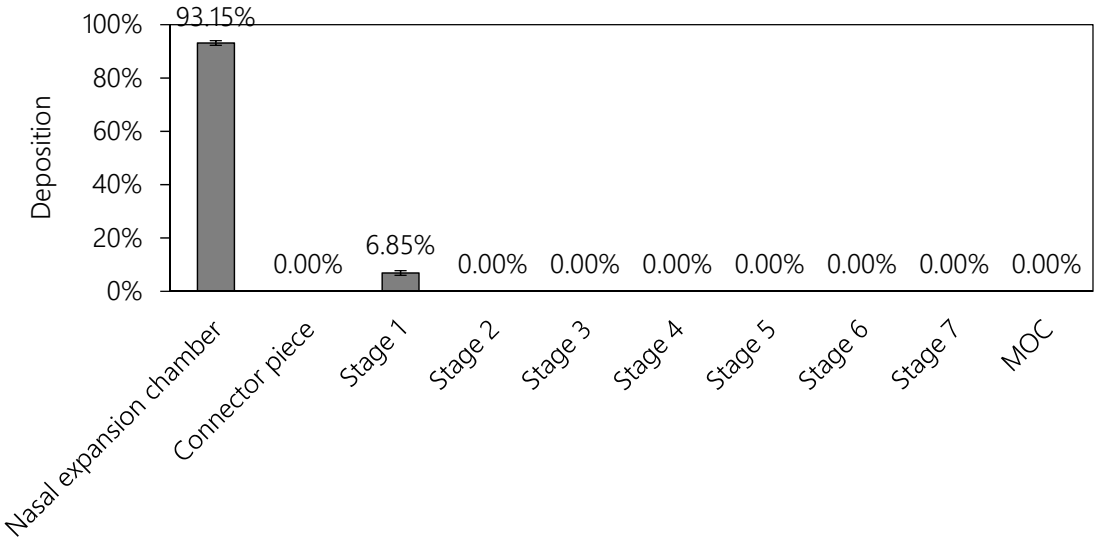

Figure 4-52. Deposition profile of the NiM formulation utilising the NGI in combination with the nasal expansion chamber at an airflow of 15 L min^{-1} (n = 3, error bars = SD).

The deposition in the nasal expansion chamber was found to be 93.15 % at a recovery of 97.5 ± 3.4 %. An FPF of only 0.4 % was calculated from these results. Hence, the formulation mostly deposited in the nose as intended.

For further characterisation of the nasal deposition profile, the nasal expansion chamber was replaced with the nasal cast. Apart from that, the same setup (including the airflow of 15 L min^{-1}) was used. The resulting deposition profile can be seen in Figure 4-53.

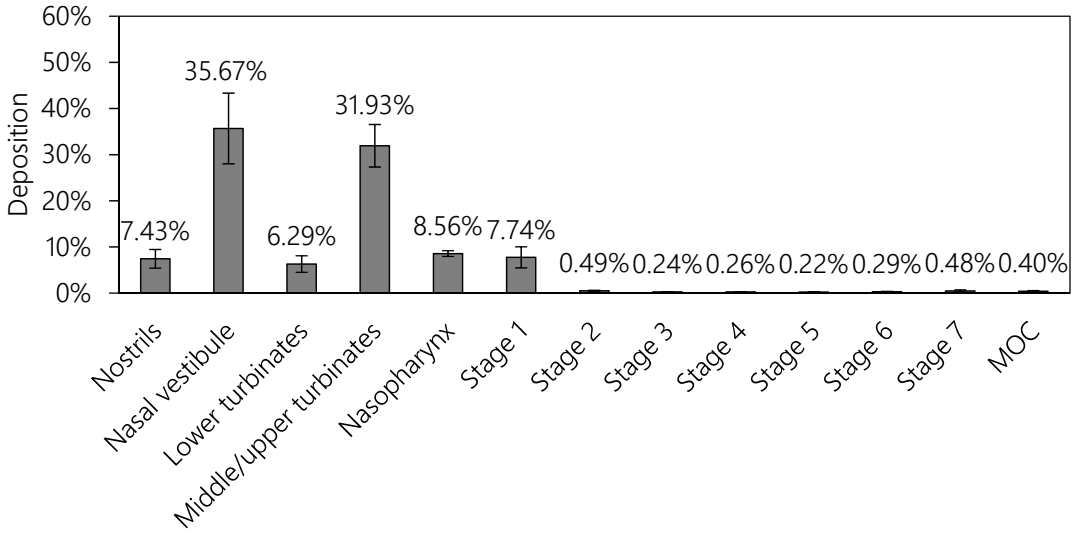

Figure 4-53. Deposition of the NiM formulation utilising the NGI in combination with the nasal cast at an airflow of 15 L min^{-1} (n = 2, error bars = min/max).

Ideally, a nasal powder intended for vaccination would be deposited equally over the nose without any deposition in nostrils and no postnasal fraction. These criteria are not met (depicted in Figure 4-54). Especially noticeable is the low deposition of 6 % in the area of the lower turbinates which is probably due to the upward administration of the powder resulting in more likely deposition in the upper parts of the nose. This effect was already described by others [131,132]. The total nasal fraction was calculated to be 90 ± 3 % and the FPF to be 1.6 %. Generally, it can be said that the results gained with the NGI in combination with the nasal expansion chamber and with the nasal cast were in good agreement.

Usually, a nasal powder would be applied while the patient breathes normally. In this project it was tried whether a patient holding his breath (no airflow applied) would decrease the postnasal fraction. Therefore, another experiment only using the nasal cast plus a cup to collect the postnasal fraction was performed to investigate the influence of the previously applied airflow on the regional deposition and especially on the postnasal fraction. The resulting nasal deposition profile was compared to the values obtained at an airflow of 15 L min^{-1} (Figure 4-54). Moreover, an ideal profile indicating equal distribution over all nasal surfaces excluding the nostrils is added in the diagram.

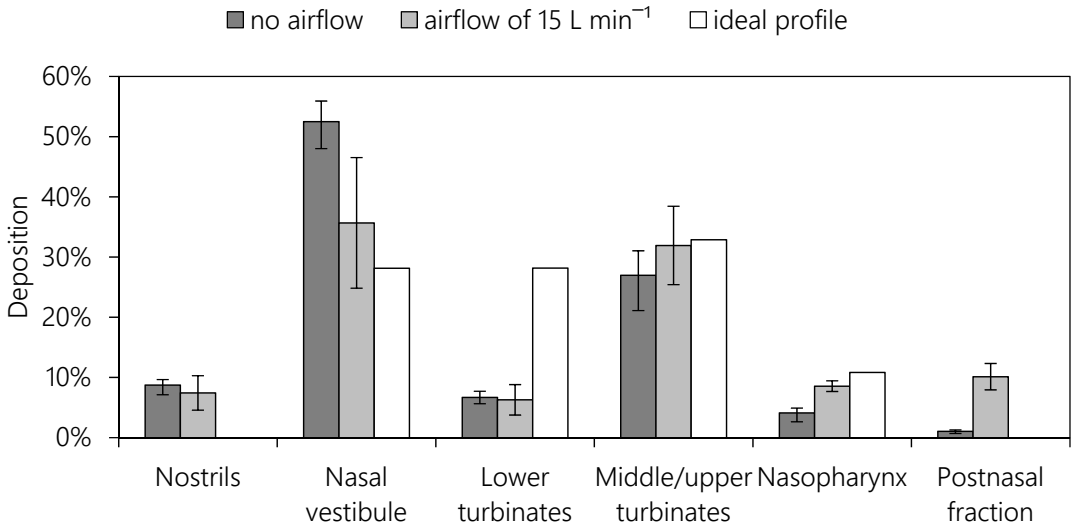

Figure 4-54. Deposition of the NiM formulation utilising the nasal cast and no airflow (n = 3, error bars = SD) in comparison to previously gained values if NGI was operated at 15 L min^{-1} (n = 2, error bars = min/max) and ideal profile.

The comparison reveals a decreased postnasal fraction of 1.0 % (instead of 10.1 %) if no airflow was applied. Generally, if an airflow was applied, a shift in deposition towards the rear parts of the nose could be observed. The deposition in the nostrils and the area of the lower turbinates was comparable while especially the deposition of powder in the upper parts of the nose was increased with no applied airflow. This can be explained by exactly this – the missing airstream towards the nasopharynx. This enables the powder to reach the upper parts of the nose instead of being drawn through the larger internal openings towards the posterior parts.

Concluding the aerodynamic characterisation experiments, it can be said, that the developed NiM formulation seems suitable for nasal deposition. Potential improvements of this formulation should aim at a lower deposition of the formulation in the area of the nostrils and the nasal vestibule.

4.6 In Vitro Uptake Experiments

First *in vitro* uptake experiments were performed with the produced NPs consisting of chitosan and CMC. To make the particles visible in FACS and ImageStream analyses the chitosan was labelled with FITC prior to particle formation with CMC.

NPs were produced with FITC-conjugated chitosan (dissolved in 2 % HAc to 1 mg mL^{-1}) and CMC (dissolved in water to 1 mg mL^{-1}). If OVA was used it was dissolved to a concentration of 1 mg mL^{-1} in the chitosan phase. NiM utilised for *in vitro* experiments were spray dried with the two-fluid instead of the ultrasonic nozzle. A lower concentration of mannitol (2 % instead of 20 %) and a refilling of the nanosuspension to its original volume after the washing was used. Refilling resulted in an identical weight ratio of mannitol to NPs of 20:1. The lower mannitol concentration led to much smaller particles of approximately 2 µm. This was done because of the higher particle yield that could be achieved with this setup. NPs were redispersed in cell culture medium before uptake experiments. For this reason, the size of the NiM was not decisive. Images of the NiM formulations (without and with OVA) are shown in Figure 4-55.

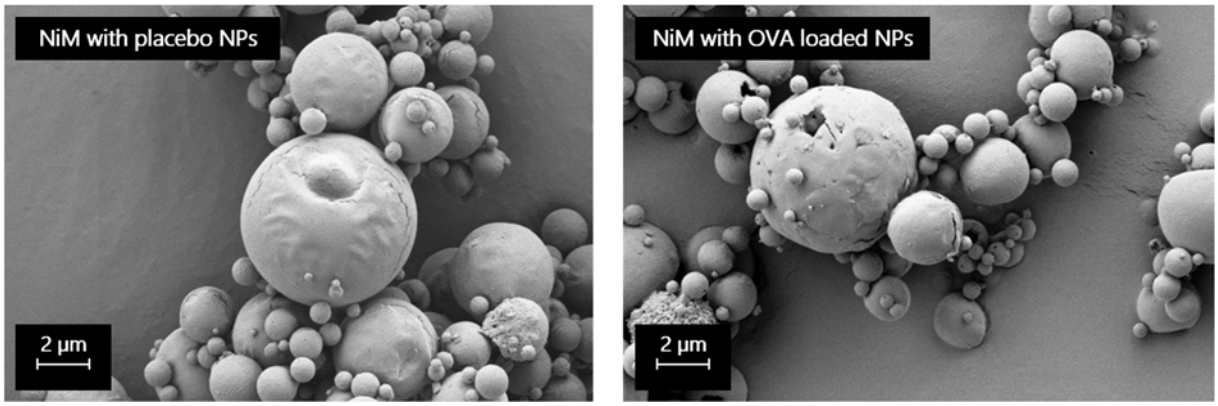

Figure 4-55. SEM images of particles created with a mannitol concentration of 2 % which was either dissolved in a nanosuspension (chitosan 90/10c and CMC in a weight ratio of 1:1) not containing or containing OVA, with mean particle sizes of 2.4 ± 0.0 µm and 1.9 ± 0.0 µm, respectively, at 5 000-fold magnification.

In vitro experiments were performed with the goal to assess whether the uptake of the NPs was concentration dependent and whether the size of the NPs influenced their uptake. FACS results from uptake experiments are shown in Figure 4-56.

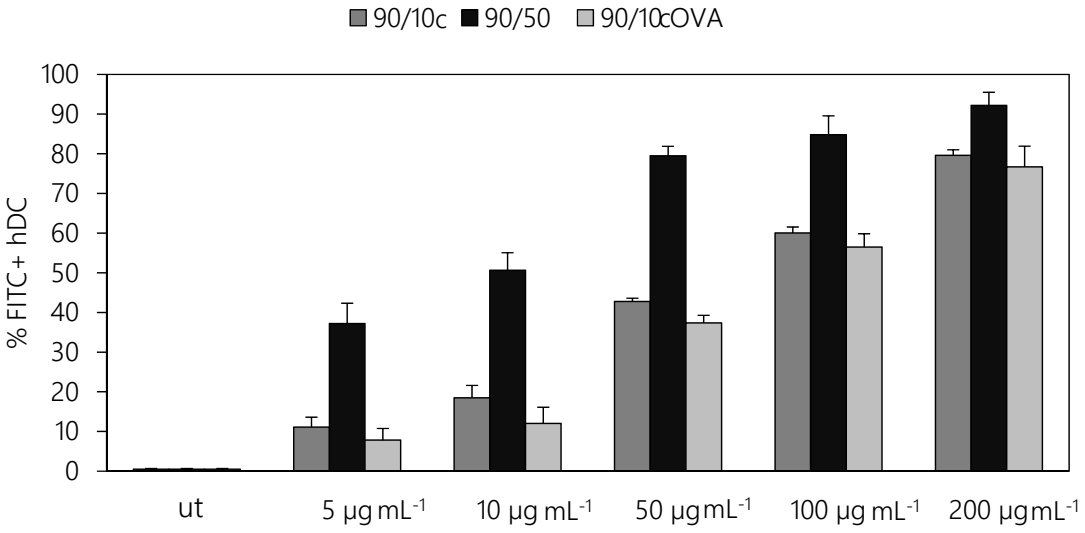

Figure 4-56. Results of flow cytometric analyses of human DCs (hDCs) incubated with FITC-conjugated NPs (chitosan and CMC in a weight ratio of 1:1, if OVA was incorporated this is indicated by "OVA") in different concentrations compared to untreated cells (ut). NP association is indicated as % FITC+ signal (n = 3, error bars = SD).

The concentration of NPs added to the cells (as indicated on the x-axis) was determined based on the assumption that all particle-forming excipients actually formed NPs. As shown earlier, this is not the case (chapter 4.1.5). Therefore, those values can only be taken as approximations. A concentration dependent uptake could be measured for all particles. Moreover, a size dependency became obvious in this experiment. Larger NPs (formed with chitosan 90/50, approximately 1 000 nm) showed a higher association than smaller ones (formed with chitosan 90/10c, approximately 350 nm). Particles with incorporated OVA (approximately 300 nm) showed a slightly lower association than their OVA-free counterparts.

Those results were unexpected. Usually smaller particles up to a size of 500 nm are described as being taken up to a higher extent into dendritic cells compared to microparticles (chapter 2.2.1.1). Further experiments were performed to verify these results. A concentration of 100 µg mL^{-1} was used for all subsequent experiments. In Figure 4-57 the FACS results using three different particle sizes (approximately 220 nm, 400 nm and 1 000 nm after redispersion) are shown, confirming the previous results. The larger the particles, the higher the share of FITC associated cells.

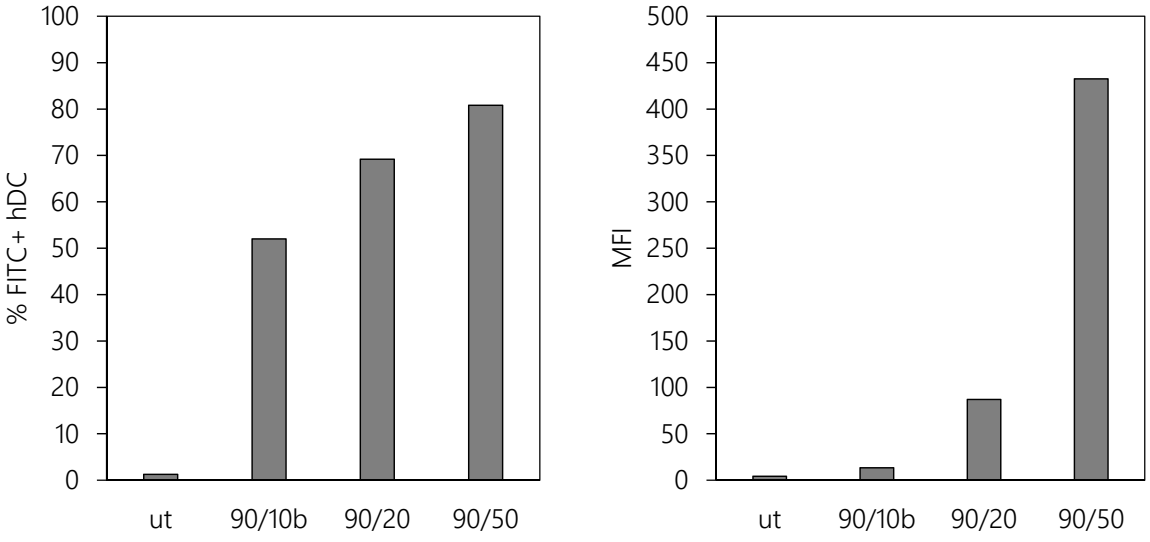

Figure 4-57. Results of flow cytometric analyses of hDCs incubated with FITC-conjugated NPs (different chitosan qualities and CMC in a weight ratio of 1:1) compared to untreated cells (ut). NP uptake is indicated as % FITC+ signal (data of one representative experiment).

In addition to the percentage of FITC+ cells (Figure 4-57, left) in the right panel of Figure 4-57 the median fluorescence intensity (MFI) is plotted. It indicates the brightness of the FITC+ cells, therefore giving an indication about the amount of FITC in the cell. This diagram shows an even higher increase with increasing particle size. This was to be expected because larger particles consist of more material which hence shines brighter.

Nonetheless, the question remained why the results did not follow the literature. To investigate this question, ImageStream analyses were performed. Via imaging they show whether a particle is in the cell or only attached to its surface, as shown in Figure 4-58. Results are shown in Figure 4-59.

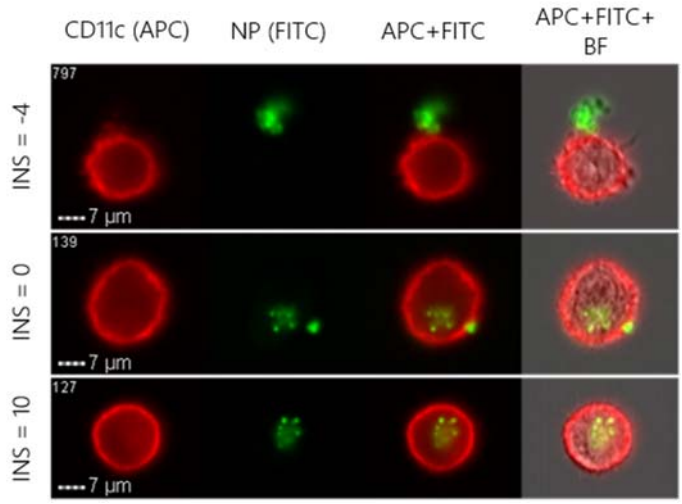

Figure 4-58. Representative images of hDCs incubated with FITC-conjugated NPs (chitosan 90/50) analysed with ImageStream. The APC channel shows CD11c membrane counterstaining. Channel overlay is indicated by "+", BF = brightfield.

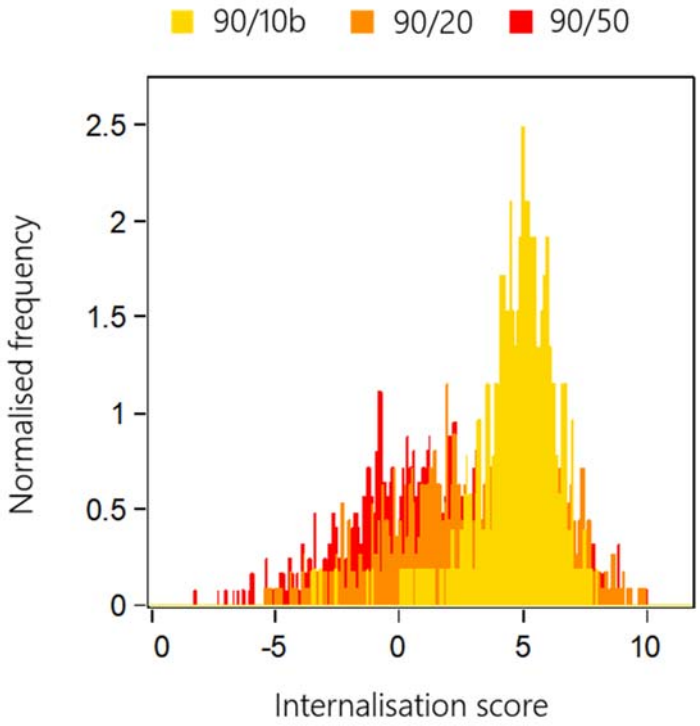

Figure 4-59. Internalisation score histogram of one representative experiment with FITC-conjugated NPs (different chitosan qualities and CMC in a weight ratio of 1:1) with median internalisation scores (INS) of 4.95, 3.42 and 1.56 for chitosan 90/10b, 90/20 and 90/50, respectively.

The results achieved by FACS analysis could be differentiated with the ImageStream results. The larger particles (chitosan 90/50) could be localised externally rather than internally, which could be described by the lower INS of 1.56 compared to 4.95 and 3.42 for NPs with chitosan 90/10b and 90/20. This indicated increased extracellular adhesion

to DCs with increasing particle size despite extensive washing prior to FACS and ImageStream analyses. Hence, the lower uptake of the NPs containing OVA, as shown in Figure 4-56, can quite possibly be explained by the smaller size of those NPs reduced in overall uptake but simultaneously a higher level of intracellular uptake, consistent with the results presented for chitosan quality 90/10b in comparison to 90/20. From these experiments, it can be concluded that the smallest particles are best suited for intracellular uptake in DCs.

Future experiments will examine the uptake of NPs in other cell types, such as macrophages and epithelial cells. Moreover, experiments to elucidate the uptake mechanisms and subsequent activation of DCs will be conducted. It is important to use unstained NPs for this, as the FITC-tag changes chitosan and hence particle characteristics.

5 Overall Findings, Concluding Remarks and Future Prospects

While the experimental results achieved in this dissertation project were presented in the previous chapters, the following chapter provides an overall discussion of those results, concluding remarks and future prospects.

The first part of the results dealt with the development and characterisation of nanoparticulate formulations consisting of chitosan and CMC or DOC. NPs consisting of chitosan and CMC could be produced in different ratios. By gradually increasing the amount of added CMC, the particle size could be decreased. However, at some point particle size started increasing dramatically (visible as agglomeration of nanosuspension, at a chitosan to CMC ratio of approximately 1:2). This instability could be correlated with the ZP. If the latter drops below +30 mV, no stable nanosuspension will be obtained. Two stable weight ratios (1:1 and 2:3) were picked for further experiments. This ZP drop was not found for NPs consisting of chitosan and DOC. ZP stayed above +30 mV even if utilising higher amounts of counterion.

In literature usually penta-sodium triphosphate (TPP) is used as cross-linker for chitosan NPs [122,133–135]. It has five charges per molecule while exhibiting an even smaller molecular weight of 253 g mol^{-1} (without sodium ions) compared to DOC (415 g mol^{-1}). Using TPP as counterion, Fan et al. [136] observed a drop of the ZP below +30 mV with a simultaneous increase in particle size. Therefore, the cross-linking capability can be ascribed completely to the availability of multiple charges per molecule rather than to the molecular weight of the counterion.

The size of resulting NPs was not only governed by the ratio of chitosan and counterion (CMC and DOC). It also depended on the chitosan quality. Chitosan is characterised by its molecular weight and DDA. The molecular weight was positively correlated with particle size. This effect was also found by others who utilised different chitosan qualities for NP production [137–140]. Nonetheless, usually only one or two qualities were used for comparison. In this project a broader overview over achievable sizes was provided by using up to 14 chitosan qualities.

By contrast, the DDA only influences particle size to a very small extent – at least as long as CMC was used as counterion. However, if utilising DOC as counterion, the particle size negatively correlated with DDA. This effect could not be explained by the methods used in this project.

Furthermore, it was not only important to measure size and ZP in order to characterise the NPs, but also to determine the yield of NPs. The term yield, as used in this thesis, signifies the amount of particle forming excipient that actually forms particles. This was of high interest for two reasons. On the one hand, it would allow a better assessment of the impact of different counterions, chitosan characteristics and utilised ratio on particle yield. On the other hand, it would facilitate a determination of the ratio of NPs to encapsulated protein. Admittedly, no reliable method for quantification of NP yield could be identified within this work. Nonetheless, making use of the degree of turbidity of nanosuspensions provided suggestive evidence about the particle yield (higher turbidity indicated higher particle yield). If more counterion (CMC or DOC) was utilised or particles were formed with CMC in contrast to DOC higher yields were achieved. Future projects should address the topic of NP quantification by either finding a suitable method to quantitatively separate the excipients (and then being able to make use of the anthrone assay which was found to quantify chitosan regardless of molecular weight and DDA) or by finding a novel technique to solve this question.

From the results it could be concluded that CMC was the more suitable counterion. It was the better cross-linker and helped achieving higher particle yields. Nonetheless, literature describes DOC for formation of NPs with chitosan for nasal administration. This is due to its penetration enhancing effect on nasal absorption which might contribute to the functionality of NPs [79]. A recommendation to be made based on the experimental results in this thesis is thus that if *in vitro* experiments show a need for an absorption enhancer, a combination of CMC and DOC as counterions could be used. Preliminary experiments showed suitable particle sizes if CMC and DOC were each dissolved to a concentration of 1 mg mL^{-1}, regardless of whether mixing took place prior

to addition to chitosan phase or whether CMC and DOC were added subsequently to chitosan phase.

It was furthermore important to not only characterise the resulting particles, but also the particle formation process. For this purpose, ITC was used in this project. This technology was also applied by other researchers to examine differences in particle formation caused by different cross-linkers or different solvents [141–143]. The effect of the two utilised counterions could not be studied within this project because no suitable common solvent for ITC was found for both chitosan and DOC, a crucial prerequisite for ITC measurements. Hence, only CMC could be used as counterion in ITC measurements. In those, ITC was utilised to assess differences between various chitosan qualities used for particle formation. Differences were found to be based on the DDA of the respective chitosan resulting in a lower enthalpy and simultaneously a lower stoichiometric ratio for a lower deacetylated quality, which indicated an effect of DDA on the particle formation process. From this, it could furthermore be concluded that the DDA influenced particle yield (positive correlation between DDA and yield).

Protein encapsulation experiments were only performed with NPs consisting of chitosan and CMC because they were regarded as advantageous over those formed with chitosan and DOC. In those experiments the DDA was found to substantially influence the protein loading of NPs. Additionally, the ratio between chitosan and CMC was decisive for encapsulation. A higher DDA and more added CMC were found to provide favourable conditions for higher LC. Other factors affecting protein encapsulation were the solvent and temperature. Increasing the concentration of OVA in the starting solution gave higher LCs but only slightly higher LEs. This meant much protein was discarded. The maximum LE was found to be 35 % (corresponding to an LC of almost 50 %) for chitosan 95/20 dissolved in 2 % HAc and with a chitosan to CMC ratio of 2:3 at ambient temperature.

As these results left room for optimisation, a new method for protein encapsulation was developed. Instead of dissolving the OVA in the chitosan phase shortly before particle formation (standard method), it was dissolved in 2 % HAc and then mixed with CMC.

This mixture was in a second step used as counterion for particle formation. Here, the highest values achieved for LE were 60 - 70 % (corresponding to an LC of approximately 8 %) with chitosan qualities exhibiting a DDA of 95 %. Such LCs were achieved with the standard method only if a higher OVA concentration of 1 mg mL^{-1} was used in the starting solution. This method has so far only been tested with OVA. Future experiments should expand the developed method to other proteins to assess its general feasibility.

Depending on the goal, to encapsulate most of the protein (expensive and effective, alternative addition sequence favourable) or achieve a rather high LC (inexpensive and/or less effective, standard method favourable) one of the described methods should be chosen. It should however be kept in mind for both methods that proteins are not as stable in an acidic medium as in buffer. Nonetheless, within this project 2 % HAc was chosen as solvent because it was necessary for chitosan dissolution. The concentration of 2 % over 1 % was chosen because it was favourable for protein loading. The residence time in acid should be kept to a minimum and if one works with a sensitive protein 2 % HAc might be an inappropriate solvent and an alternative must be selected.

To transfer the developed NPs to a dry powder, spray drying with a matrix was utilised. Prior to this, the nanosuspension was washed because not all starting substances formed NPs. Washing of the nanosuspension was performed via centrifugation. However, depending on the particle size and their amount (larger and higher), particle sizes tended to increase over the course of this procedure. An optimisation of this process would be advisable in future projects to not affect the original particle size by this step at all.

Mannitol was used as matrix in spray drying in this project. This method not only makes the NPs applicable but stabilises them as well, which is also reported in the literature [123,144,145]. Depending on the deposition target of the formulation, the size must be adapted. Particles with a size suitable for nasal deposition could be obtained utilising the lab spray dryer B-290 in combination with the ultrasonic nozzle and a mannitol concentration of 20 wt%. Particles appeared hollow and had an overall smooth but

slightly indented surface. This appearance was dependent on the incorporation of OVA in the NPs or not. It was however not further influenced by the kind of NPs incorporated (used chitosan quality or ratio between chitosan and CMC). The scheme of the NiM formulation proposed in the objectives was adjusted accordingly (Figure 5-1).

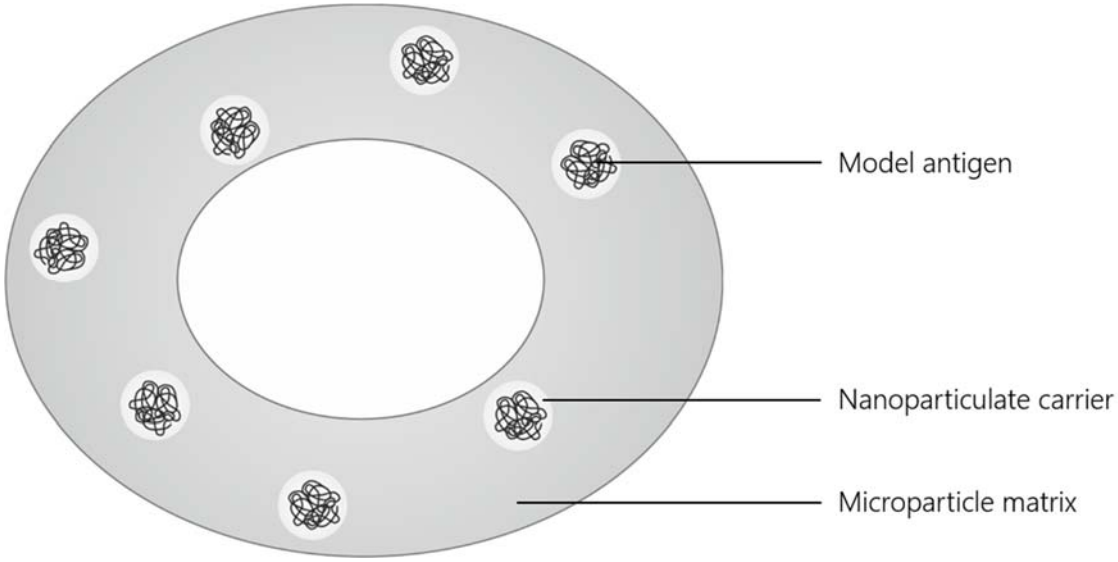

Figure 5-1. Scheme of a produced NiM.

NiM particles had a geometrical size of approximately 20 µm. Larger particle sizes might be better suited for nasal deposition. They could be obtained if inlet and outlet temperatures and/or higher matrix concentrations were used for the process. However, as a low outlet temperature (maximum of 40 °C) was necessary to ensure redispersibility of NPs this could not be tried within this project. A second reason why it was not possible to produce larger particles is that mannitol cannot be dissolved to a higher concentration in the aqueous solvent. Nonetheless, the obtained particles meet the > 10 µm requirement. DVS measurements showed only slight hygroscopicity of the powder making it a suitable dosage form for nasal administration.

The aerodynamic characterisation was particularly important for the developed formulation. The geometric diameter measured by laser diffraction suggested a size suitable for nasal deposition. But because particles were hollow, the aerodynamic behaviour might have deviated from expectations based on the assumption of solid particles of this size. It could however be shown that approximately 90 % of the formulation was deposited in the nose. The regional nasal deposition was further

investigated using a nasal cast. Results showed a preferential deposition in the upper and anterior parts of the nose due to the upward application of the powder, which is typical for this device. This effect was also found by others [131,132] who examined the nasal deposition of dry powders. A lower share in the upper parts of the nose and a generally more uniform distribution over the mucosa would be favourable in order to maximise the potential uptake in immune competent cells. Nonetheless, the results indicate an almost exclusive deposition in the nose, which was aimed for. It must however be kept in mind that the experiments were only *in vitro* experiments with a nasal cast which probably does not adequately mimic the complex physiology (flexibility, ciliae) of the human nasal cavity. Therefore, those results only have suggestive character [21].

In vitro experiments were performed examining the uptake into DCs of redispersed NPs. They showed a positive correlation between concentration as well as size and uptake. The higher uptake of larger particles (1 000 nm) could be differentiated via ImageStream analyses. Those particles were adhered to the outer surface of the cell, rather than being internalised. The internalisation of particles was negatively correlated with particle size. Future experiments will deal with the uptake mechanisms and subsequent activation of the DCs.

Overall, this work contributes to the deeper understanding of forming NPs with chitosan via ionic gelation. Influencing factors on particle characteristics were identified. Incorporating the NPs in a matrix made them suitable for nasal application. Aerodynamic characterisation showed a predominantly nasal deposition. The redispersed NPs can be taken up into immune competent cells but in the presence of epithelial cells, particles are rather taken up into those. Hence, optimisation of NPs, e.g. immune attractive additives such as pattern recognition ligands or cytokines to NPs or matrix, should be further examined. Future experiments should moreover investigate the activation of APC by those particles. A review by Bahamondez-Canas and Cui published in 2018 stressed the need for new effective vaccine formulations, especially

those for nasal administration [28]. Dry powder formulations are ascribed favourable properties as improved patient compliance and possible self-administration. However, until now, no dry powder for nasal vaccination is registered. Consequently, it can be concluded that this dissertation project was and future research on this topic will be timely and topical.

6 Summary

Nanoparticles (NPs) have been identified as a promising carrier and adjuvant system in mucosal vaccination. Chitosan is widely used as excipient for NPs for this purpose. To make such NPs applicable as dry powder, they can be incorporated into a microparticulate matrix (Nano-in-Microparticles). For an efficient nasal deposition of those microparticles, they should exhibit a particle size above 10 µm. Upon deposition the microparticulate matrix should release the NPs in their original size. The range of suitable sizes for an uptake of the NP in immune competent cells, especially in dendritic cells, is between 100 nm and 500 nm, as known from literature.

This work focussed on the preparation and characterisation of the NPs. They were prepared from chitosan and carboxymethylcellulose. Ovalbumin was used as model antigen. The particle formation between the two polymers is based on cross-linking via ionic gelation (charge equalisation between the positively charged chitosan and the negatively charged carboxymethylcellulose). Effects on particle stability, particle size and protein encapsulation were tested. NPs in the range between 100 - 500 nm could be produced. The model antigen could be loaded in the NPs, depending on the method used rather high loading efficiencies of up to 60 - 70 % (related to the total protein amount) or loading capacities of up to 50 % (related to the total excipient amount) were achieved. Moreover, NPs consisting of chitosan and sodium deoxycholate were characterised for comparison. As a result, the latter particle forming approach was not pursued further because the NPs consisting of chitosan and carboxymethylcellulose were regarded as more promising.

Furthermore, a dosage form for the nasal application of the NPs was developed. For that purpose, they were spray dried with mannitol to get embedded in microparticles. This way the NPs were stabilised. Using an ultrasonic nozzle in combination with a high mannitol concentration of 20 %, particles in a suitable size range for nasal deposition of approximately 20 µm could be generated. Experiments with a nasal cast model showed the suitability of the formulation for nasal application.

The NPs could be redispersed from the microparticles almost in their original size. First *in vitro* uptake experiments in dendritic cells showed a concentration- and size-dependent uptake. Smaller particles up to 500 nm were internalised in cells while larger particles (1 000 nm) stuck to the surface of the cells. Follow-up experiments will examine potential uptake mechanisms and subsequent activation of the dendritic cells.

7 Summary (German)

Die Forschung zu mukosaler Impfung hat Nanopartikel (NP) als vielversprechenden Antigenträger mit adjuvanten Eigenschaften identifiziert. Häufig wird dabei Chitosan als Material zur Herstellung der NP verwendet. Um solche NP als trockenes Pulver applizierbar zu machen, können sie in eine mikropartikuläre Matrix (Nano-in-Mikropartikel) inkorporiert werden. Die Mikropartikel sollen über die Nase appliziert werden und daher eine Partikelgröße von über 10 µm aufweisen, um eine nasale Deposition sicherzustellen. Nach erfolgter Deposition soll die mikropartikuläre Matrix die NP in ihrer ursprünglichen Größe freigeben. Für die Aufnahme der NP in immunkompetente, insbesondere in dendritische, Zellen eignet sich eine Größe von 100 - 500 nm, wie aus der Literatur bekannt ist.

Der Fokus dieser Arbeit lag insbesondere auf der Herstellung und Charakterisierung der NP. Diese wurden aus Chitosan und Carboxymethylcellulose hergestellt. Als Modellantigen wurde Ovalbumin verwendet. Die Partikelbildung zwischen den beiden Polymeren beruht auf einer Quervernetzung durch ionische Gelierung (Ladungsausgleich zwischen positiv geladenem Chitosan und negativ geladener Carboxymethylcellulose). Es wurden Einflüsse auf die Partikelstabilität, resultierende Partikelgröße und die Proteinverkapselung untersucht. NP im geeigneten Größenbereich von 100 - 500 nm konnten hergestellt werden. Das Modellantigen konnte mit den Nanopartikeln assoziiert werden. Abhängig von der verwendeten Methode konnte eine hohe Verkapselungseffizienz von bis zu 60 - 70 % (bezogen auf den gesamten Proteingehalt) oder eine hohe Partikelbeladung von bis zu 50 % (bezogen auf die gesamte Menge Partikelausgangsstoffe) erreicht werden. Darüber hinaus wurden auch NP bestehend aus Chitosan und Natriumdeoxycholat vergleichend charakterisiert. Daraus ergab sich, dass dieser Partikelformulierungsansatz nicht weiterverfolgt wurde, da die Partikel aus Chitosan und Carboxymethycellulose als vielversprechender angesehen werden.

Im Weiteren wurde eine Darreichungsform für die nasale Gabe der NP entwickelt. Dafür wurden sie mittels Sprühtrocknung mit Mannitol in Mikropartikel eingebettet und

dadurch stabilisiert. Durch die Verwendung einer Ultraschalldüse und einer hohen Mannitol-Konzentration von 20 % konnten Partikel in einem geeigneten Größenbereich von ca. 20 µm generiert werden. Durch Versuche mit einem Nasenmodell konnte gezeigt werden, dass die entwickelte Formulierung prinzipiell geeignet für eine nasale Deposition ist.

Die NP sind nach Auflösen der Mikropartikel annähernd in ihrer ursprünglichen Größe rekonstituiert worden. Es wurden erste *in vitro* Versuche zur Aufnahme in dendritischen Zellen durchgeführt. Diese zeigten, dass die Partikel konzentrations- und größenabhängig aufgenommen werden. Kleinere Partikel (bis 500 nm) wurden in die Zellen aufgenommen, während größere (1 000 nm) eher außen an den Zellen anhefteten. Weiterführende Untersuchungen werden sich mit möglichen Aufnahmemechanismen und der anschließenden Aktivierung der dendritischen Zellen beschäftigen.

8 References

[1] I. Zündorf, A.M. Vollmar, T. Dingermann, Immunologische Grundlagen des Impfens. Hightech-Training für das Immunsystem, Pharm. Unserer Zeit 37 (2008) 20–27.

[2] T. Sunil, R. Dilbarova, R. Rappuoli, Future Challenges for Vaccinologists, in: T. Sunil (Ed.), Vaccine Design.: Methods in Molecular Biology, Humana Press, New York, 2016, pp. 41–55.

[3] P.H. Nambiar, A. Delgado Daza, L.L. Livornese Jr, Clinical Impact of Vaccine Development, in: T. Sunil (Ed.), Vaccine Design.: Methods in Molecular Biology, Humana Press, New York, 2016, pp. 3–39.

[4] R.S. Kallerup, C. Foged, Classification of Vaccines, in: C. Foged, T. Rades, Y. Perrie, S. Hook (Eds.), Subunit Vaccine Delivery, pp. 15–29.

[5] G.A. Sautto, G.A. Kirchenbaum, T.M. Ross, Towards a universal influenza vaccine: Different approaches for one goal, Virology journal 15 (2018) 17.

[6] FDA, Statement from FDA Commissioner Scott Gottlieb, M.D. on the efficacy of the 2017-2018 influenza vaccine, 2018.

[7] S. Mitragotri, Immunization without needles, Nature Reviews Immunology 5 (2005) 905–916.

[8] S.R. Bonam, C.D. Partidos, S.K.M. Halmuthur, S. Muller, An Overview of Novel Adjuvants Designed for Improving Vaccine Efficacy, Trends in pharmacological sciences 38 (2017) 771–793.

[9] R. Bastola, G. Noh, T. Keum, S. Bashyal, J.-E. Seo, J. Choi, Y. Oh, Y. Cho, S. Lee, Vaccine adjuvants: Smart components to boost the immune system, Archives of Pharmacal Research (2017).

[10] B. Bernocchi, R. Carpentier, D. Betbeder, Nasal nanovaccines, International Journal of Pharmaceutics (2017).

[11] A.S. McKee, P. Marrack, Old and new adjuvants, Current Opinion in Immunology 47 (2017) 44–51.

[12] E.C. Carroll, L. Jin, A. Mori, N. Muñoz-Wolf, E. Oleszycka, H.B.T. Moran, S. Mansouri, C.P. McEntee, E. Lambe, E.M. Agger, P. Andersen, C. Cunningham, P. Hertzog, K.A. Fitzgerald, A.G. Bowie, E.C. Lavelle, The Vaccine Adjuvant Chitosan Promotes Cellular Immunity via DNA Sensor cGAS-STING-Dependent Induction of Type I Interferons, Immunity 44 (2016) 597–608.

[13] V. Cimica, J.M. Galarza, Adjuvant formulations for virus-like particle (VLP) based vaccines, Clinical immunology (Orlando, Fla.) 183 (2017) 99–108.

[14] J. Huang, R.J. Garmise, T.M. Crowder, K. Mar, C.R. Hwang, A.J. Hickey, J.A. Mikszta, V.J. Sullivan, A novel dry powder influenza vaccine and intranasal delivery technology: induction of systemic and mucosal immune responses in rats, Vaccine 23 (2004) 794–801.

[15] S.S. Davis, Nasal vaccines, Advanced Drug Delivery Reviews 51 (2001) 21–42.

[16] P.G. Djupesland, Nasal delivery of vaccines (2003).

[17] A. Kumar, A. Vimal, A. Kumar, Why Chitosan? From properties to perspective of mucosal drug delivery, International journal of biological macromolecules 91 (2016) 615–622.

[18] A. Smith, M. Perelman, M. Hinchcliffe, Chitosan, Human Vaccines & Immunotherapeutics 10 (2014) 797–807.

[19] L. Illum, I. Jabbal-Gill, M. Hinchcliffe, A.N. Fisher, S.S. Davis, Chitosan as a novel nasal delivery system for vaccines, Advanced Drug Delivery Reviews 51 (2001) 81–96.

[20] L. Illum, Nasal drug delivery — Recent developments and future prospects, Journal of Controlled Release 161 (2012) 254–263.

[21] S.P. Newman, G.R. Pitcairn, R.N. Dalby, Drug delivery to the nasal cavity: In vitro and in vivo assessment, Critical Reviews in Therapeutic Drug Carrier Systems 21 (2004) 21–66.

[22] R.U. Agu, Challenges in nasal drug absorption: How far have we come?, Therapeutic delivery 7 (2016) 495–510.

[23] P.G. Djupesland, J.C. Messina, R.A. Mahmoud, The nasal approach to delivering treatment for brain diseases: An anatomic, physiologic, and delivery technology overview, Therapeutic delivery 5 (2014) 709–733.

[24] N. Csaba, M. Garcia-Fuentes, M.J. Alonso, Nanoparticles for nasal vaccination, Advanced Drug Delivery Reviews 61 (2009) 140–157.

[25] W. Becker, H.H. Naumann, C.R. Pfaltz, Hals-Nasen-Ohren-Heilkunde: Kurzgefasstes Lehrbuch mit Atlasteil, differentialdiagnostische Tabellen, Prüfungsfragen, 3., neubearb. Aufl. ed., G. Thieme, Stuttgart, New York, 1986.

[26] E. Mutschler, G. Thews, H.-G. Schaible, P. Vaupel, Anatomie, Physiologie, Pathophysiologie des Menschen: 140 Tabellen, 6., völlig überarb. und erw. Aufl. ed., Wiss. Verl.-Ges, Stuttgart, 2007.

[27] T.P. Crowe, M.H.W. Greenlee, A.G. Kanthasamy, W.H. Hsu, Mechanism of intranasal drug delivery directly to the brain, Life sciences 195 (2018) 44–52.

[28] T.F. Bahamondez-Canas, Z. Cui, Intranasal immunization with dry powder vaccines, European Journal of Pharmaceutics and Biopharmaceutics 122 (2018) 167–175.

[29] H.R. Costantino, L. Illum, G. Brandt, P.H. Johnson, S.C. Quay, Intranasal delivery: Physicochemical and therapeutic aspects, International Journal of Pharmaceutics 337 (2007) 1–24.

[30] H.-G. Boenninghaus, Hals-Nasen-Ohrenheilkunde für Medizinstudenten: Gegliedert nach dem 1979 erschienenen Gegenstandskatalog 3 im Anhang 280 Prüfungsaufgaben, 5. neubearbeitete und erw. Aufl. ed., Springer-Verlag, Berlin, New York, 1980.

[31] A.J. Hickey, R.J. Garmise, Dry powder nasal vaccines as an alternative to needle-based delivery, Critical Reviews in Therapeutic Drug Carrier Systems 26 (2009) 1–27.

[32] P. Verdugo, Mucin exocytosis, The American Review of Respiratory Disease 144 (1991) 7.

[33] P.G. Djupesland, Nasal drug delivery devices: characteristics and performance in a clinical perspective-a review, Drug Delivery and Translational Research 3 (2013) 42–62.

[34] F. Zepp, Principles of Vaccination, in: T. Sunil (Ed.), Vaccine Design.: Methods in Molecular Biology, Humana Press, New York, 2016, pp. 57–84.

[35] A. Helmstädter, Zur Geschichte der aktiven Immunisierung. Vorbeugen ist besser als Heilen, Pharmazie in unserer Zeit 37 (2008) 12–18.

[36] I. Hajj Hussein, N. Chams, S. Chams, S. El Sayegh, R. Badran, M. Raad, A. Gerges-Geagea, A. Leone, A. Jurjus, Vaccines Through Centuries: Major Cornerstones of Global Health, Frontiers in public health 3 (2015) 269.

[37] S. Plotkin, History of vaccination, Proceedings of the National Academy of Sciences of the United States of America 111 (2014) 12283–12287.

[38] World Health Organization, Vaccine Safety Basics E-Learning Course: Module 3: Adverse events following immunization, 2018, http://vaccine-safety-training.org/classification-of-aefis.html, accessed 1 March 2018.

[39] R.T. Chen, S.C. Rastogi, J.R. Mullen, S.W. Hayes, S.L. Cochi, J.A. Donlon, S.G. Wassilak, The Vaccine Adverse Event Reporting System (VAERS), Vaccine 12 (1994) 542–550.

[40] K.M. Murphy, P. Travers, M. Walport, Janeway Immunologie, 7., Aufl. 2009. Korrigierter Nachdruck 2014 ed., Springer Berlin, Berlin, 2014.

[41] A.J. Highton, R.A. Kemp, Immunological Background, in: C. Foged, T. Rades, Y. Perrie, S. Hook (Eds.), Subunit Vaccine Delivery, pp. 3–14.

[42] C.P. Karch, P. Burkhard, Vaccine technologies: From whole organisms to rationally designed protein assemblies, Biochemical pharmacology 120 (2016) 1–14.

[43] M. Perry, A. Whyte, Immunology of the tonsils, Immunology Today 19 (1998) 414–421.

[44] H. Kiyono, S. Fukuyama, NALT- versus Peyer's-patch-mediated mucosal immunity, Nature reviews. Immunology 4 (2004) 699–710.

[45] M. Tafaghodi, S. Abolghasem Sajadi Tabassi, M.-R. Jaafari, S.R. Zakavi, M. Momen-Nejad, Evaluation of the clearance characteristics of various microspheres in the human nose by gamma-scintigraphy, International Journal of Pharmaceutics 280 (2004) 125–135.

[46] R. Scherließ, Nasal Administration of Vaccines, in: C. Foged, T. Rades, Y. Perrie, S. Hook (Eds.), Subunit Vaccine Delivery, pp. 287–306.

[47] M.-L. de Temmerman, J. Rejman, J. Demeester, D.J. Irvine, B. Gander, S.C. de Smedt, Particulate vaccines: On the quest for optimal delivery and immune response, Drug Discovery Today 16 (2011) 569–582.

[48] S. Hamdy, A. Haddadi, R.W. Hung, A. Lavasanifar, Targeting dendritic cells with nano-particulate PLGA cancer vaccine formulations, Advanced Drug Delivery Reviews 63 (2011) 943–955.

[49] R. Rietscher, M. Schröder, J. Janke, J.A. Czaplewska, M. Gottschaldt, R. Scherließ, A. Hanefeld, U.S. Schubert, M. Schneider, P.A. Knolle, C.-M. Lehr, Antigen delivery via hydrophilic PEG-b-PAGE-b-PLGA nanoparticles boosts vaccination induced T cell immunity, European Journal of Pharmaceutics and Biopharmaceutics 102 (2016) 20–31.

[50] C.F. Kuper, P.J. Koornstra, D.M.H. Hameleers, J. Biewenga, B.J. Spit, A.M. Duijvestijn, P.J.C. van Breda Vriesman, T. Sminia, The role of nasopharyngeal lymphoid tissue, Immunology Today 13 (1992) 219–224.

[51] J. Holmgren, C. Czerkinsky, Mucosal immunity and vaccines, Nature Medicine 11 (2005) 53.

[52] S. Sharma, T.K.S. Mukkur, H.A.E. Benson, Y. Chen, Pharmaceutical aspects of intranasal delivery of vaccines using particulate systems, Journal of Pharmaceutical Sciences 98 (2009) 812–843.

[53] H. Wagner, A. Vollmar, A. Bechthold, D. Hoffmeister, Biogene Arzneistoffe und Grundlagen von Gentechnik und Immunologie, 7., völlig neu bearb. Aufl. ed., Wiss. Verl.-Ges, Stuttgart, 2007.

[54] R.B. Baleeiro, M. Schweinlin, R. Rietscher, A. Diedrich, J.A. Czaplewska, M. Metzger, C.-M. Lehr, R. Scherließ, A. Hanefeld, M. Gottschaldt, P. Walden, Nanoparticle-Based Mucosal Vaccines Targeting Tumor-Associated Antigens to Human Dendritic Cells, Journal of biomedical nanotechnology 12 (2016) 1527–1543.

[55] G. Curigliano, M. Rescigno, A. Goldhirsch, Immunology and breast cancer: Therapeutic cancer vaccines, Breast (Edinburgh, Scotland) 16 Suppl 2 (2007) S20-6.

[56] M.F. Bachmann, M.R. Dyer, Therapeutic vaccination for chronic diseases: A new class of drugs in sight, Nature reviews. Drug discovery 3 (2004) 81–88.

[57] H. Boukhebza, N. Bellon, J.M. Limacher, G. Inchauspé, Therapeutic vaccination to treat chronic infectious diseases: Current clinical developments using MVA-based vaccines, Human Vaccines & Immunotherapeutics 8 (2012) 1746–1757.

[58] B. Slütter, N. Hagenaars, W. Jiskoot, Rational design of nasal vaccines, Journal of Drug Targeting 16 (2008) 1–17.

[59] S. Chadwick, C. Kriegel, M. Amiji, Nanotechnology solutions for mucosal immunization, Advanced Drug Delivery Reviews 62 (2010) 394–407.

[60] Partidos, Intranasal vaccines: Forthcoming challenges, Pharmaceutical science & technology today 3 (2000) 273–281.

[61] A.K. Shakya, M.Y.E. Chowdhury, W. Tao, H.S. Gill, Mucosal vaccine delivery: Current state and a pediatric perspective, Journal of controlled release official journal of the Controlled Release Society 240 (2016) 394–413.

[62] A.S. Cordeiro, M.J. Alonso, Recent advances in vaccine delivery, Pharmaceutical patent analyst 5 (2016) 49–73.

[63] M. Frühwein, Basiswissen Impfen - Lehrtext, 2014, https://www.curacampus.de/campus-web/app/medienfile.8088315.3e486467-b000-44b7-95aa-8df66788b0dc.original.pdf;jsessionid=B65DE68FBC08DA703B37D351CF5D142E/Basiswissen%20Impfen.pdf, accessed 22 February 2018.

[64] M. Bröker, C. Beyer, Adjuvantien für Humanvakzinen. Alte und neue Hilfsstoffe, Pharm. Unserer Zeit 37 (2008) 42–51.

[65] M. Moser, O. Leo, Key concepts in immunology, Vaccine 28 Suppl 3 (2010) C2-13.

[66] D.T. O'Hagan, G.S. Ott, G. van Nest, R. Rappuoli, G.D. Giudice, The history of MF59(®) adjuvant: A phoenix that arose from the ashes, Expert review of vaccines 12 (2013) 13–30.

[67] G. Leroux-Roels, Unmet needs in modern vaccinology: Adjuvants to improve the immune response, Vaccine 28 Suppl 3 (2010) C25-36.

[68] D. Newsted, F. Fallahi, A. Golshani, A. Azizi, Advances and challenges in mucosal adjuvant technology, Vaccine 33 (2015) 2399–2405.

[69] L. Zeng, Mucosal adjuvants: Opportunities and challenges, Human Vaccines & Immunotherapeutics 12 (2016) 2456–2458.

[70] J.d.S. Apostólico, V.A.S. Lunardelli, F.C. Coirada, S.B. Boscardin, D.S. Rosa, Adjuvants: Classification, Modus Operandi, and Licensing, Journal of immunology research 2016 (2016) 1459394.

[71] I.F. Uchegbu, Fundamentals of Pharmaceutical Nanoscience, Springer-Verlag, New York, 2016.

[72] Food and Drug Administration (Ed.), Guidance for Industry - Considering Whether an FDA-Regulated Product Involves the Application of Nanotechnology, 2014.

[73] B. Sarmento, J.d. Neves, Chitosan-Based Systems for Biopharmaceuticals: Delivery, Targeting and Poly, John Wiley & Sons, 2012.

[74] M.A. Elgadir, M.S. Uddin, S. Ferdosh, A. Adam, A.J.K. Chowdhury, M.Z.I. Sarker, Impact of chitosan composites and chitosan nanoparticle composites on various drug delivery systems: A review, Journal of food and drug analysis 23 (2015) 619–629.

[75] S. Rodrigues, M. Dionísio, C.R. López, A. Grenha, Biocompatibility of chitosan carriers with application in drug delivery, Journal of functional biomaterials 3 (2012) 615–641.

[76] L. Casettari, L. Illum, Chitosan in nasal delivery systems for therapeutic drugs, Journal of Controlled Release (2014).

[77] R. Hendrickson, J.P. Remington, Remington: The science and practice of pharmacy, 21st ed. ed., Lippincott Williams & Wilkins, Philadelphis, PA, 2006.

[78] DrugBase: Excipient: Sodium carboxymethylcellulose, 2016, http://www.drugbase.de/nc/de/datenbanken/fiedler/excipient.html?tx_crondavdbfiedler_pi[uid]=25925&tx_solr[filter][0]=owndb%3Aall, accessed 22 January 2018.

[79] A. Cadete, L. Figueiredo, R. Lopes, C.C.R. Calado, A.J. Almeida, L.M.D. Goncalves, Development and characterization of a new plasmid delivery system based on chitosan-sodium deoxycholate nanoparticles, European Journal of Pharmaceutical Sciences 45 (2012) 451–458.

[80] A.D. Nisbet, R.H. Saundry, A.J. Moir, L.A. Fothergill, J.E. Fothergill, The complete amino-acid sequence of hen ovalbumin, European Journal of Biochemistry 115 (1981) 335–345.

[81] J.A. Huntington, P.E. Stein, Structure and properties of ovalbumin, Journal of Chromatography B: Biomedical Sciences and Applications 756 (2001) 189–198.

[82] G. Swaminathan, E.A. Thoryk, K.S. Cox, S. Meschino, S.A. Dubey, K.A. Vora, R. Celano, M. Gindy, D.R. Casimiro, A.J. Bett, A novel lipid nanoparticle adjuvant significantly enhances B cell and T cell responses to sub-unit vaccine antigens, Vaccine 34 (2016) 110–119.

[83] H. Sun, K.G.J. Pollock, J.M. Brewer, Analysis of the role of vaccine adjuvants in modulating dendritic cell activation and antigen presentation in vitro, Vaccine 21 (2003) 849–855.

[84] A. Hanninen, A. Braakhuis, W.R. Heath, L.C. Harrison, Mucosal Antigen Primes Diabetogenic Cytotoxic T-Lymphocytes Regardless of Dose or Delivery Route, Diabetes 50 (2001) 771–775.

[85] P.D. Hulseberg, A. Zozulya, H.H. Chu, J.A. Triccas, Z. Fabry, M. Sandor, The same well-characterized T cell epitope SIINFEKL expressed in the context of a cytoplasmic or secreted protein in BCG induces different CD8+ T cell responses, Immunology letters 130 (2010) 36–42.

[86] I.R. Badell, W.H. Kitchens, M.E. Wagener, A.E. Lukacher, C.P. Larsen, M.L. Ford, Pathogen Stimulation History Impacts Donor-Specific CD8(+) T Cell Susceptibility to Costimulation/Integrin Blockade-Based Therapy, American journal of transplantation official journal of the American Society of Transplantation and the American Society of Transplant Surgeons 15 (2015) 3081–3094.

[87] D(-)-Mannit, https://www.carlroth.com/de/de/Chemikalien/A-Z-Chemikalien/M/D%28-%29-Mannit/D%28-%29-Mannit/p/0000000500008cb4000f0023_de, accessed 29 January 2018.

[88] DrugBase: Excipient: Mannitol, 2016, http://www.drugbase.de/de/datenbanken/fiedler/excipient.html?tx_crondavdbfiedler_pi%5Buid%5D=17016&cHash=d42b70a44dff565f08816ef05980c7f6, accessed 29 January 2018.

[89] Fachinformation: Bronchitol 40 mg, Hartkapseln mit Pulver zur Inhalation, 2017, accessed 29 January 2018.

[90] M. Johnson, FITC/Fluorescein, MATER METHODS 1 (2011).

[91] W. Luttmann, K. Bratke, M. Küpper, D. Myrtek, Der Experimentator: Immunologie, 4., vollst. überarb. u. korr. Aufl. 2014 ed., Springer Berlin, Berlin, 2014.

[92] A. Diedrich, Entwicklung einer nanopartikulären Formulierung zur Vakzinierung über den Respirationstrakt, 2015.

[93] C. Colonna, B. Conti, P. Perugini, F. Pavanetto, T. Modena, R. Dorati, P. Iadarola, I. Genta, Ex vivo evaluation of prolidase loaded chitosan nanoparticles for the enzyme replacement therapy, European Journal of Pharmaceutics and Biopharmaceutics 70 (2008) 58–65.

[94] H.A. Schiffter, Sprühtrocknung - So schnell kann Trocknung gehen, Deutsche Apotheker Zeitung 152 (2012) 78–88.

[95] R. Vehring, Pharmaceutical Particle Engineering via Spray Drying, Pharmaceutical Research 25 (2008) 999–1022.

[96] Büchi Labortechnik, Training Papers Spray Drying (2002).

[97] Büchi Labortechnik, Bedienungsanleitung, Ultrasonic Controller (2014).

[98] Sartorius Stedim Data Analytics, User Guide to MODDE, 2017, accessed 5 February 2018.

[99] P. Sorlier, C. Rochas, I. Morfin, C. Viton, A. Domard, Light scattering studies of the solution properties of chitosans of varying degrees of acetylation, Biomacromolecules 4 (2003) 1034–1040.

[100] G. Rücker, M. Neugebauer, G.G. Willems, Instrumentelle Analytik für Pharmazeuten: Lehrbuch zu spektroskopischen, chromatografischen, elektrochemischen und thermischen Analysenmethoden, 4., durges. und akt. Aufl. ed., Wissenschaftliche Verlagsgesellschaft, Stuttgart, 2008.

[101] M. Lavertu, Z. Xia, A.N. Serreqi, M. Berrada, A. Rodrigues, D. Wang, M.D. Buschmann, A. Gupta, A validated 1H NMR method for the determination of the degree of deacetylation of chitosan, Journal of Pharmaceutical and Biomedical Analysis 32 (2003) 1149–1158.

[102] Malvern Instruments, Zetasizer Nano User Manual, 2013.

[103] I. Horiba Instruments, A Guidebook to Particle Size Analysis, 2014, https://www.horiba.com/fileadmin/uploads/Scientific/Documents/PSA/PSA_Guidebook.pdf.

[104] Malvern Instruments, FAQ: What is the Z average?

[105] A. Fahr, R. Voigt, Voigt Pharmazeutische Technologie: Für Studium und Beruf ; mit ... 113 Tabellen, 12., völlig neu bearb.Aufl. ed., Dt. Apotheker-Verl., Stuttgart, 2015.

[106] D.A. Skoog, F.J. Holler, S.R. Crouch, Instrumentelle Analytik: Grundlagen - Geräte - Anwendungen, 6., vollst. überarb. erw. Aufl. 2014 ed., Springer, Berlin, 2014.

[107] C. Demetzos, Pharmaceutical nanotechnology: Fundamentals and practical applications, Adis, Singapore, Singapore, 2016.

[108] Microcal ITC Systems - Understanding Biomolecular Interactions, 2015, https://www.malvern.com/en/assets/MRK2058_tcm22-23553.pdf, accessed 16 January 2018.

[109] F. Lottspeich, Bioanalytik, 3., [aktualisierte und erweiterte] Aufl. ed., Springer, Heidelberg, 2012.

[110] Thermo Fisher Scientific, Thermo Scientific Pierce Protein Assay Technical Handbook, 2017, assets.thermofisher.com/TFS-Assets/LSG/brochures/protein-assay-technical-handook.pdf, accessed 16 January 2018.

[111] P.K. Smith, R.I. Krohn, G.T. Hermanson, A.K. Mallia, F.H. Gartner, M.D. Provenzano, E.K. Fujimoto, N.M. Goeke, B.J. Olson, D.C. Klenk, Measurement of protein using bicinchoninic acid, Analytical Biochemistry 150 (1985) 76–85.

[112] Surface Measurement Systems, Dynamic vapor sorption (DVS), https://www.surfacemeasurementsystems.com/solutions/dynamic_vapor_sorption/

[113] 2.9.18 Zubereitungen zur Inhalation: Aerodynamische Beurteilung feiner Teilchen, in: Europäisches Arzneibuch 9. Ausgabe, Grundwerk 2017: Amtliche deutsche Ausgabe, Deutscher Apotheker Verlag, Stuttgart, 2017.

[114] Copley Scientific, Quality Solutions for Inhaler Testing, 2015.

[115] Abnova, D-Mannitol Assay Kit (Colorimetric).

[116] O. Helm, J. Held-Feindt, E. Grage-Griebenow, N. Reiling, H. Ungefroren, I. Vogel, U. Krüger, T. Becker, M. Ebsen, C. Röcken, D. Kabelitz, H. Schäfer, S. Sebens, Tumor-associated macrophages exhibit pro- and anti-inflammatory properties by which they impact on pancreatic tumorigenesis, International journal of cancer 135 (2014) 843–861.

[117] M.M. Leane, R. Nankervis, A. Smith, L. Illum, Use of the ninhydrin assay to measure the release of chitosan from oral solid dosage forms, International Journal of Pharmaceutics 271 (2004) 241–249.

[118] S. Prochazkova, K.M. Vårum, K. Ostgaard, Quantitative determination of chitosans by ninhydrin, Carbohydrate Polymers 38 (1999) 115–122.

[119] S.A. Abouelmagd, Y.J. Ku, Y. Yeo, Low molecular weight chitosan-coated polymeric nanoparticles for sustained and pH-sensitive delivery of paclitaxel, Journal of Drug Targeting 23 (2015) 725–735.

[120] M. Friedman, Applications of the ninhydrin reaction for analysis of amino acids, peptides, and proteins to agricultural and biomedical sciences, Journal of agricultural and food chemistry 52 (2004) 385–406.

[121] C. Scaramboni, R.C. Urban, M. Lima-Souza, R.F.P. Nogueira, A.A. Cardoso, A.G. Allen, M.L.A.M. Campos, Total sugars in atmospheric aerosols: An alternative tracer for biomass burning, Atmospheric Environment 100 (2015) 185–192.

[122] N. Sawtarie, Y. Cai, Y. Lapitsky, Preparation of chitosan/tripolyphosphate nanoparticles with highly tunable size and low polydispersity, Colloids and surfaces. B, Biointerfaces 157 (2017) 110–117.

[123] A. Grenha, B. Seijo, C. Serra, C. Remuñán-López, Chitosan Nanoparticle-Loaded Mannitol Microspheres: Structure and Surface Characterization, Biomacromolecules 8 (2007) 2072–2079.

[124] F. Gütter, Understanding nano-stabiliser and nano-bio interactions of nanocrystals, 2018.

[125] J. Janke, PLGA-Nanopartikel für die inhalative Vakzinierung, 2014.

[126] S. Buske, Chitosan as adjuvant and particle forming excipient in a nano-in-microparticulate dry powder for nasal and pulmonary vaccine delivery, 2014.

[127] M.D. Chavanpatil, P.R. Vavia, The influence of absorption enhancers on nasal absorption of acyclovir, European Journal of Pharmaceutics and Biopharmaceutics 57 (2004) 483–487.

[128] R. Scherließ, S. Buske, K. Young, B. Weber, T. Rades, S. Hook, In vivo evaluation of chitosan as an adjuvant in subcutaneous vaccine formulations, Vaccine 31 (2013) 4812–4819.

[129] 5.11 Zum Abschnitt "Eigenschaften" in Monographien, in: Europäisches Arzneibuch 9. Ausgabe, Grundwerk 2017: Amtliche deutsche Ausgabe, Deutscher Apotheker Verlag, Stuttgart, 2017.

[130] Food and Drug Administration (Ed.), Draft Guidance for Industry - Bioavailability and Bioequivalence Studies for Nasal Aerosols and Nasal Sprays for Local Action, 2003.

[131] P.G. Djupesland, A. Skretting, Nasal deposition and clearance in man: comparison of a bidirectional powder device and a traditional liquid spray pump, Journal of Aerosol Medicine and Pulmonary Drug Delivery 25 (2012) 280–289.

[132] K. Inthavong, J. Wen, J.-Y. Tu, Modelling the inhalation of drug aerosols in a human nasal cavity, JBiSE 03 (2010) 52–58.

[133] P.R. Kamath, D. Sunil, Nano-Chitosan Particles in Anticancer Drug Delivery: An Up-to-Date Review, Mini reviews in medicinal chemistry 17 (2017) 1457–1487.

[134] G. Kanojia, R.T. Have, P.C. Soema, H. Frijlink, J.-P. Amorij, G. Kersten, Developments in the formulation and delivery of spray dried vaccines, Human Vaccines & Immunotherapeutics 13 (2017) 2364–2378.

[135] S.A. Agnihotri, N.N. Mallikarjuna, T.M. Aminabhavi, Recent advances on chitosan-based micro- and nanoparticles in drug delivery, Journal of Controlled Release 100 (2004) 5–28.

[136] W. Fan, W. Yan, Z. Xu, H. Ni, Formation mechanism of monodisperse, low molecular weight chitosan nanoparticles by ionic gelation technique, Colloids and surfaces B: Biointerfaces 90 (2012) 21–27.

[137] Q. Gan, T. Wang, C. Cochrane, P. McCarron, Modulation of surface charge, particle size and morphological properties of chitosan-TPP nanoparticles intended for gene delivery, Colloids and surfaces. B, Biointerfaces 44 (2005) 65–73.

[138] M. Alameh, M. Lavertu, N. Tran-Khanh, C.-Y. Chang, F. Lesage, M. Bail, V. Darras, A. Chevrier, M.D. Buschmann, siRNA Delivery with Chitosan: Influence of Chitosan Molecular Weight, Degree of Deacetylation, and Amine to Phosphate Ratio on in Vitro Silencing Efficiency, Hemocompatibility, Biodistribution, and in Vivo Efficacy, Biomacromolecules 19 (2018) 112–131.

[139] S. Hassani, A. Laouini, H. Fessi, C. Charcosset, Preparation of chitosan–TPP nanoparticles using microengineered membranes – Effect of parameters and encapsulation of tacrine, Colloids and Surfaces A: Physicochemical and Engineering Aspects 482 (2015) 34–43.

[140] N. Csaba, M. Köping-Höggård, M.J. Alonso, Ionically crosslinked chitosan/tripolyphosphate nanoparticles for oligonucleotide and plasmid DNA delivery, International Journal of Pharmaceutics 382 (2009) 205–214.

[141] J. Mirtič, J. Ilaš, J. Kristl, Influence of different classes of crosslinkers on alginate polyelectrolyte nanoparticle formation, thermodynamics and characteristics, Carbohydrate Polymers 181 (2018) 93–102.

[142] P.L. Ma, M. Lavertu, F.M. Winnik, M.D. Buschmann, Stability and binding affinity of DNA/chitosan complexes by polyanion competition, Carbohydrate Polymers 176 (2017) 167–176.

[143] G. Giacalone, H. Hillaireau, P. Capiau, H. Chacun, F. Reynaud, E. Fattal, Stabilization and cellular delivery of chitosan-polyphosphate nanoparticles by incorporation of iron, Journal of Controlled Release 194 (2014) 211–219.

[144] N. Tsapis, D. Bennett, B. Jackson, D.A. Weitz, D.A. Edwards, Trojan particles. Large porous carriers of nanoparticles for drug delivery, Proceedings of the National Academy of Sciences of the United States of America 99 (2002) 12001–12005.

[145] N. Anton, A. Jakhmola, T.F. Vandamme, Trojan microparticles for drug delivery, Pharmaceutics 4 (2012) 1–25.

9 Appendix

9.1 Abbreviations

APC	Antigen presenting cells
BCA	Bicinchoninic acid
BF	Brightfield
CD	Cluster of differentiation
CMC	Sodium carboxymethylcellulose
DC	Dendritic cell
DDA	Degree of deacetylation
DLS	Dynamic light scattering
DOC	Sodium deoxycholate
DoE	Design of Experiments
DVS	Dynamic vapour sorption
FITC	Fluorescein isothiocyanate isomer I
FPF	Fine particle fraction
HAc	Acetic acid
hDC	Human dendritic cells
HPMC	Hydroxypropyl methylcellulose
IEP	Isoelectric point
Ig	Immunoglobulin
INS	Internalisation score
ITC	Isothermal titration calorimetry
LC	Loading capacity
LE	Loading efficiency
MALS	Multiple angle light scattering
M-cells	Microfold cells
MFI	Median fluorescence intensity
MHC	Major histocompatibility complex
MOC	Micro-orifice collector

NALT	Nose-associated lymphoid tissue
NGI	Next Generation Impactor
NiM	Nano-in-Microparticle
NMR	Nuclear magnetic resonance spectroscopy
NP	Nanoparticle
OVA	Ovalbumin
PBS	Phosphate buffered saline
PDI	Polydispersity index
PEG	Polyethylene glycol
Ph. Eur.	European Pharmacopoeia
PVA	Polyvinyl alcohol
Q3	Cumulant frequency of a volume-based distribution
q3*	Probability density function of a volume-based distribution
RSD	Relative standard deviation
SD	Standard deviation
SEC	Size exclusion chromatography
SEM	Scanning electron microscopy
sIg	Secretory immunoglobulin
T_H	Helper T-cell
TPP	Penta-sodium triphosphate
TSP	Deuterated sodium trimethylsilyl propionate
UDS	Unit dose system
UK	United Kingdom
USA	United States of America
WHO	World Health Organisation
ZP	Zeta potential

9.2 Units

%	Per cent, 10^{-2}
°	Degree(s)
°C	Degree(s) Celsius
µ	Micro (if followed by another unit), 10^{-6}
bar	Bar, 10^{5} N
c*	Centi (if followed by another unit), 10^{-2}
d	Day(s)
Da	Dalton, corresponds to g mol^{-1}
g	Gram(s)
Hz	Hertz, s^{-1}
k*	Kilo (if followed by another unit), 10^{3}
L	Litre(s)
M	Molar, mol L^{-1}
m	Metre(s)
m*	Milli (if followed by another unit), 10^{-3}
M*	Mega (if followed by another unit), 10^{6}
min	Minute(s)
N	Newton
n*	Nano (if followed by another unit), 10^{-9}
Pa	Pascal, N m^{-2}
pH	Potential of hydrogen
ppm	Part(s) per million
rcf	Relative centrifugal field
rpm	Rounds per minute, min^{-1}
s	Second(s)
S	Siemens
wt%	Mass fraction, 10^{-2}

9.3 Buffers

10x PBS, pH 7.4

NaCl	80 g
KH_2PO_4	2 g
Na_2HPO_4	11.5 g
KCl	2 g
Ultrapure water	ad 1.0 L

PBS, pH 7.4

10x PBS	100 mL
Ultrapure water	ad 1.0 L

Modified 10x PBS

NaCl	100 g
10x PBS	ad 1.0 L

Acetate buffer, pH 3.7

0.2 M NaAc	10 mL
0.2 M HAc	90 mL

Acetate buffer, pH 4

0.2 M NaAc	18 mL
0.2 M HAc	82 mL

Acetate buffer, pH 4.5

0.2 M NaAc	43 mL
0.2 M HAc	57 mL

Erklärung nach § 8 der Promotionsordnung

Hiermit erkläre ich gemäß § 8 der Promotionsordnung der Mathematisch-Naturwissenschaftlichen Fakultät der Christian-Albrechts-Universität zu Kiel, dass ich die vorliegende Arbeit, abgesehen von der Beratung durch meinen Betreuer, selbstständig und ohne fremde Hilfe verfasst habe. Weiterhin habe ich keine anderen als die angegebenen Quellen oder Hilfsmittel benutzt und die den benutzten Werken wörtlich oder inhaltlich entnommenen Stellen als solche kenntlich gemacht. Die vorliegende Arbeit ist unter Einhaltung der Regeln guter wissenschaftlicher Praxis entstanden und wurde bei keiner anderen Universität zur Begutachtung eingereicht.

Judith Maria Heidland

Danksagung

Ich möchte an dieser Stelle die Gelegenheit nutzen, vielen Personen Danke zu sagen, ohne die die letzten vier Jahre sicher anders verlaufen wären.

Mein erster Dank geht dabei an meine Doktormutter Regina Scherließ. Vielen Dank für dieses spannende und herausfordernde Promotionsthema, für die Unterstützung bei der Bearbeitung dessen und vor allem auch dafür, dass ich es auf so vielen Konferenzen vorstellen konnte.

Vielen Dank auch an Susanne Sebens für die gute Zusammenarbeit bei den Zellversuchen und die Übernahme des Zweitgutachtens. Danke hier auch an Ole Helm und Elsa Winter für die Planung und Durchführung der Versuche.

Hanna Göttsche, Regina Krehl, Denissa Gummels, Anna Muhs, Simone Diekjobst – Vielen Dank für die Unterstützung. Sei es die Bestellung von Substanzen, das Abfüllen von Proben oder einfach nur ein aufmunterndes Gespräch. Der Arbeitskreis wäre ohne euch ein anderer. Danke auch an Volkmar Kleppa und Detlef Rödiger für die stets schnelle Lösung sämtlicher IT-Probleme. Das gleiche gilt für Kalle Bock, der immer schnell zu Stelle war, wenn es irgendwo ein Problem gab. Vielen Dank, Dirk Böhme, für die häufig auch kreative Hilfe bei Fragen und für viele Gespräche beim morgendlichen Kaffee und damit einen entspannten Start in den Tag.

Ein sehr großer Dank gilt Rüdiger Smal, der nicht nur sämtliche Abbildungen dieser Arbeit angefertigt hat (und einige davon auch mehr als einmal, da mir immer noch Verbesserungsmöglichkeiten eingefallen sind…), sondern auch für seine immer wieder spontane Hilfe und die unglaublich vielen Gespräche, bei denen ich häufig gar nicht mehr weiß, wie wir von einem Thema auf's nächste, auf's nächste und immer weitergekommen sind.

Vielen Dank auch an alle, mit denen ich viele Stunden gemeinsam im Praktikum verbracht habe und dafür, dass wir uns gegenseitig unterstützt haben, wenn's mal eng

wurde: Ann-Kathrin Menge, Eric Lahrsen, Annika Heel, Friederike Gütter, Nancy Rhein, Kirsten Seidel, Marie Hellfritzsch und Simon Bock.

Viele Kollegen sind in dieser Zeit für mich zu guten Freunden geworden. Danke Andrea Arntz für die Unterstützung bei meinen ersten Schritten mit den Chitosan-Nanopartikeln; danke Phillip Arntz für viele Gespräche, bei denen wir uns gegenseitig aufgebaut haben; danke Ann-Kathrin Menge für einen schönen Einstieg ins Praktikum; danke Dorothea Gutekunst für viele schöne Momente in und außerhalb der Uni; danke Mathias Mönckedieck für viele tolle Erinnerungen an diverse DDL-Konferenzen im winterlichen Edinburgh; danke Marie Hellfritzsch für deine unerschöpfliche Motivation; danke Annika Heel für unsere zwei Praktikumssemester und die gegenseitige Unterstützung; danke Friederike Gütter für unsere gemeinsame Büro-Zeit, das wortlose Verständnis füreinander und für alles drum herum. Danke auch an unseren „externen Arbeitskreis" – Steffen Wöll, Claudia Hildebrandt, Fabian Stahlkopf. Ich bin froh, dass ich euch kennen gelernt habe und viele gemeinsame Erinnerungen mit euch teilen darf.

An dieser Stelle möchte ich mich auch noch ganz herzlich bei meinen Korrekturlesern bedanken. Danke Friederike Gütter, Annika Heel, Claudia Hildebrandt und Tobias Stöhr, dass ihr mir so viel geholfen habt. Ohne euch wäre die Arbeit nicht so geworden, wie sie jetzt ist!

Natürlich gilt mein Dank auch meinen Eltern und meiner Schwester. Vielen Dank für die Unterstützung und Aufmunterung – je nachdem, was gerade nötig war.

Und nicht zuletzt: danke Tobias Stöhr, dass du immer da bist und ich immer auf dich zählen kann!